Westinghouse Non-Proprietary Class 3

WCAP-16794-NP
Revision 0

October 2007

Steam Generator Tube Alternate Repair Criteria for the Portion of the Tube Within the Tubesheet at the Vogtle 1 & 2 Electric Generating Plants

WCAP-16794-NP
Revision 0

Steam Generator Tube Alternate Repair Criteria for the Portion of the Tube Within the Tubesheet at the Vogtle 1 & 2 Electric Generating Plants

October 2007

Author: *
G. W. Whiteman
Regulatory Compliance and Plant Licensing

Reviewer: *
C. D. Cassino
Steam Generator Design and Analysis

*Electronically Approved Records Are Authenticated in the Electronic Document Management System.

Westinghouse Electric Company LLC
P.O. Box 355
Pittsburgh, PA 15230-0355

TABLE OF CONTENTS

TABLE OF CONTENTS (cont.)

LIST OF TABLES

LIST OF TABLES (cont.)

LIST OF TABLES (cont.)

LIST OF FIGURES

LIST OF FIGURES (cont.)

LIST OF FIGURES (cont.)

LIST OF FIGURES (cont.)

LIST OF FIGURES (cont.)

ABSTRACT

Nondestructive examination indications of primary water stress corrosion cracking were found in the Westinghouse Model D5 Alloy 600 thermally treated steam generator tubes at the Catawba 2 nuclear power plant in the fall of 2004. Most of the indications were located in the tube-to-tubesheet welds with a few of the indications being reported as extending into the parent tube. In addition, a small number of tubes were reported with indications about 3/4 inch above the bottom of the tube within a region referred to as the tack expansion, and multiple indications were reported in one tube at internal bulge locations in the upper third of the tubesheet. The tube-end weld indications were dominantly axial in orientation and almost all of the indications were concentrated in one steam generator. Circumferential cracks were also reported at internal bulge locations in two of the Alloy 600 thermally treated steam generator tubes at the Vogtle 1 plant site in the spring of 2005. Internal tube bulges within the tubesheet are created in a number of locations as an artifact of the manufacturing process. Based on interpretations of requirements published by the NRC staff in GL 2004-01 and IN 2005-9, the Southern Nuclear Operating Company (SNC) requested that a recommendation be developed for future examinations of the tubesheet regions of the steam generator tubes at the Vogtle 1 & 2 Electric Generating Plant. An evaluation was performed that considered the requirements of the ASME Code, Regulatory Guides, NRC Generic Letters, NRC Information Notices, the Code of Federal Regulations, NEI 97-06, and additional industry requirements. Recent NRC RAI (Reference 39) have been considered and responses to those that pertain directly to Vogtle Units 1 and 2 are provided in Appendix A of this report. The conclusions of the technical evaluation are that:

1. the structural integrity of the primary-to-secondary pressure boundary is unaffected by tube degradation of any magnitude below a tube location-specific depth ranging from 7.24 to 13.38 inches (Hot Leg Only) depending on the tube leg and bundle zone being considered (and assuming the divider plate-to-stub runner weld is non-functional), designated as H*, and,

2. that the accident condition leak rate integrity can be bounded by a specified factor of the normal operation leak rate from degradation at or below a calculated distance, designated as B*, from the top of the nominally 21-inch thick tubesheet, including degradation of the tube-end welds.

These results follow from analyses demonstrating that the tube-to-tubesheet hydraulic joints make it extremely unlikely that any operating or faulted condition loads are transmitted below the H* elevation, and the contact pressure dependent leak rate resistance increases below the B* elevation within the tubesheet. The possibility of degradation at such locations in the Vogtle 1 & 2 steam generator tubes exists based on the reported degradation at Catawba 2 and previously at Vogtle 1. The determination of the required engagement depth was based on results from finite element model structural analyses and a steam line break to normal operation comparative leak rate evaluation. The cold leg requirements are greater than the hot leg requirements with regard to leak rate and pullout resistance (See Table 9-1). Application of the structural analysis and leak rate evaluation results to eliminate inspection and/or repair of tube indications in the tube end region, which is below the H* or B* elevation, is interpreted to constitute a redefinition of the primary-to-secondary pressure boundary relative to the original design of the SG and requires the approval of the NRC staff through a license amendment.

1 INTRODUCTION

Indications of cracking were reported from the nondestructive, eddy current examination of the steam generator (SG) tubes during the fall 2004 outage at the Catawba 2 nuclear power plant operated by the Duke Power Company, References 1, 2, and 3. The tube indications at Catawba 2 were reported about 7.6 inches from the top of the tubesheet in one tube, and just above the tube-to-tubesheet welds in a region of the tube known as the tack expansion (TE) in several other tubes. Moreover, indications were also reported in the tube-end welds (TEWs), also known as tube-to-tubesheet welds, joining the tube to the tubesheet, with a small number of those indications extending into the tube material. The Catawba 2 plant has Westinghouse designed, Model D5 SGs fabricated with Alloy 600 (thermally-treated) (A600TT) tubes. Subsequently, one indication was reported in each of two SG tubes at the Vogtle Unit 1 plant operated by the Southern Nuclear Operating Company (Reference 4). The Vogtle 1 & 2 SGs are of the Westinghouse Model F design with slightly smaller diameter and thickness A600TT tubes than in the Catawba 2 Model D5 SGs. It was concluded from those observations that there is the potential for similar tube indications to be reported during future inspections of the Vogtle 1 & 2 SGs.

The findings in the Catawba 2 and Vogtle 1 SG tubes present three distinct issues with regard to future inspections of A600TT SG tubes which have been hydraulically expanded into the tubesheet:

1. indications in internal bulges within the tubesheet (created in a number of tubes as an artifact of the manufacturing process),

2. indications at the elevation of the tack expansion transition, and,

3. indications in the tube-to-tubesheet welds, including some extending into the tube.

The scope of this document is to:

a. address the applicable requirements, including the original design basis, Reference 5, and regulatory issues, Reference 6, and,

b. provide analysis support for technical arguments to limit tube inspection in the tubesheet region to an area above which degradation could result in potentially not meeting the SG performance criteria, i.e., the depths specified in Section 7 and 9 of this report.

An evaluation was performed that considered the requirements of the ASME Code, Regulatory Guides, NRC Generic Letters, NRC Information Notices, Responses to NRC RAI, the Code of Federal Regulations, NEI 97-06, responses to NRC RAI and additional industry requirements. The conclusion of the technical evaluation is that:

1. the structural integrity of the primary-to-secondary pressure boundary is unaffected by tube degradation of any magnitude below a tube location-specific depth designated as H*, and,

2. the accident condition leak rate integrity can be bounded by twice the normal operation leak rate from degradation at or below a depth designated herein as B* from the top of the 21-inch thick tubesheet.

These results follow from analyses demonstrating that the tube-to-tubesheet hydraulic joints make it extremely unlikely that any operating or faulted condition loads are transmitted below the H* elevation, and that the tube-to-tubesheet contact leak rate resistance increases below the B* elevation within the tubesheet. The determination of the required engagement depth was based on the use of finite element model structural analyses and of a bounding leak rate evaluation based on the change in contact pressure between the tube and the tubesheet between normal operation and postulated accident conditions. The results provide the technical rationale to eliminate inspection of the region of the tube below the H* or B* elevation. Such an approach is interpreted to constitute a redefinition of the primary-to-secondary pressure boundary relative to the original design of the SG and requires the approval of the NRC staff through a license amendment.

A similar type of Technical Specification change has been approved, on a one-time basis, limiting inspections of Model F, Model D5 and Model 44F SGs to above 17 inches from the top of the tubesheet. This report was prepared to justify the specialized probe, e.g., rotating probe coil (RPC), exclusion zone to the portion of the tube below specific elevations from the top of the tubesheet based on meeting the structural and leak rate performance criteria for both the hot and cold leg, and to provide the necessary information for a detailed NRC staff review of the technical basis for that request. The major difference between the current evaluation of the Vogtle 1 & 2 SGs and prior applications is the identification of tube location-specific minimum depths for which inspection is required to ensure SG tube performance criteria is met instead of simply requiring a bounding value of 17 inches from the top of the tubesheet. Therefore, the report demonstrates the high level of conservatism which is maintained through the practice of inspecting to a depth of 17 inches from the top of the hot leg (HL) side of the tubesheet.

The H* values were determined to assure meeting the structural performance criteria for the operating SG tubes as delineated in NEI 97-06, Revision 2, Reference 7. The B* values were determined based on meeting the accident condition leak rate performance criteria. Compliance is based on demonstrating both structural and leakage integrity during normal operation and postulated accident conditions. The structural model was based on standard analysis techniques and finite element models as used for the original design of the SGs and documented in numerous submittals for the application of criteria to deal with tube indications within the tubesheet of other models of Westinghouse designed SGs with tube-to-tubesheet joints fabricated by other techniques, e.g., explosive expansion.

All full depth expanded tube-to-tubesheet joints in Westinghouse-designed SGs have a residual radial preload interface pressure between the tube and the tubesheet. Early vintage SGs involved hard rolling which resulted in the largest magnitude of the residual interface pressure. Hard rolling was replaced by explosive expansion which resulted in a reduced magnitude of the residual interface pressure. Finally, hydraulic expansion replaced explosive expansion for the installation of SG tubes, resulting in a further reduction in the residual interface pressure. In general, it was found that the leak rate through the joints in hard rolled tubes is insignificant. Subsequent testing demonstrated that the leak rate resistance of explosively expanded tubes was not as great as that of hard rolled tubes and prediction methods based on empirical data to support theoretical models were developed to deal with the potential for leakage. The same approach was followed to develop a prediction methodology for hydraulically expanded tubes. However, the model has been under review since its inception by Westinghouse and the NRC staff, with the intent of verifying its accuracy because it involved analytically combining the results from independent tests of leak rate through cracks with the leak rate through the tube-to-tubesheet crevice. An alternative approach, provided in this report, was developed for application at Vogtle 1 & 2 from

engineering expectations of the relative leak rate between normal operation and postulated accident conditions based on a first principles engineering evaluation.

A summary of the evaluation is provided in Section 2 of this report. Section 3 addresses plant operating conditions at Vogtle 1 & 2. Section 4 discusses the tube pullout and leakage test programs that are applicable to the Model F SGs at Vogtle 1 & 2. A summary of the conclusions from the structural analysis of the joint is provided in Section 5, the leak rate analysis in Section 6, determination of the requisite inspection depth based on leak rate considerations is in Section 7, a review of the qualitative arguments used by the NRC Staff for the tube joint inspection length approved for other plants is discussed in Section 8, conclusions from the structural and leak rate evaluations and recommended tube inspection plans are contained in Section 9 of this report. Responses to recent NRC Staff RAI as they pertain to Vogtle Units 1 and 2 are provided in Appendix A of this report. A letter summary of changes to the H* and B* analysis due to new crevice pressure and divider plate data, Reference 21, is included as Appendix B of this report.

2 SUMMARY DISCUSSION

Evaluations were performed to assess the need for addressing degradation in the region of the SG tubes within the tubesheet at the Vogtle 1 & 2 Electric Generating Plant. The conclusions from the evaluation are that a redefinition of the pressure boundary can be effected while still assuring that the structural and leak rate performance criteria would be met during both normal operation and limiting postulated accident conditions.

Implementation of the redefinition of the pressure boundary results in the elimination of examination of the tube end region of the tubes, which includes an allowance for a feature referred to as the bottom of the expansion transition (BET) and excludes the region of the tube-to-tubesheet joint referred to as the tack expansion or the tack expansion transition near the bottom of the tubesheet. In addition, consideration was given to the need to perform inspections of the tube-to-tubesheet weld in spite of the fact that the weld is specifically not part of the tube in the sense of the plant technical specification, see Reference 2. It is concluded that there is no need to inspect the tube-to-tubesheet welds for degradation because the tube in these regions has been shown to meet structural and leak rate criteria regardless of the level of degradation. The results from the evaluations performed as described herein demonstrate that the inspection of the tube within 7.65 inches of the tube-to-tubesheet weld and of the weld is not necessary for structural adequacy of the SG during normal operation or during postulated faulted conditions, nor for the complying with leak rate limits during postulated faulted events.

However, the leak rate during postulated accident conditions would be expected to be less than that during normal operation for indications near the bottom of the tubesheet (including indications in the tube-end welds) based on the observation that while the driving pressure increases by about a factor of almost two, the flow resistance increases because the tube-to-tubesheet contact pressure also increases. Flow resistance has been shown to have a log-linear relationship with contact pressure as discussed in Section 7 of this report. Depending on the depth within the tubesheet, the relative increase in resistance could easily be larger than that of the pressure potential. Therefore, the leak rate under normal operating conditions could exceed its allowed value before the accident condition leak rate would be expected to exceed its allowed value. This approach is termed an application of the "bellwether principle." The evaluations were performed to specifically determine relative changes in the leak rate resistance as a function of tube location from the center of the tubesheet and degradation distance from the top of the tubesheet. The assessment envelopes postulated circumferential cracking of the tube or the tube-to-tubesheet weld that is 100% deep by 360° in extent because it is based on the premise that the tube and weld are not present below the analyzed elevations. It has been determined that accident condition leak rate integrity can be bounded by twice the normal operation leak rate from degradation of any magnitude below 6.81 inches from the top of a nominally 21.03-inch thick tubesheet, designated as the B* distance (Hot Leg Only).

Based on the information summarized above, inspection to the H* depths as defined in Reference 33, are the minimum distances that are necessary to assure compliance with the structural requirements for the SGs. In addition, based on the results from consideration of application of the bellwether principle regarding potential leakage during postulated accident conditions, inspection depths as a function of tube location established using the results from these analyses are conservative and justified.

The limiting length (H* value) determined for structural compliance bounds the required length for leak rate compliance as discussed in Sections 5 and 9 of this report depending on the allowable relative leak rates. For example, compare the results in Table 5-12 and 5-12a to those in Table 7-2. The application of the bellwether approach to the leak rate analysis as described in Section 6.1 of this report negates the need to consider specific leak rates from individual cracks because it relies only on the relative magnitude of the joint contact pressures between the tube and the tubesheet. The B* distances determined in this report represent the distances from the top of the tubesheet where the integrated resistance is the same during a postulated SLB and NOp conditions. As discussed later in this report, these distances vary by radial location from the center of the tube bundle. This means that the leak rate during a postulated SLB from any or all indications below the B* distance will be bounded by a multiple of the leak rate during normal operating conditions based on the relative driving pressure for the two conditions.

3 OPERATING CONDITIONS

The Vogtle 1 & 2 Electric Generating Plant is a four-loop nuclear power plant with Westinghouse designed and fabricated Model F SGs; there are 5626 tubes in each SG. The design of these SGs includes Alloy 600 thermally-treated (A600TT) tubing, full-depth hydraulically expanded tubesheet joints, and broached hole quatrefoil tube support plates constructed of stainless steel.

3.1 BOUNDING OPERATING CONDITIONS

Values that bound the current Vogtle 1 & 2 SG thermal-hydraulic parameters during normal operation are tabulated below (Note: these values assume a 10% SG tube plugging level.):

Parameter and Units		Bounding NOp Conditions[1]		Current NOp Conditions[2]
		Case 1	Case 2	(Reference 40)
Power – NSSS	MWt	3653	3653	3579
Reactor Vessel Outlet Temperature	°F	603.8	620.0	603.8
Reactor Coolant System Pressure	psig	2235	2235	2235
SG Steam Temperature	°F	518.1	531.3	534
SG Steam Pressure	psig	810	926	901
Primary-to-Secondary Pressure Difference	psi	1425	1309	1334
Steam Line Break Pressure Difference	psig	2560	2560	2560

1. Reference 9.
2. The H*/B* values calculated using the current limiting operating parameters are equivalent to the H*/B* values calculated using the limiting margin uncertainty recapture (MUR) uprate parameters identified in Reference 9.

3.2 FAULTED CONDITIONS

In addition to the Regulatory Guide 1.121 (Reference 41) criteria, it is necessary to satisfy the updated final safety analysis report (UFSAR) accident condition assumptions for primary-to-secondary leak rates. Calculated primary-to-secondary side leak rate during postulated events should:

1. not exceed the total charging pump capacity of the primary coolant system, and

2. be such that the off-site radiological dose consequences do not exceed Title 10 of the Code of Federal Regulations (10 CFR) Part 100 guidelines.

The accident condition primary-to-secondary leakage must be limited to acceptable values established by plant-specific UFSAR evaluations. Pressure differentials associated with a postulated accident condition event can result in leakage from a through-wall crack through the interface between a hydraulically expanded tube in the tubesheet and the tube hole surface. Therefore, a steam generator leakage evaluation for faulted conditions is provided in this report. The accidents that are affected by primary-to-secondary leakage are those that include, in the activity release and off-site dose calculation, modeling of leakage and secondary steam release to the environment. For Vogtle Units 1 and 2, these accidents include a postulated control rod ejection, locked rotor, and a postulated SLB event. Steam line break (SLB) is the limiting condition with respect to overall dose consequences because:

1. the SLB primary-to-secondary leak rate in the faulted loop is greater than the operating leak rate for the longest period of time with the largest sustained increase in differential pressure, and

2. leakage in the faulted steam generator is released directly to the environment.

For evaluating the radiological consequences due to a postulated SLB, the activity released from the affected SG (which is connected to the broken steam line) is released directly to the environment. The unaffected steam generators are assumed to continually discharge steam and entrained activity via the safety and relief valves up to the time when initiation of the RHR (reactor heat removal) system can be accomplished. The radiological consequences evaluated, based on meteorological conditions, usually assume that all of this flow goes to the affected SG. With the analytically determined level of leakage, the resultant doses are expected to be well within the guideline values of 10 CFR 100.

4 STEAM GENERATOR TUBE LEAKAGE AND PULLOUT TEST PROGRAMS DISCUSSION

Data is available with regard to pullout testing for the Model F SG geometry. The original testing of Reference 9 was performed to investigate postulated extreme effects on the tube-to-tubesheet weld from a loose part on the primary side of SG 4 at Vogtle Unit 1. Data was available from both Model D5 testing and Model F testing to assess the potential for crevice leakage. These data were subsequently used to support the model specific development of the required H* engagement length to resist pullout and to characterize the leak rate from throughwall tube indications within the tubesheet as a function of the contact pressure between the tube and the tubesheet, e.g., Reference 10 was originally written for the Vogtle 1 & 2 SGs. The testing also provides valuable information regarding the calculation of B* once a relative SLB to NOp leak rate has been identified.[1]

- The results from strength tests were used to establish the joint lengths needed to meet the structural performance criteria during normal operation and postulated accident conditions, the required engagement length being designated as H*. The inherent strength of the joint coupled with the results from a finite element model of the loading conditions is used to calculate the required H* values subsequently described in Section 5. The H* results described in this WCAP supercede prior H* analysis.

- The results from leak rate tests for Model D5 and Model F test specimens were used to support the methodology to quantify the leak rate during postulated accident conditions as a function of the leak rate during normal operation. The required engagement length to meet a specific leak rate objective is designated as B*. For example, it may be desired to determine the engagement length needed so that the leak rate expected during a postulated accident event is no more than twice that during normal operation. The calculation of the relative leak rates as a function of engagement length is described in Section 7 of this report.

The test programs, their results, and the analysis of the results are described in the following sections.

4.1 TUBE PULLOUT RESISTANCE PROGRAM

Two testing programs were performed to determine the pullout resistance of Model F tube-to-tubesheet joints at [

]^{a,c,e} All of the test results are listed in Table 4-5. The mechanical loading, or pullout, tests were run on a mechanical testing machine, [

]^{a,c,e} The objective was to develop input information for analytically determining tube-to-tubesheet contact pressure and pullout resistance (lb/inch–axial). In this

1 It is noted that the discussion in Section 7 shows that the B* depths are not very sensitive to changes in the correlating parameters between the leak rate and contact pressure.

configuration, there is no contribution to tube-to-tubesheet contact pressure from tube internal pressurization. Internal pressurization also resists Poisson contraction associated with the axial load.

4.1.1 Model F Test Sample Assembly

The SG factory tube installation drawing specifies a [

]^{a,c,e} to facilitate the tube weld to the cladding on the tubesheet face and it was omitted from the test. Following welding of the tube to the tubesheet, a full-length hydraulic expansion of the tube into the tubesheet is performed. The hydraulic expansion pressure range for the Model F SGs was approximately [ ]^{a,c,e}. The majority of the test samples were expanded using a specified pressure of [ ]^{a,c,e} to conservatively bound the lower expansion pressure limit used for SG fabrication.

The tube expansion tool used in the factory consisted of a pair of seals, spaced by a tie rod between them. The hydraulically expanded zone was positioned relative to the lower surface of the tubesheet, overlapping the upper end of the tack expanded region. It extended to within a short distance of the upper surface of the tubesheet. This produced a hydraulically expanded length of approximately [ ]^{a,c,e} inch nominal tubesheet thickness. The majority of the test specimens were fabricated using [

]^{a,c,e} Previous test programs which employed a segmented approach to expansion confirmed the expectation that uniform results from one segment to the next would result. This approach produced the desired expansion pressures for a conservative length of [ ]^{a,c,e} inch expanded length being simulated. The remaining length of tube was expanded to the pressure at which the expansion bladder failed, usually between [ ]^{a,c,e} These samples are described as "Segmented Expansion" types. A tube expansion schematic is shown on Figure 4-2.

Data were also available from a small group of the test samples that had been previously fabricated using a [ ]^{a,c,e} tool which had been fabricated expressly for such tests. These samples were described as "Full-Depth Expansion" types. The expansion method with regard to the segmented or full-length aspect does not have a bearing on the test results.

4.1.2 Model F Tube Pullout Test Results Discussion

The data from the series of pullout tests are listed in Table 4-5 and in Table 4-6 for the 0.25 inch displacement data at 600°F. The room temperature pullout test results shown in Table 4-5 were not used in the determination of the H* distances using the theory of elasticity. [

]^{a,c,e}

[

]^{a,c,e} The use of a larger coefficient of friction results in calculating a lower value of the contact pressure. Subsequent use of the lower coefficient of friction results in calculating a larger required engagement length. A conservative value used for the pullout force in the H* calculations was the lower 95th percentile, i.e., [ ]^{a,c,e} lbf/inch. The 95th percentile was used because the standard deviation value was so small. It is possible that the [

]^{a,c,e} As noted in the response to NRC RAI No. 1 in Appendix A of this report, only the room temperature data from Table 4-5 is utilized to determine the force per unit length value of [ ]^{a,c,e} that is used to calculate the H* distances included in this report.

4.2 MODEL F AND MODEL D5 LEAK RATE TESTING PROGRAMS

The purpose of the testing programs was to provide quantified data with which to determine the [

]^{a,c,e} As discussed in detail in Section 7, the analytical model for the leak rate is referred to as the Darcy or Hagen-Poiseuille formulation. The volumetric flow is a function of the pressure potential, the inverse of the crevice length, the inverse of the fluid viscosity, and the inverse of a resistance term characteristic of the geometry of the tube-to-tubesheet joint and referred to as the loss coefficient. Thus, the purpose of the testing programs is to obtain data with which to determine the loss coefficient. Data were available from leak rate test programs that independently addressed the Model F and the Model D5 tube-to-tubesheet joints:

a. The Model F tube joint leakage resistance program involved tests at [

]^{a,c,e}

b. The Model D5 tube joint leakage resistance program involved tests at [

]^{a,c,e}

The Model F program and results are described in Sections 4.2.1.1, 4.2.1.2, and 4.2.1.3 followed by the description and results of the Model D5 program in Sections 4.2.2.1, 4.2.2.2, and 4.2.2.3.

4.2.1 Model F Tube Joint Leakage Resistance Program

A total of [ ]^{a,c,e} were used in the leak test program. The tubesheet simulants were collars with the nominal tubesheet hole diameter. All tubes were perforated within the collar so that the only resistance to leakage was the tube-to-tubesheet joint. The measured leak rates were converted into leakage resistances for the tubesheet crevice using Darcy's law for flow through porous media. The leakage resistance data were calculated for the test conditions listed in Table 4-1.

2 The value of 0.2 was first justified as a conservative value for this type of use in Reference 16.

4.2.1.1 Model F Test Specimen Configuration

The intent of the test samples was to model key features of the Model F tube-to-tubesheet joint for [ ]^{a,c,e} The following hardware was used:

A Model F tubesheet simulating collar which mimicked the radial stiffness of a Model F tubesheet unit cell with an outside diameter of approximately [ ]^{a,c,e} The length of the test collars was [ ]^{a,c,e} thickness of the steam generator tubesheet. This allowed for the introduction and collection of leakage in unexpanded sections of the tube, while retaining conservative or typical hydraulic expansion lengths. The collars were drilled to the nominal design value inside diameters with the surface finish based on drawing tolerances. In addition, the run-out tolerance for the collar drilling operation was held to within [ ]^{a,c,e} of the tubesheet nominal hole diameter.

[

]^{a,c,e}

Model F A600TT tubing with a yield strength approximately the same as that of the tubes in the operating plants, which ranges from [ ]^{a,c,e} was used. The tubing used was from a certified heat and lot conforming to ASME SB163, Section III Class 1 and was maintained in a Quality Systems-controlled storeroom prior to use.

The intent of the leakage portion of the test program was to determine the leakage resistance of simulated Model F tube-to-tubesheet joints, disregarding the effect of the tube-to-tubesheet weld and the [

]^{a,c,e} see Figure 4-1. The welds were a feature of the test specimen design and made

no contribution to the hydraulic resistance. All of the leak tests conducted for the Model F test specimens discharged to atmospheric pressure, 15 psia.

4.2.1.2 Model F Leakage Resistance Tests

The testing reported herein was performed according to a test procedure which outlined two types of leak tests as follows:

1. Model F room temperature primary-to-secondary side leak tests were performed on all test samples, [
   ]^{a,c,e}

2. Model F elevated temperature primary-to-secondary leak tests were performed using an
   [
   ]^{a,c,e} These tests were performed following the room temperature primary-to-secondary side leak tests on the chosen samples.

4.2.1.3 Model F Leak Test Results

The leak tests on segmented expansion collars averaged [
]^{a,c,e} (As a point of reference, there are approximately 75,000 drops in one gallon.) The test results showed a [
]^{a,c,e}

4.2.2 Model D5 Tube Joint Leakage Resistance Program

A total of [
]^{a,c,e}

The lower bound leakage resistance distribution for the collars with the nominal tubesheet hole diameter was used in the present leakage evaluation. This lower bound leakage resistance was made using data for the test conditions shown in Table 4-2 below combined with the Model F leak test results discussed in Section 4.2.1.

4.2.2.1 Model D5 Test Specimen Configuration

The intent of the test samples was to model key features of the Model D5 tube-to-tubesheet joint for [ ]^{a,c,e} The following hardware was used:

1. A Model D5 tubesheet simulating collar matching the radial stiffness of a Model D5 tubesheet unit cell, utilizing an appropriate outside diameter of approximately [

]^{a,c,e}

Model D5 Tubing with an average yield strength for the SG Alloy 600 tubing in the Model D plants is [ ]^{a,c,e} The Alloy 600 tubing used for these tests was from heats conforming to ASME SB163, Section III Class 1. It was obtained from a Quality Systems-controlled Storeroom.

The intent of the leakage portion of the test program was to determine the leakage resistance of simulated Model D5 tube-to-tubesheet joints, disregarding the effect of the [ ]^{a,c,e}

Tube-to-tubesheet stimulant samples of the Model D5 configuration were designed and fabricated. The steam generator factory tubing drawing specifies a [

]^{a,c,e}

The hydraulic expansion pressure range for the Model D5 steam generators was [ ]^{a,c,e} This value conservatively bounds the lower expansion pressure limit used for the Model D5 steam generators. Refer to Figure 4-5 for the details of the configuration for the leak test. The test equipment consisted of a make-up tank (MUT), primary water autoclave (AC1) and a secondary autoclave (AC2) connected by insulated pressure tubing. Two specimens were installed into the secondary autoclave to minimize setup time and variability across test runs. AC1 was run with deoxygenated primary water containing specified amounts of boron, lithium, and dissolved hydrogen. The primary chemistry conditions were controlled in the MUT and a pump and backpressure system allowed the primary water to re-circulate from the MUT to the AC1. The primary autoclave had the normal controls for heating, monitoring pressure and safety systems including rupture discs. Figure 4-5 shows the entire test system with key valves and pressure transducers identified. In addition to the normal controls for heating, monitoring pressure, and maintaining safety, the secondary autoclave was outfitted with water cooled condensers that converted any steam escaping from the specimens into room temperature water. The pressure in the secondary side (in the main body of AC2, was monitored by pressure transducers. For most tests, the leakage was collected in a graduated cylinder on a digital balance connected to a computer so that the amount of water could be recorded as a function

of time. For some normal operating tests, the leakage was calculated based on changes in the secondary side pressure. All relevant autoclave temperatures and pressures were recorded with an automatic data acquisition system at regular time intervals.

4.2.2.2 Model D5 Leakage Resistance Tests

For the Model D5 testing, primary-to-secondary leak tests were performed on all test samples, using simulated primary water as a pressurizing medium. Refer to [

]^{a,c,e} to simulate a perforation of the tube wall due to corrosion cracking. All of the elevated temperature primary-to-secondary side leak tests were performed using an [

]^{a,c,e} as the pressurizing/leakage medium. In the case of 800 psid back pressure tests, the leakage was collected in the autoclave as it issued from the tube-to-collar crevice. In the remainder of the autoclave tests, the leakage was collected in the autoclave as it issued from the tube-to-collar crevice but it was piped to a condenser/cooler and weighed on an instrumented scale.

4.2.2.3 Model D5 Leak Test Results

The leakage rates for the Model D5 600°F normal operating and accident pressure differential conditions were similar to the respective Model F values. Leakage ranged from [

]^{a,c,e} Leakage data were also recorded at room temperature conditions to provide input for the low contact pressure portion of the flow loss coefficient-versus-contact pressure correlation.

Table 4-1 Model F Leak Test Program Matrix

a.c.e

a,c,e

Table 4-2 Model D5 Leak Test Program Matrix

a,c,e

Table 4-3 Model F Leak Rate Testing Data

Table 4-3 Model F Leak Rate Testing Data (cont.)

a,c,e

Table 4-3 Model F Leak Rate Testing Data (cont.)

a,c,e

Table 4-4 Model D5 Experimental Loss Coefficients

a,c,e

a,c,e

Table 4-4 Model D5 Experimental Loss Coefficients (cont.)

Table 4-4 Model D5 Experimental Loss Coefficients (cont.)

a,c,e

Table 4-5 Model F Pullout Test Data a,c,e

Table 4-6 Model F 0.25 Inch Displacement Data at 600°F

a,c,e

a,c,e

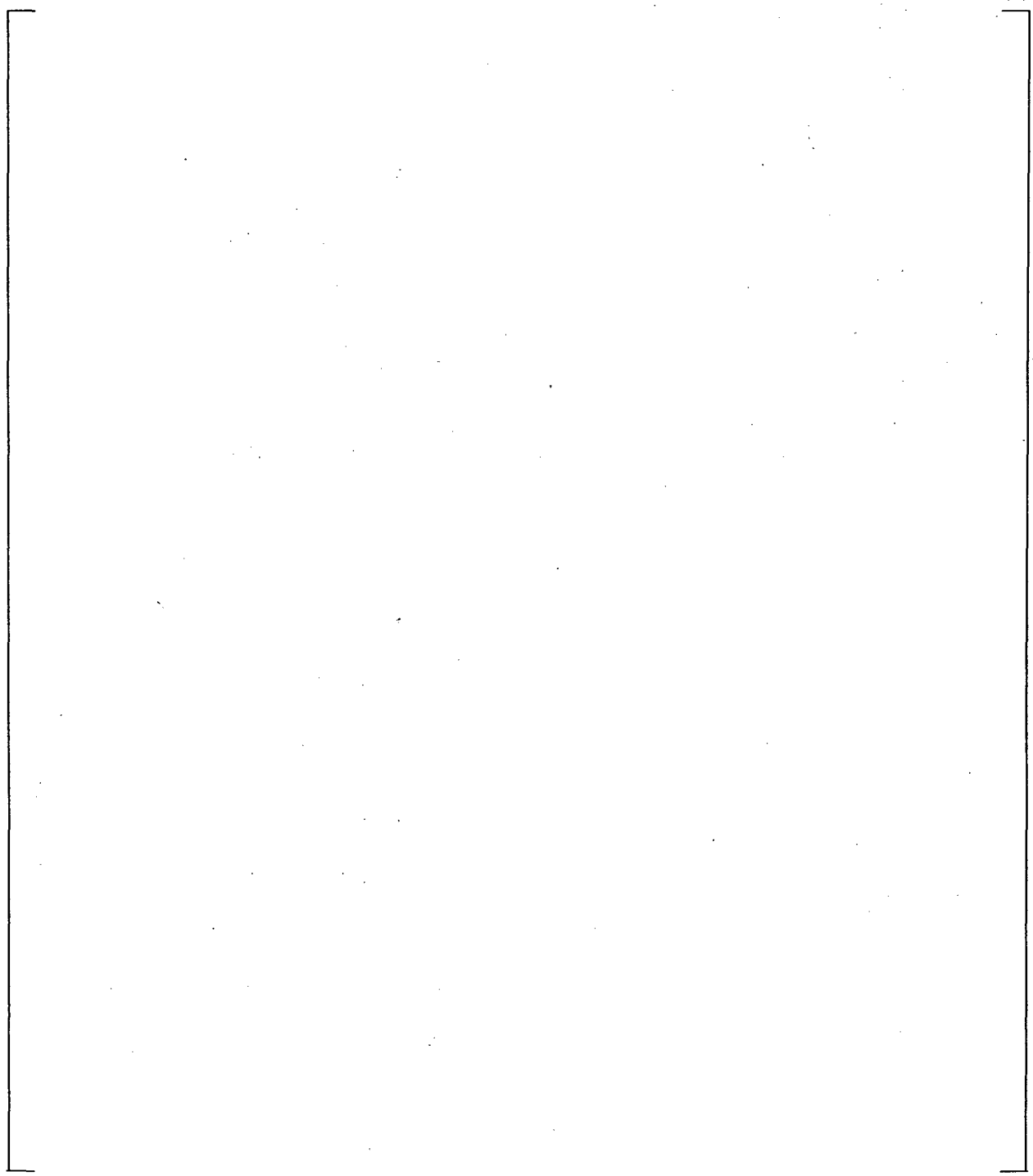

Figure 4-1 Example Leakage Test Schematic (Model F Testing Only)

a,c,e

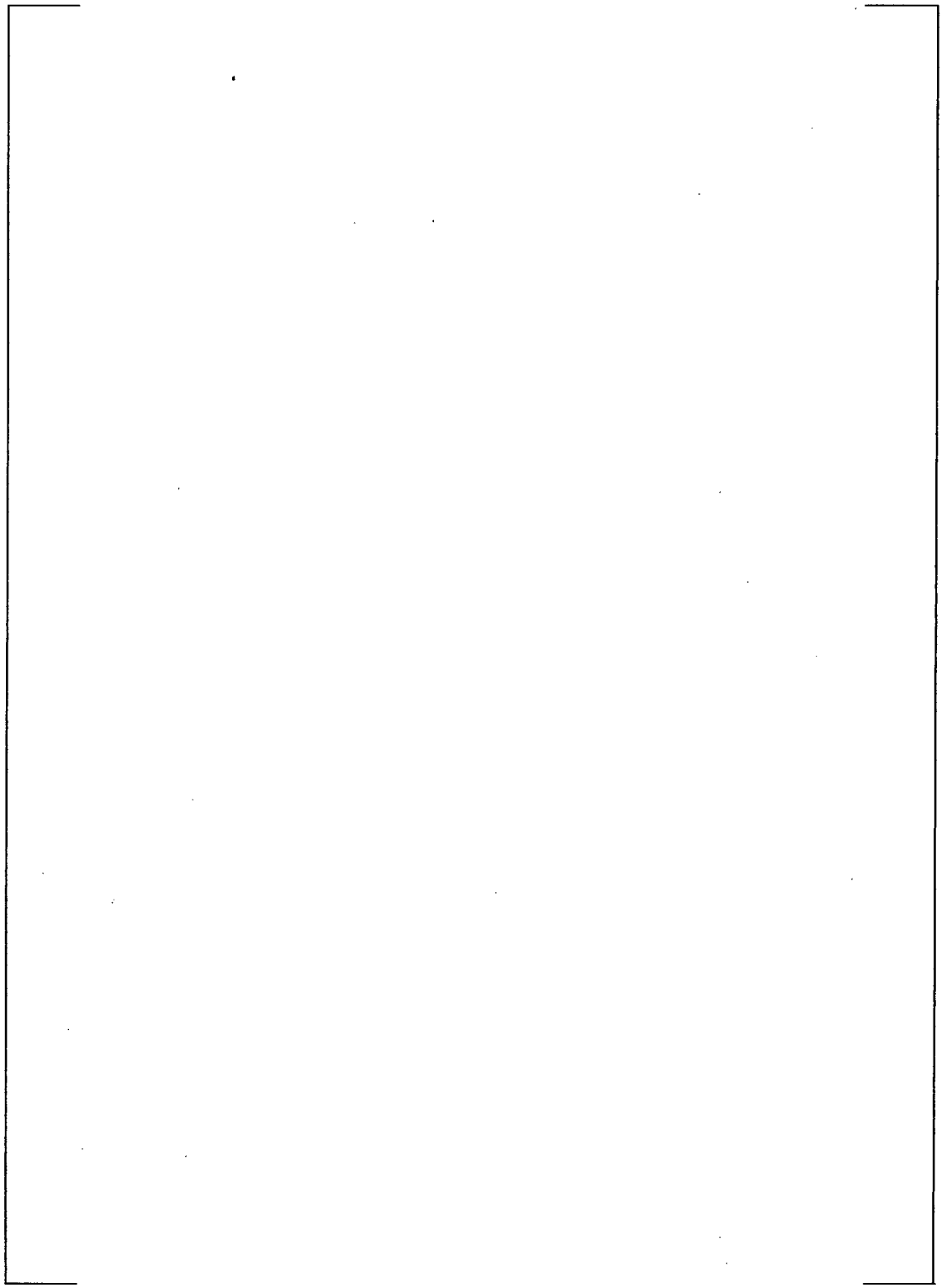

Figure 4-2 Example Tube Hydraulic Expansion Process Schematic

a,c,e

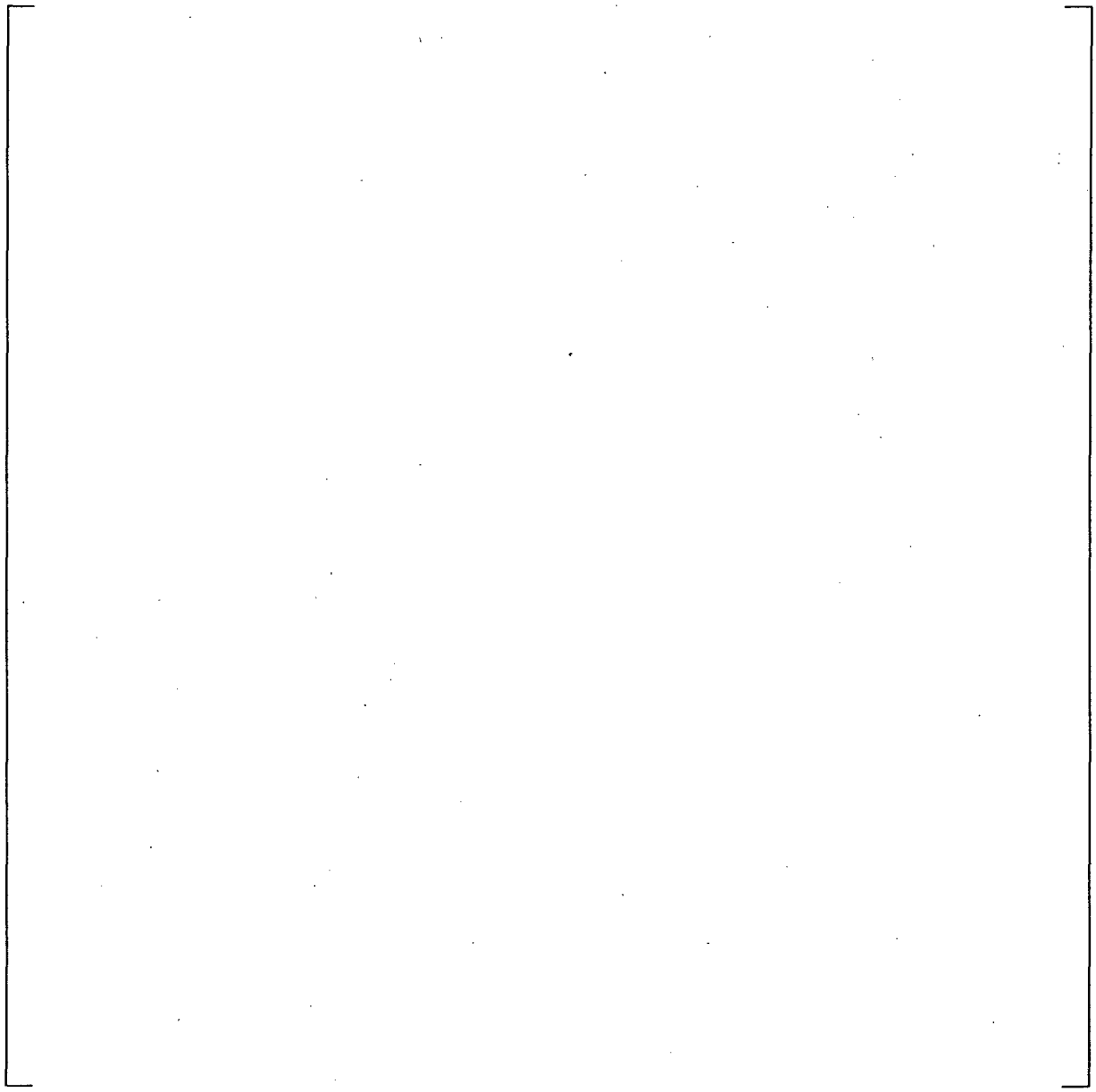

Figure 4-3 Example Tube Joint Leakage Test Configuration

a,c,e

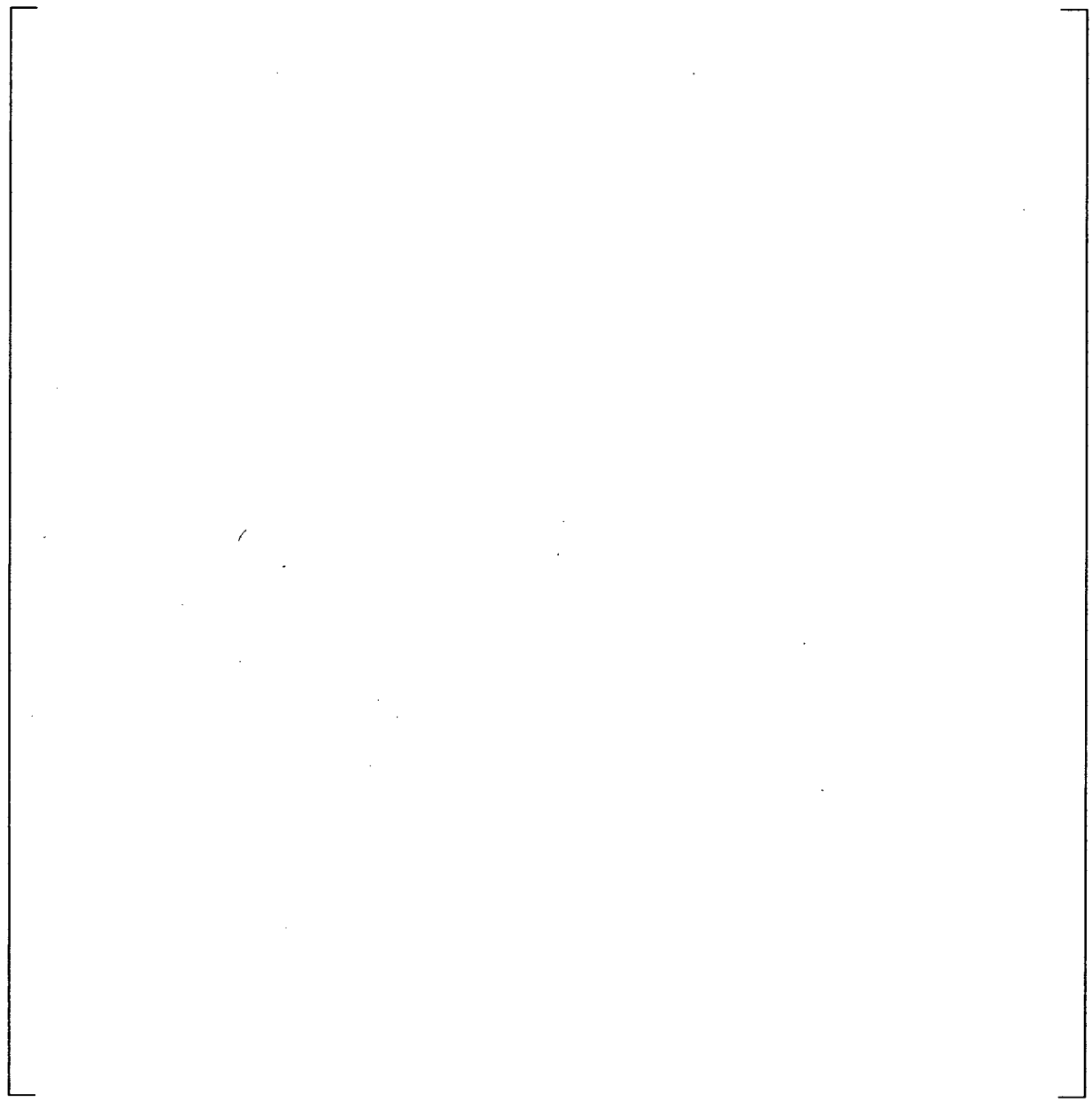

Figure 4-4 Example Tube Joint Sample Pullout Test Configuration

a,c,e

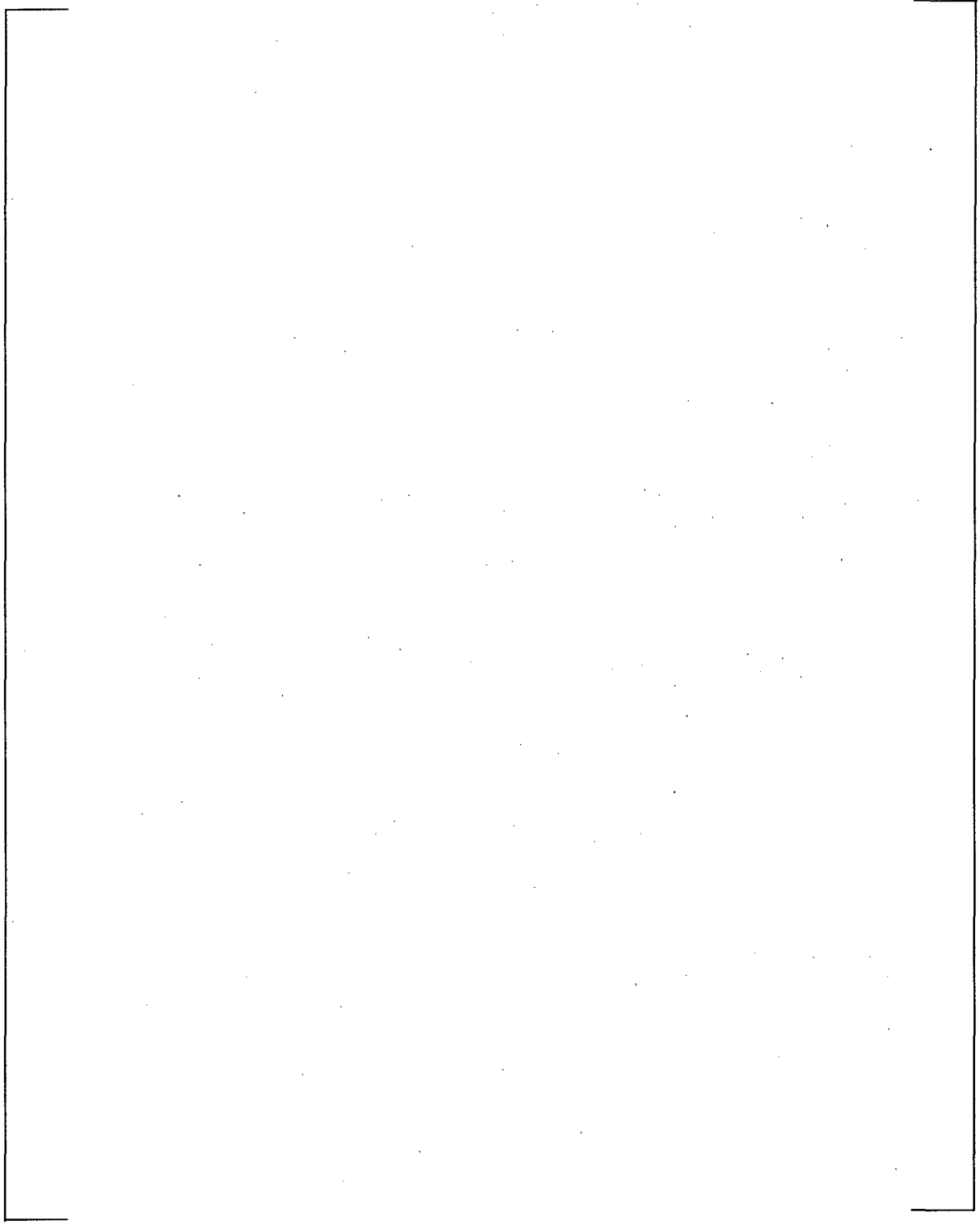

Figure 4-5 Schematic for the Test Autoclave Systems for Leak Rate Testing (Model D5 Testing Only)

5 STRUCTURAL ANALYSIS OF TUBE-TO-TUBESHEET JOINT

This section summarizes the structural aspects and analysis of the entire tube-to-tubesheet joint region. The tube-end weld was originally designed as a pressure boundary structural element in accordance with the requirements of Section III of the ASME (American Society of Mechanical Engineers) Boiler and Pressure Vessel Code, Reference 5. The design and construction code for the Vogtle 1 & 2 SGs was the 1971 Edition with the Summer 1972 Addenda. This means that there were no strength considerations made with regard to the expansion joint between the tube and the tubesheet, including the tack expansion regardless of whether it was achieved by rolling or Poisson expansion of a urethane plug.

An extensive empirical and analytical evaluation of the structural capability of the as-installed tube-to-tubesheet joints based on considering the weld to be absent was performed specifically for the Vogtle 1 & 2 Model F SGs and the results are reported below. Typical Model F hydraulic expansion joints with lengths comparable to those being proposed in what follows for limiting specialized probe examination were tested for pullout resistance strength at temperatures ranging from 70 to 600°F (References 11 and 35). The results of the tests coupled with those from finite element evaluations of the effects of temperature and primary-to-secondary pressure on the tube-to-tubesheet interface loads have been used to determine the engagement lengths that would be sufficient to equilibrate the axial loads resulting from consideration of 3 times the normal operating and 1.4 times the limiting accident condition pressure differences (Reference 33). Variation in required engagement length is a function of tube location, i.e., row and column, and decreases away from the center of the SG where the maximum value applies. The tubesheet bows, i.e., deforms, upward from the primary-to-secondary pressure difference and results in the tube holes becoming dilated above the neutral plane (i.e., the tubesheet concave side (primary surface) is in compression and the convex side (secondary surface) is in tension. The two surfaces are divided by the neutral plane which is the surface of the tubesheet that experiences no stress due to bending) , which is a little below the mid-plane of the thickness of the tubesheet because of the effect of the tensile membrane stress from the pressure loading. The amount of dilation is a maximum very near the radial center of the tubesheet (restricted by the divider plate in its as-built configuration) and diminishes with increasing radius outward. Moreover, the tube-to-tubesheet joint becomes tighter below the neutral plane and is a maximum at the bottom of the tubesheet[3].

In conclusion, the need for the weld is obviated by the interference fit between the tube and the tubesheet. Axial forces due to end cap loads are not transmitted to the portion of the tube below the H* distance during operation or faulted conditions, by factors of safety of at least 3 and 1.4 respectively, including postulated loss-of-coolant accidents (LOCA), and inspection of the tube below the H* distance including the tube-to-tubesheet weld is not technically necessary. Even if the expansion joint were not present, tubes with circumferential cracks up to about 180° by 100% deep would have sufficient strength to meet the nominal ASME Code structural requirements, based on the margins of safety reported in Reference 12. (The tube expansion joint cracking that has occurred to date is typically limited to less than 40° in azimuthal extent (Reference 37).

3 There is a small reversal of the bending stress beyond a radius of about 55 inches because the support ring prevents rotation and the hole dilation is at the bottom of the tubesheet.

An examination of Table 5-6 through Table 5-10 (and Tables 5-6a through 5-10a) illustrates that the holding strength of the tube-to-tubesheet joint in the vicinity of the mid-plane of the tubesheet thickness is much greater than at the top of the tubesheet. The radii reported in these tables were picked to conservatively represent the entire radial zones of consideration as defined on Figure 5-1. For example, Zone C has a maximum radius of 30.19 inches. However, in order to establish the H* value for Zone C, the tube radial location in which the H* distance was calculated to be the longest from the top of the tubesheet was reported. The H* value calculated for a tube at a radius of 4.02 inches from the center of the bundle was reported for Zone D. Likewise for tubes in Zone B under the heading 48.61 inches, the basis for the calculation was a tube at a radius of 34.4 inches. To illustrate the extreme conservatism associated with the holding strength of the joint slightly above and slightly below the neutral surface of the tubesheet, and to identify the proper tube radii for consideration the following is noted:

- In the center of the tubesheet, the incremental holding strength in the 4 inch distance between 12 to 16 inches below the top of the tubesheet during NOp is 581 lbf per inch using a coefficient of friction of 0.3. The performance criterion for $3 \cdot \Delta P$ is met by the first 1.38 inches of engagement below the upper elevation. At a radius of 58 inches, the length of engagement needed to meet the 3 Δp performance criterion is 7.24 inches from the top of the tubesheet.

- The performance criterion of 1.40 ΔP_{SLB} is met by the first 3.31 inches of engagement below 8 inches from the top of the tubesheet for a postulated SLB at the center of the tube bundle. At a radius of 58 inches, the length of engagement needed is met at 4.46 inches from the top of the tubesheet.

Table 5-11 and 5-11a show the limiting H* distances for each radial location for both the tube bundle hot and cold legs.

The defining point for a tube location is the tube centerline. To find the distance from the center stay rod of the tubesheet, the Pythagorean Theorem was used, with the X and Y lengths being the sides of the triangle and the radius to be solved for being the hypotenuse.

5.1 EVALUATION OF TUBE-TO-TUBESHEET CONTACT PRESSURE

A finite element model was developed (for the Model F tubesheet, channel head, and shell region) to determine the tubesheet hole dilations in the Vogtle 1 & 2 SGs (Reference 20 and 33). Background information on the finite element model is provided in Appendix A, Response to Wolf Creek NRC RAI 16. [

]^{a,c,e} loads in the tube. The contact pressures were evaluated using the specific assumptions and methods as described in Appendix A, Response to Wolf Creek NRC RAI Question 2.

5.1.1 Material Properties and Tubesheet Equivalent Properties

The tubes in the Vogtle 1 & 2 SGs are fabricated from A600TT material. Summaries of the applicable mechanical and thermal properties for the tube material are provided in Table 5-1. The tubesheets are fabricated from SA-508, Class 2a, material for which the properties are listed in Table 5-2. The shell material is SA-533, Grade A, Class 2, and its properties are in Table 5-3. Finally, the channel head material is SA-216, Grade WCC, and its properties are in Table 5-4. The material properties were obtained from the ASME B&PV (Boiler and Pressure Vessel) Code, Reference 14.

The perforated tubesheet in the Model F channel head assembly is treated as an equivalent solid plate in the finite element analysis. An accurate model of the overall plate behavior was achieved by using the concept of an equivalent elastic material with anisotropic properties. For square pitch tubesheet hole patterns, the equivalent material properties depend on the orientation of loading with respect to the symmetry axes of the pattern. An accurate approximation was developed in Reference 15, where energy principles were used to derive effective average isotropic elasticity matrix coefficients for the in-plane loading. The average isotropic stiffness formulation gives results that are consistent with those using the Minimum Potential Energy Theorem, and the elasticity problem thus becomes axisymmetric. The solution for strains is sufficiently accurate for design purposes, except in the case of very small ligament efficiencies, which are not an issue for the evaluation of the SG tubesheet.

The stress-strain relations for the axisymmetric perforated part of the tubesheet (Reference 16) are given by:

$$\begin{bmatrix} \sigma_R^* \\ \sigma_\theta^* \\ \sigma_Z^* \\ \tau_{RZ}^* \end{bmatrix} = \begin{bmatrix} D_{11} & D_{12} & D_{13} & 0 \\ D_{21} & D_{22} & D_{23} & 0 \\ D_{31} & D_{32} & D_{33} & 0 \\ 0 & 0 & 0 & D_{44} \end{bmatrix} \begin{bmatrix} \varepsilon_R^* \\ \varepsilon_\theta^* \\ \varepsilon_Z^* \\ \gamma_{RZ}^* \end{bmatrix}$$

with the elasticity coefficients calculated as:

$$D_{11} = D_{22} = \frac{\overline{E}_p^*}{f(1+\overline{\nu}_p^*)}\left[1 - \frac{\overline{E}_p^*}{E_Z^*}\nu^2\right] + \frac{1}{2}\left[\overline{G}_p^* - \frac{\overline{E}_p^*}{2(1+\overline{\nu}_p^*)}\right]$$

$$D_{21} = D_{12} = \frac{\overline{E}_p^*}{f(1+\overline{\nu}_p^*)}\left[\overline{\nu}_p^* + \frac{\overline{E}_p^*}{E_Z^*}\nu^2\right] - \frac{1}{2}\left[\overline{G}_p^* - \frac{\overline{E}_p^*}{2(1+\overline{\nu}_p^*)}\right]$$

$$D_{13} = D_{23} = D_{31} = D_{32} = \frac{\overline{E}_p^*\nu}{f}$$

$$D_{33} = \frac{E_Z^*(1-\overline{\nu}_p^*)}{f} \quad \text{and} \quad D_{44} = \overline{G}_Z^*$$

where $f = 1 - \overline{\nu}_p^* - 2\frac{\overline{E}_p^*}{E_Z^*}\nu^2$ and $\overline{G}_p^* = \frac{\overline{E}_d^*}{2(1+\overline{\nu}_d^*)}$

$\bar{E}_p^*$ = Effective elastic modulus for in-plane loading in the pitch direction,
E_z^* = Effective elastic modulus for loading in the thickness direction,
$\bar{\nu}_p^*$ = Effective Poisson's ratio for in-plane loading in the pitch direction,
$\bar{G}_p^*$ = Effective shear modulus for in-plane loading in the pitch direction,
$\bar{G}_z^*$ = Effective modulus for transverse shear loading,
$\bar{E}_d^*$ = Effective elastic modulus for in-plane loading in the diagonal direction,
$\bar{\nu}_d^*$ = Effective Poisson's ratio for in-plane loading in the diagonal direction, and,
ν = Poisson's ratio for the solid material.
E = Elastic modulus of solid material
L = Width of ligament minimum section
γ_{RZ} = Transverse shear strain
τ_{RZ} = Transverse shear stress,
[D] = Elasticity coefficient matrix required to define the anisotropy of the material

The tubesheet is a thick plate and the application of the pressure load results in a generalized plane strain condition. The pitch of the square, perforated hole pattern is 0.98 inches and nominal hole diameters are 0.703 inch. The ID of the tube after expansion into the tubesheet is taken to be about 0.625 inch based on an approximation of 1% thinning during installation associated with constant material volume. Equivalent properties of the tubesheet are calculated without taking credit for the stiffening effect of the tubes, which results in conservatism in the calculations regarding tubesheet deflection.

$$\text{Ligament Efficiency, } \eta = \frac{h_{\text{nominal}}}{P_{\text{nominal}}}$$

where:

h_{nominal} = $P_{nominal}$ - d_{maximum} (ligament thickness)
P_{nominal} = 0.980 inches, the pitch of the square hole pattern
d_{maximum} = .706 inches, the tube hole diameter

Therefore, $h_{nominal}$ = 0.2745 inches (0.980-0.706), and η = 0.2796 when the tubes are not included. From Slot, Reference 16, the in-plane mechanical properties for Poisson's ratio of 0.3 are:

Property		Value
E_p^*/E	=	0.3977
ν_p^*	=	0.1630
E_d^*/E	=	0.2137
ν_d^*	=	0.5531
E^*/E	=	0.3057
ν^*	=	0.3580
E	=	Elastic modulus of solid material

where the subscripts p and d refer to the pitch and diagonal directions, respectively. These values are substituted into the expressions for the anisotropic elasticity coefficients given previously. The coordinate system used in the analysis and derivation of the tubesheet equations given in Reference 16 and Reference 17 is different from the coordinate system in Reference 18. In the global model, defined in Reference 18, the X-axis corresponds to the radial direction, the Y-axis to the vertical or tubesheet thickness direction, and the Z-axis to the hoop direction. The directions assumed in the derivation of the elasticity coefficients were X- and Y-axes in the plane of the tubesheet and the Z-axis through the thickness. In addition, the order of the stress components in the WECAN/Plus (Reference 17) elements used for the global model is σ_{xx}, σ_{yy}, τ_{xy}, and σ_{zz}. The mapping between the Reference 15 equations and WECAN/+ is therefore:

Coordinate Mapping	
Reference 15	WECAN/+
1	1
2	4
3	2
4	3

Table 5-2 gives the modulus of elasticity, E, of the tubesheet material at various temperatures. Using the equivalent property ratios calculated above in the equations presented at the beginning of this section yields the elasticity coefficients for the equivalent solid plate in the perforated region of the tubesheet for the finite element model.

Potential impacts on yield strength due to temperature variations are reviewed in Appendix A, Response to Wolf Creek NRC RAI 4.

5.1.2 Evaluation Methodology Discussion

The analysis of the contact pressures utilizes conventional (thick shell equations) and finite element analysis techniques. A finite element analysis (FEA) model was developed for the Model F SG channel head/tubesheet/shell region in order to determine the tubesheet rotations (References 20 and 33). The elements used for the models of the channel head/tubesheet/shell region were the quadratic version of the 2-D axisymmetric isoparametric elements STIF53 and STIF56 of WECAN-Plus (Reference 17). The model for the Model F SG is shown on Figure 5-2. The dimensions used for the Model F FEA inputs were the same as those of the Vogtle Model F SGs. The FEA model results are only used to determine the effects of tubesheet bow caused by system pressure and temperatures on the tube contact pressures.

The pullout forces were calculated using a first principles approach. In-depth technical description is provided in Appendix A, Response to Wolf Creek NRC RAI 1. Basis for the calculations included room temperature pullout force test data."

The unit loads applied to this model are listed below:

Unit Load	Magnitude
Primary Side Pressure	1000 psi
Secondary Side Pressure	1000 psi
Tubesheet Thermal Expansion	500°F
Shell Thermal Expansion	500°F
Channel Head Thermal Expansion	500°F

The three temperature loadings consist of applying a uniform thermal expansion to each of the three component members, one at a time, while the other two remain at ambient conditions. The boundary conditions imposed for all five cases are: UX = 0 at all nodes on the centerline, and UY = 0 at one node on the lower surface of the tubesheet support ring. In addition, an end-cap load was applied to the top of the secondary side shell for the secondary side pressure unit load equal to:

$$P_{endcap} = -\frac{R_i^2}{R_o^2 - R_i^2} P$$

where:

R_i = Inside radius of secondary shell in finite element model = 64.69 in.
R_o = Outside radius of secondary shell in finite element model = 68.0 in.
P = Secondary pressure unit load = 1000 psi.

This procedure yielded displacements throughout the tubesheet for the unit loads.

5.1.2.1 Tubesheet Rotation Effects

Loads are imposed on the tube OD as a result of tubesheet rotations under pressure and temperature conditions. Previous calculations performed [

]^{a,c,e} The analysis results in this report conservatively assume that the stub-runner-to divider plate weld is non-functional (i.e., there is no restraint provided to the vertical displacement of the tubesheet by the weld).

The radial deflection, U_R, at any point within the tubesheet is found by scaling and combining the unit load radial deflections at that location according to:

a,c,e

[ ]

This expression is used to determine the radial deflections along a line of nodes at a constant axial elevation (e.g., top of the tubesheet) within the perforated area of the tubesheet. The expansion of a hole of diameter D in the tubesheet at a radius R is given by:

a,c,e

[ ]

U_R is available directly from the finite element results. dU_R/dR may be obtained by numerical differentiation.

The maximum expansion of a hole in the tubesheet is in either the radial or circumferential direction. [

]^{a,c,e}

Where *SF* is a scale factor between zero and one. For the eccentricities typically encountered during tubesheet rotations, [ ]^{a,c,e} These values are listed in the following table:

a,c,e

[

]

Data of initial eccentricities were fit to the following polynomial equation (Reference 20):

a,c,e

[

]

The hole expansion calculation as determined from the finite element results includes the effects of tubesheet rotations and deformations caused by the system pressures and temperatures. It does not include the local effects produced by the interactions between the tube and tubesheet hole.

5.1.2.2 Calculation of Local Effects Due to Interaction of the Tube and Tubesheet Hole

Standard thick shell equations, including accountability for the end-cap axial loads in the tube (Reference 18), in combination with the hole expansions from above are used to calculate the contact pressures between the tube and the tubesheet.

The unrestrained radial expansion of the tube OD due to thermal expansion is calculated as:

$$\Delta R_t^{th} = c\,\alpha_t\,(T_t - 70)$$

and from pressure acting on the inside and outside of the tube as,

$$\Delta R_{to}^{pr} = \frac{P_i c}{E_t}\left[\frac{(2-\nu)b^2}{c^2-b^2}\right] - \frac{P_o c}{E_t}\left[\frac{(1-2\nu)c^2+(1+\nu)b^2}{c^2-b^2}\right],$$

where:

P_i = Internal primary side pressure, P_{pri} psi
P_o = Crevice pressure, P_{cp} psi
b = Inside radius of tube = 0.3138 in.
c = Outside radius of tube = 0.3534 in.
α_t = Coefficient of thermal expansion of tube, in/in/°F
E_t = Modulus of Elasticity of tube, psi
T_t = Temperature of tube, °F, and,
ν = Poisson's Ratio of the material.

The thermal expansion of the hole ID is included in the finite element results and does not have to be expressly considered in the algebra; however, the expansion of the hole ID produced by pressure is given by:

$$\Delta R_{TS}^{pr} = \frac{P_i c}{E_{TS}}\left[\frac{d^2 + c^2}{d^2 - c^2} + \nu\right],$$

where:

E_{TS} = Modulus of Elasticity of tubesheet, psi

d = Outside radius of cylinder which provides the same radial stiffness as the tubesheet, that is, [ ]^{a,c,e}

If the unrestrained expansion of the tube OD is greater than the expansion of the tubesheet hole, then the tube and the tubesheet are in contact. The inward radial displacement of the outside surface of the tube produced by the contact pressure is given by: (Note: The use of the term δ in this section is unrelated to its potential use elsewhere in this report.)

$$\delta_t = \frac{P_2 c}{E_t}\left[\frac{c^2 + b^2}{c^2 - b^2} - \nu\right]$$

The radial displacement of the inside surface of the tubesheet hole produced by the contact pressure between the tube and hole is given by:

$$\delta_{TS} = \frac{P_2 c}{E_{TS}}\left[\frac{d^2 + c^2}{d^2 - c^2} + \nu\right]$$

The equation for the contact pressure (P_2) is obtained from:

$$\delta_{to} + \delta_{TS} = \Delta R_{to} - \Delta R_{TS} - \Delta R_{ROT}$$

where ΔR_{ROT} is the hole expansion produced by tubesheet rotations obtained from finite element results. The ΔR's are:

$$\Delta R_{to} = c\alpha_t (T_t - 70) + \frac{P_{pri} c}{E_t}\left[\frac{(2-\nu)b^2}{c^2 - b^2}\right] - \frac{P_{cp} c}{E_t}\left[\frac{(1-2\nu)c^2 + (1+\nu)b^2}{c^2 - b^2}\right]$$

$$\Delta R_{TS} = \frac{P_{cp} c}{E_{TS}}\left[\frac{d^2 + c^2}{d^2 - c^2} + \nu\right]$$

The resulting equation is:

a,c,e

[ ]

where:

P_i = Internal primary side pressure, P_{pri} psi
P_o = Crevice pressure, P_{cp} psi
b = Inside radius of tube = 0.3138 in.
c = Outside radius of tube = 0.3534 in.
α_t = Coefficient of thermal expansion of tube, in/in/°F
E_t = Modulus of Elasticity of tube, psi
T_t = Temperature of tube, °F, and,
ν = Poisson's Ratio of the material.
P_2 = Contact Pressure

For a given set of primary and secondary side pressures and temperatures, the above equation is solved for selected elevations in the tubesheet to obtain the contact pressures between the tube and tubesheet as a function of radius. The elevations selected ranged from the top to the bottom of the tubesheet. Negative "contact pressure" indicates a gap condition.

The OD of the tubesheet cylinder is equal to that of the cylindrical (simulate) collars [ ]^{a,c,e} designed to provide the same radial stiffness as the tubesheet, which was determined from a finite element analysis of a section of the tubesheet (References 19 and 20).

The tube inside and outside radii within the tubesheet are obtained by assuming a nominal plus 2 sigma diameter for the hole in the tubesheet (0.7068 inch) and wall thinning in the tube equal to the average of that measured during hydraulic expansion tests. That thickness is 0.0396 inch for the tube (Model F tube wall thickness after hydraulic expansion). The following table lists the values used in the equations above, with the material properties evaluated at 600°F. (Note that the properties in the following sections are evaluated at the primary fluid temperature).

Thick Cylinder Equations Parameter	Value*
b, inside tube radius, in.	0.3138
c, outside tube radius, in.	0.3534
d, outside radius of cylinder w/ same radial stiffness as TS, in.	[ ]^{a,c,e}
α_t, coefficient of thermal expansion of tube, in/in °F	$7.44 \cdot 10^{-6}$
E_t, modulus of elasticity of tube, psi	$29.7 \cdot 10^{6}$
α_{TS}, coefficient of thermal expansion of tubesheet, in/in °F	$7.25 \cdot 10^{-6}$
E_{TS}, modulus of elasticity of tubesheet, psi	$25.7 \cdot 10^{6}$
* The basis for the values for the parameters listed in this table used in the H*/B* analyses for Vogtle Units 1 and 2 are further clarified in the response to NRC RAI No. 2 in Appendix A of this report.	

5.1.2.3 Crevice Pressure Discussion

It has been shown by experiment that, for most of the distance through the tubesheet, the crevice pressure does not drop to below saturation pressure for large cracks in series with a crevice. The 1900 psi test pressure would be expected to result in less leakage because the test pressure is lower than the primary pressure during normal operating conditions of 2235 psig. The secondary side pressure does not significantly influence the crevice pressure.

There are two possible bases for determining which pressure to use during specific operating conditions: empirical test data and conservative assumptions based on engineering judgment. The empirical test data collected during tests performed on a simulated tubesheet collar with a hydraulically expanded tube consisted of measuring the pressure between the tube wall and the inner collar surface. The tube had six [

]^{a,c,e} The purpose of the hole positioning and geometry was to eliminate any geometry based flaw effects. The results of the tests for steam line break (SLB) and normal operating (NOp) conditions are described in detail in the White Paper submitted to the NRC under Docket Numbers STN 50- 454, 50-455, 50-546, and 50-547 (Reference 21). The results from the White Paper (Reference 21) show that a limiting crevice pressure can be defined as a fraction of the primary side pressure for both SLB and NOp. The specific fractions, denoted as crevice pressure ratios in the White Paper, are [ ]^{a,c,e}

The crevice pressure is determined by taking the primary pressure and multiplying by the appropriate crevice pressure ratio. For example, a NOp primary pressure of 2250 psi would result in a crevice pressure of [ ]^{a,c,e} Similarly, the crevice pressure for a primary pressure of 2560 psi during SLB results in a crevice pressure of approximately [ ]^{a,c,e} The leak rate is directly proportional to the pressure drop across the tube wall into the crevice. The pressure drop across the tube wall during NOp is 2250 psi minus [ ]^{a,c,e} The pressure drop from the example SLB condition is 2560 psi minus [ ]^{a,c,e} The change in driving head on any leaked fluid, combined with the change in contact pressure due to the

increased pressure in the tube/tubesheet crevice, still results in a leak rate ratio, defined as the leakage during SLB divided by the leakage during NOp, of less than two (Reference 21).

The crevice pressure interpretation in Reference 21 is conservative and focuses on the largest differences in operating conditions and how to apply them in a fashion that has the greatest impact on contact pressure. Another conclusion that is equally supported by the test data is that different crevice pressure ratios can be used that show that the leak rate would either not increase, or would potentially decrease, during accident conditions. For instance, in the White Paper, if the median is used to calculate the crevice pressure ratios from the total set of all available test data then ratios of [ ]^{a,c,e} are obtained for NOp and SLB conditions, respectively. Using those values to determine the pressure in the crevice gives a pressure drop across the tube wall of approximately [ ]^{a,c,e} during NOp and SLB conditions, respectively. The difference between the pressure drop for NOp and SLB using the total set median values is approximately [ ]^{a,c,e} Such a small difference in driving pressure on the leak, combined with the change in temperature and tubesheet bow during accident conditions, reduce the leak rate during a SLB so that the leakage during NOp is [ ]^{a,c,e}

In smaller cracks, it is possible for geometry based effects to change the way that the pressure develops in the tube/tubesheet crevice. In such a case, the pressure in the crevice may be much lower than suggested by the test results reported in Reference 21. In that event, the assumption of secondary side pressure in the crevice is conservative during both NOp and SLB conditions. In the case of NOp, the lower the pressure in the crevice the greater the pressure drop across the tube wall. For example, assuming a secondary side pressure of 750 psi in the crevice during NOp results in a pressure drop of 2250 psi minus 750 psi which equals 1500 psi. Similarly, assuming the secondary pressure in the crevice during SLB conditions results in a pressure differential of 2560 psi (assuming 0 psi secondary side pressure during an SLB event). The difference between the pressure during the NOp and SLB conditions is 1060 psi which results in a SLB to NOp leak rate ratio of less than two. If the crevice pressure during NOp was lower than the secondary side pressure, say that it was equal to 0 psi, the pressure drop across the tube wall during NOp would be equal to 2250 psi. The difference between the drop in pressure during the NOp and SLB conditions would then become 310 psi. The leak rate ratio between the NOp and SLB conditions, with a much smaller difference in the driving head on the leakage between NOp and SLB, would be much less than two.

5.1.2.4 Divider Plate Impact Discussion

Indications of cracks in the divider plates have been reported in French steam generators located at the Chinon, Saint-Laurent, Dampierre and Gravelines nuclear power stations. The cracks were observed on both sides of the divider plate in the stub runner divider plate weld, stub runner base metal and in the divider plate itself.

Figure 5-8 is a sketch of the region where cracking has been observed to occur.

The divider plate has typically been accounted for in B* and H* analyses via a divider plate factor, which is the ratio of the maximum vertical tubesheet displacements with an intact divider plate compared to the maximum vertical displacements of a tubesheet with no divider plate present. The factor is based on the ASME Code Stress Report provided for the SGs, which considered both to conservatively calculate

stresses in the tubesheet and stresses in the components attached to the tubesheet. Based on the original ASME Code stress analysis, the ratio of the maximum tubesheet displacement with and without the benefit of the divider plate is [ ]^{a,c,e} which means that the maximum vertical displacement of the tubesheet with an intact divider plate is [ ]^{a,c,e} less than the maximum vertical displacement of a tubesheet without a divider plate. This value [ ]^{a,c,e} was used for the divider plate factor in the B* and H* analyses prior to 2007.

The divider plate factor from the ASME stress report was determined by comparing the results of finite element models that included a divider plate with the nominal material properties and dimensions to a divider plate with an artificially low stiffness (e.g. Young's Modulus = 10 psi). The finite element models utilized for the code stress report to determine the divider plate effect were overly conservative because they did not account for features in the lower steam generator assembly that act to increase the resistance of the tubesheet to vertical deflections. For example, in the early analysis models used to calculate tubesheet displacements, the tube lane and the channel head to divider plate weld were not modeled. Research by Terakawa (Reference 22) indicates that the presence of the tube material within the tubesheet acts to stiffen the tubesheet with respect to bending and vertical deflection. A more detailed finite element model than that used in the original stress analysis shows that the impact of a non-degraded divider plate on tubesheet deflection is significantly greater and that the appropriate value to use for the divider plate factor in H* and B* analyses is [ ]^{a,c,e} (Reference 21), that is, the tubesheet deflection with an intact divider plate is significantly less than originally estimated [ ]^{a,c,e}

The B*/H* results presented in this report include a non-functional divider plate-to-stub runner weld (DP = 0.64) except where noted as otherwise (See the response to NRC RAI Questions Nos. 16, 17 and 18 included in Appendix A of the report). Note that in this context the term "non-functional" applies only to the divider plate-to-stub runner weld's ability to restrain the vertical deflections of the tubesheet. Evaluation of the current divider plate degradation indicates that the progression of degradation is small, and that very significant divider plate degradation is required before the function of the divider plate relative to the deflection of the tubesheet would be degraded; thus, the assumption of a non-functional stub runner to divider plate weld is extremely conservative (Reference 38).

5.1.3 Vogtle 1 & 2 Contact Pressures

5.1.3.1 Normal Operating Conditions

The loadings considered in the analysis are based on an umbrella set of conditions as defined in References 15, 16 and 14. The current operating parameters from Reference 8 are used. The temperatures and pressures for normal operating conditions at Vogtle 1 & 2 are bracketed by the following two cases:

Loading	Case 1[1]	Case 2[2]
Primary Pressure	2235 psig	2235 psig
Secondary Pressure	901 psig	926 psig
Primary Fluid Temperature (T_{hot})	603.8°F	620.0°F
Secondary Fluid Temperature	534.0°F	537.3°F
1. T_{hot} = 603.8°F. 2. T_{hot} = 620.0°F.		

The primary pressure [

]^{a,c,e}

5.1.3.2 Faulted Conditions

Of the faulted conditions, Feed Line Break (FLB) and Steam Line Break (SLB) are the most limiting. FLB has a higher ΔP across the tubesheet, while the lower temperature of SLB results in less thermal tightening. Both cases are considered in the tube contact pressure calculation.

Previous analyses have shown that FLB and SLB are the limiting faulted conditions, with tube lengths required to resist push out during a postulated loss of coolant accident (LOCA) being typically less than one-fourth of the tube lengths required to resist pull out during FLB and SLB (References 18, 19 and 23). Therefore LOCA was not considered in this analysis.

Other transients are considered in the Vogtle Units 1 and 2 response to Wolf Creek NRC RAI No. 10 included in Appendix A of this report.

Feed Line Break

The temperatures and pressures for the FLB event at Vogtle 1 & 2 are bracketed by the following two cases:

Loading	Case 1[1]	Case 2[2]
Primary Pressure	2650 psig	2650 psig
Secondary Pressure	0 psig	0 psig
Primary Fluid Temperature (T_{hot})	603.8°F	620.0°F
Secondary Fluid Temperature	534.0°F	537.3°F

1. T_{hot} = 603.8°F.
2. T_{hot} maintained at a maximum value of 620°F.

The FLB condition [

]^{a,c,e}

5.1.3.3 Steam Line Break

As a result of SLB, the faulted SG will rapidly blow down to atmospheric pressure, resulting in a large ΔP across the tubes and tubesheet. The entire flow capacity of the auxiliary feedwater system would be delivered to the dry, hot shell side of the faulted SG. The primary side re-pressurizes to the pressurizer safety valve set pressure. The pertinent parameters are listed below. The combination of parameters yielding the most limiting results is used.

Primary Pressure	=	2560 psig
Secondary Pressure	=	0 psig
Primary Fluid Temperature (T_{hot})	=	420°F
Secondary Fluid Temperature	=	260°F

For this set of primary and secondary side pressures and temperatures, the equations derived in Section 5.2 below are solved for the selected elevations in the tubesheet to obtain the contact pressures between the tube and tubesheet as a function of tubesheet radius for the hot leg.

5.1.3.4 Summary of Tube-to-Tubesheet Contact Pressure Results

For Vogtle 1 & 2, the contact pressures between the tube and tubesheet for various plant conditions are listed in Table 5-5 (Hot Leg Results) and Table 5-5a (Cold Leg Results) and plotted versus radius on through Figure 5-3 through Figure 5-7 (Hot Leg Results) and Figure 5-3a through 5-7a (Cold Leg Results). The application of these values to the determination of the required engagement length is discussed in Section 5.3.

5.2 TUBE-TO-TUBESHEET HYDRAULIC EXPANSION JOINT CREVICE DEPTH

The tube holes for Model F SGs were drilled from the bottom side of the tubesheet (standard practice), and the fabrication drawings required that the holes be deburred after drilling. Deburring effectively results in a chamfer of the hole and the maximum allowable depth for the chamfer was specified to be [ ]^{a,c,e} inch. The tube installation hydraulic expansion process can also result in a short tapered crevice between the tube and the tubesheet at the secondary face of the tubesheet. This is an artifact of the expansion process equipment and its location within the tube at the time of application of the expansion pressure was a controlled dimension during fabrication. The maximum allowable crevice depth for the Vogtle 1 & 2 SGs was specified as [ ]^{a,c,e} inch on the Reference 24 drawing. In order to better quantify the requirements for controlling the crevice depth, and recognizing the stochastic nature of the manufacturing process, the hydraulic expansion procedure specification, Reference 25, stipulated statistical controls on the mean and the standard deviation of the crevice depth for a SG bundle. It was also stipulated that 99% of the population of crevice depths would be less than or equal to [ ]^{a,c,e} inch although the allowable mean depth was increased. For the purpose of establishing the depth of engagement required to assure meeting both the structural and leak rate performance criteria for the Vogtle 1 & 2 SGs, the requirements of the latter procedure were considered and an allowance of 0.3 inch was selected for application. Although there can be circumstances where the crevice depth allowance would not be necessary, e.g., if the elevation of zero contact pressure from tubesheet bow induced tube hole dilation were below the 0.3 inch allowance depth, such instances would be expected to be rare and the allowance has been added to all structurally required depths for final application.

5.3 DETERMINATION OF REQUIRED ENGAGEMENT LENGTH OF THE TUBE IN THE TUBESHEET

The elimination of a portion of the tube within the tubesheet from the in-service inspection (ISI) requirement constitutes a change in the location of the pressure boundary. The technical justification of the omission of the lower portion of the tube from examination relies on knowledge of the tube-to-tubesheet interference fit contact pressure at all elevations in the tube joint. In order to maintain consistency with other reports on this subject, the required length of engagement of the tube in the tubesheet to resist tube end-cap loads associated with the structural performance criteria is designated as H*. This length is based on structural requirements only and does not include any consideration of the potential leak rate, except perhaps in a supporting role with regard to the leak rate expectations relative to normal operating conditions. The contact pressure is used to calculate the magnitude of the force

resisting pullout of the tube from the tubesheet over the H* length. It is also used in estimating the impact of changes in the contact pressure on potential primary-to-secondary leak rate during postulated accident conditions.

The determination of H* depths was performed using the specific assumptions and methods as described in Appendix A, Response to Wolf Creek NRC RAI Question 2.

The end-cap loads to be resisted during NOp and faulted conditions are (Hot Leg Only):

Normal (maximum):	$\pi \cdot (2235\text{-}901) \cdot (0.7068)^2 /4 = 523.41$ lbs
Faulted (FLB):	$\pi \cdot 2650 \cdot (0.7068)^2 /4 = 1039.75$ lbs
Faulted (SLB):	$\pi \cdot 2560 \cdot (0.7068)^2 /4 = 1004.44$ lbs

Seismic loads have also been considered, but they are not significant in the tube joint region of the tubes. The normal operation load is multiplied by a factor of 3 and the faulted condition loads by a factor of 1.4 to obtain the associated structural performance criteria.

The tube-to-tubesheet contact pressure consists of the residual from the installation of the tube in the tubesheet plus the added effects discussed in Section 9 with regard to internal pressure in the tube, the differences in thermal expansion, and tubesheet rotation effects. The residual contact pressure from the tube installation was evaluated semi-empirically. It was determined by test for the as-fabricated condition and then analytically projected to the pertinent plant conditions. The tests involved pullout testing of tube-to-tubesheet specimens using thick collars to simulate the tubesheet as described in Section 4.1.

The initial element in estimating the strength (i.e., resistance to pullout) of the tube-to-tubesheet joint during normal operation or postulated accident conditions is the residual strength of the joint stemming from the expansion preload due to the manufacturing process, i.e., hydraulic expansion. During operation the preload increases because the thermal expansion of the tube is greater than that of the tubesheet and because a portion of the internal pressure in the tube is transmitted to the interface between the tube and the tubesheet. However, the tubesheet bows upward leading to a dilation of the tubesheet holes at the top of the tubesheet and a contraction at the bottom of the tubesheet when the primary-to-secondary pressure difference is positive. The dilation of the holes acts to reduce the contact pressure between the tubes and the tubesheet. The H* lengths are based on the pullout resistance associated with the net contact pressure during normal or accident conditions. The calculation of the residual strength involves a conservative approximation that the strength is uniformly distributed along the entire length of the tube within the tubesheet. This leads to a lower bound estimate of the strength for the determination of H*.

For the partial-length RPC evaluation, tube-to-tubesheet contact pressure was calculated [

]^{a,c,e}

The force resisting pullout acting on a length of a tube between elevations h_1 and h_2 is given by:

$$F_i = (h_2 - h_1)F_{HE} + \mu \pi d \int_{h_1}^{h_2} P \, dh$$

where:

F_{HE} = Resistance per length to pull out due to the installation hydraulic expansion,

P = Contact pressure acting over the incremental length segment *dh*, and,

μ = Coefficient of friction between the tube and tubesheet, conservatively assumed to be 0.3 for the pullout analysis to determine H*.

The contact pressure is assumed to vary linearly between adjacent elevations in the top part of Table 5-6 through Table 5-10 (Hot Leg), Table 5-6a through Table 5-10a (Cold Leg) so that between elevations L_1 and L_2,

$$P = P_1 + \frac{(P_2 - P_1)}{(L_2 - L_1)}(h - L_1)$$

or,

a,c,e

[redacted]

so that,

a,c,e

[redacted]

The latter equation was used to accumulate the force resisting pullout from the top of the tubesheet to each of the elevations listed in the lower parts of Table 5-6 through Table 5-10 (Hot Leg), Table 5-6a through Table 5-10a (Cold Leg). The above equation is also used to find the minimum contact lengths needed to meet the pullout force requirements; a summary for the various zones is provided in Table 5-11 (Hot Leg) and Table 5-11a (Cold Leg).

The top part of Table 5-8 (Hot Leg) lists the contact pressures through the thickness at each of the radial sections for the SLB faulted condition. The last parameter row, "h(0)" , of the central portion of the table lists the maximum tubesheet elevation as measured downward from the top of the tubesheet at which the contact pressure (P_c) is greater-than-or-equal-to zero. The above equation is used to accumulate the force resisting pull out from the top of the tubesheet to each of the elevations listed in the lower part of Table 5-8 (Hot Leg). In Zone C for example, this length is 11.30 inches for the $1.4 \cdot \Delta P_{SLB}$ performance criterion which corresponds to a pullout force of 1406.21 lbs in the hot leg. The minimum contact length

needed to meet the pullout force requirement of 1570.22 lbs for the Faulted (FLB) condition is less as is shown in Table 5-9 and Table 5-10 (Hot Leg). The H* calculations for each loading condition at each of the radii considered are summarized in Table 5-11 (Hot Leg). The H* results for each zone are summarized in Table 5-12 (Hot Leg). The bounding condition for the determination of the H* length for the hot leg is the normal operating condition performance criterion.

The cold leg results are provided in Tables 5-5a through 5-12a. The top part of Table 5-8a lists the contact pressures through the thickness at each of the radial sections for the SLB faulted condition. The last parameter row, "h(0)", of the central portion of the table lists the maximum tubesheet elevation measured downward from the top of the tubesheet at which the contact pressure (P_c) is greater-than-or-equal-to zero. The above equation is used to accumulate the force resisting pull out from the top of the tubesheet to each of the elevations listed in the lower part of Table 5-8a. In Zone C for example, this length is 11.30 inches for the $1.4 \cdot \Delta P_{SLB}$ performance criterion which corresponds to a pullout force of 1406.21 lbs in the cold leg. The minimum contact length needed to meet the pullout force requirement of 1455.65 lbs for the Faulted (FLB) is shown in 5-9a and Table 5-10a. The H* calculations for each loading condition at each of the radii considered are summarized in Table 5-11a. The H* results for each zone are summarized in Table 5-12a. The bounding condition for the determination of the H* length for the cold leg is the normal operating condition performance criterion.

The limiting loading condition and the corresponding force required to resist pullout used to establish the H* distances (Hot Leg Only) included in Table 5-6 through Table 5-10 are summarized below:

Plant Condition	Axial End Cap Force Due to Pressure Differential Across Tubesheet (Lbf)	Limiting Loading Condition	Force Required to Resist Pullout (Lbf)
Normal Operation (T_{hot} = 603.8°F)	523.41	3 ΔP_{NOp}	1570.22
Normal Operation (T_{hot} = 620.0°F)	513.60	3 ΔP_{NOp}	1540.79
Steam Line Break	1004.44	1.4 ΔP_{SLB}	1406.21
Feed Line Break	1039.75	1.4 ΔP_{FLB}	1455.65

The H* distances and the limiting loading conditions for the Vogtle Unit 1 and 2 SGs for Zones A-D are identified in Table 5-11 and 5-11a (H* distances) and Table 5-12 and 5-12a (limiting loading conditions) for the hot and cold leg of the tube bundles.

5.4 REVIEW OF COMPRESSIVE FAILURE SUSCEPTIBILITY

Reviews have demonstrated that it is not possible for a SG tube with an intact cross section to compressively fail due to the applied pressures calculated in the H* and B* analysis. Additional technical material to support this conclusion with respect to VEGP is provided in Appendix A, Response to Wolf Creek NRC RAI Question 5.

5.5 REVIEW FOR TUBE-TO-TUBESHEET SUSCEPTIBILITY TO TUBE SLIPPAGE

The impacts to the tube-to-tubesheet joint due to tube slippage are addressed in Appendix A, Response to Wolf Creek NRC RAI Question 8 and Question 9.

Table 5-1 Summary of Material Properties Alloy 600 Tube Material

Property	Temperature (°F)						
	70	200	300	400	500	600	700
Young's Modulus ($psi \cdot 10^6$)	31.00	30.20	29.90	29.50	29.00	28.70	28.20
Thermal Expansion ($in/in/°F \cdot 10^{-6}$)	6.90	7.20	7.40	7.57	7.70	7.82	7.94
Density ($lb\text{-}sec^2/in^4 \cdot 10^{-4}$)	7.94	7.92	7.90	7.89	7.87	7.85	7.83
Thermal Conductivity ($Btu/sec\text{-}in\text{-}°F \cdot 10^{-4}$)	2.01	2.11	2.22	2.34	2.45	2.57	2.68
Specific Heat ($Btu\text{-}in/lb\text{-}sec^2\text{-}°F$)	41.2	42.6	43.9	44.9	45.6	47.0	47.9

Table 5-2 Summary of Material Properties for SA-508 Class 2a Tubesheet Material

Property	Temperature (°F)						
	70	200	300	400	500	600	700
Young's Modulus ($psi \cdot 10^6$)	29.20	28.50	28.00	27.40	27.00	26.40	25.30
Thermal Expansion ($in/in/°F \cdot 10^{-6}$)	6.50	6.67	6.87	7.07	7.25	7.42	7.59
Density ($lb\text{-}sec^2/in^4 \cdot 10^{-4}$)	7.32	7.30	7.29	7.27	7.26	7.24	7.22
Thermal Conductivity ($Btu/sec\text{-}in\text{-}°F \cdot 10^{-4}$)	5.49	5.56	5.53	5.46	5.35	5.19	5.02
Specific Heat ($Btu\text{-}in/lb\text{-}sec^2\text{-}°F$)	41.9	44.5	46.8	48.8	50.8	52.8	55.1

Table 5-3 Summary of Material Properties SA-533 Grade A Class 2 Shell Material

Property	Temperature (°F)						
	70	200	300	400	500	600	700
Young's Modulus ($psi \cdot 10^6$)	29.20	28.50	28.00	27.40	27.00	26.40	25.30
Thermal Expansion ($in/in/°F \cdot 10^{-6}$)	7.06	7.25	7.43	7.58	7.70	7.83	7.94
Density ($lb\text{-}sec^2/in^4 \cdot 10^{-4}$)	7.32	7.30	7.283	7.265	7.248	7.23	7.211

Table 5-4 Summary of Material Properties SA-216 Grade WCC Channel Head Material							
Property	**Temperature (°F)**						
	70	**200**	**300**	**400**	**500**	**600**	**700**
Young's Modulus ($psi \cdot 10^6$)	29.50	28.80	28.30	27.70	27.30	26.70	25.50
Thermal Expansion ($in/in/°F \cdot 10^{-6}$)	5.53	5.89	6.26	6.61	6.91	7.17	7.41
Density ($lb\text{-}sec^2/in^4 \cdot 10^{-4}$)	7.32	7.30	7.29	7.27	7.26	7.24	7.22

HOT LEG RESULTS

Table 5-5 Tube/Tubesheet Maximum & Minimum Contact Pressures and H* Depths for Vogtle 1 & 2 Steam Generators

a,c,e

Table 5-6 Cumulative Forces Resisting Pull Out from the TTS Vogtle 1 & 2 Hot Leg Normal Conditions –T_{hot} = 603.8°F, P_{sec} = 901 psig, DP Factor = 0.64

a,c,e

Table 5-7 Cumulative Forces Resisting Pull Out from the TTS Vogtle 1 & 2 Hot Leg Normal Conditions – T_{hot} = 620°F, P_{sec} = 926 psig , DP Factor = 0.64

a,c,e

Table 5-8 Cumulative Forces Resisting Pull Out from the TTS Vogtle 1 & 2 Hot Leg Faulted (SLB) Conditions, P_{sec} = 0 psig, DP Factor = 0.64

a,c,e

Table 5-9 Cumulative Forces Resisting Pull Out from the TTS Vogtle 1 & 2 Hot Leg FLB Conditions, T_{hot} = 603.8°F, DP Factor = 0.64

a,c,e

Table 5-10 Cumulative Forces Resisting Pull Out from the TTS Vogtle 1 & 2 Hot Leg FLB Conditions, T_{hot} = 620°F, DP Factor = 0.64

a,c,e

Table 5-11 Summary of H* Calculations for Vogtle 1 & 2 (Hot Leg)

a,c,e

Table 5-12 H* Summary Table Structural Criteria Required Engagement

Zone	Limiting Hot Leg Loading Condition	Engagement from TTS (inches)
		Hot Leg

a,c,e

COLD LEG RESULTS

Table 5-5a Tube/Tubesheet Maximum & Minimum Contact Pressures and H* Depths for Vogtle 1 & 2 Steam Generators a,c,e

Table 5-6a Cumulative Forces Resisting Pull Out from the TTS Vogtle 1 & 2 Cold Leg Normal Conditions – T_{hot} = 603.8°F, P_{sec} = 901 psig, DP Factor = 0.64

a,c,e

Table 5-7a Cumulative Forces Resisting Pull Out from the TTS Vogtle 1 & 2 Cold Leg Normal Conditions – T_{hot} = 620°F, P_{sec} = 926 psig ; DP Factor =0.64

a,c,e

Table 5-8a Cumulative Forces Resisting Pull Out from the TTS Vogtle 1 & 2 Cold Leg Faulted (SLB) Conditions, $P_{sec} = 0$ psig

a,c,e

Table 5-9a Cumulative Forces Resisting Pull Out from the TTS Vogtle 1 & 2 Cold Leg FLB Conditions, T_{hot} = 603.8°F, DP Factor = 0.64

a,c,e

Table 5-10a Cumulative Forces Resisting Pull Out from the TTS Vogtle 1 & 2 Cold Leg FLB Conditions, T_{hot} = 620°F; DP Factor = 0.64

a,c,e

Table 5-11a Summary of H* Calculations for Vogtle 1 & 2

a,c,e

Table 5-12a H* Summary Table Structural Criteria Required Engagement

Zone	Limiting Cold Leg Loading Condition	Engagement from TTS (inches)
		Cold Leg

a,c,e

a,c,e

Figure 5-1 Definition of H* Zones
(Zone D is the most inboard and Zone A the most outboard)

a,c,e

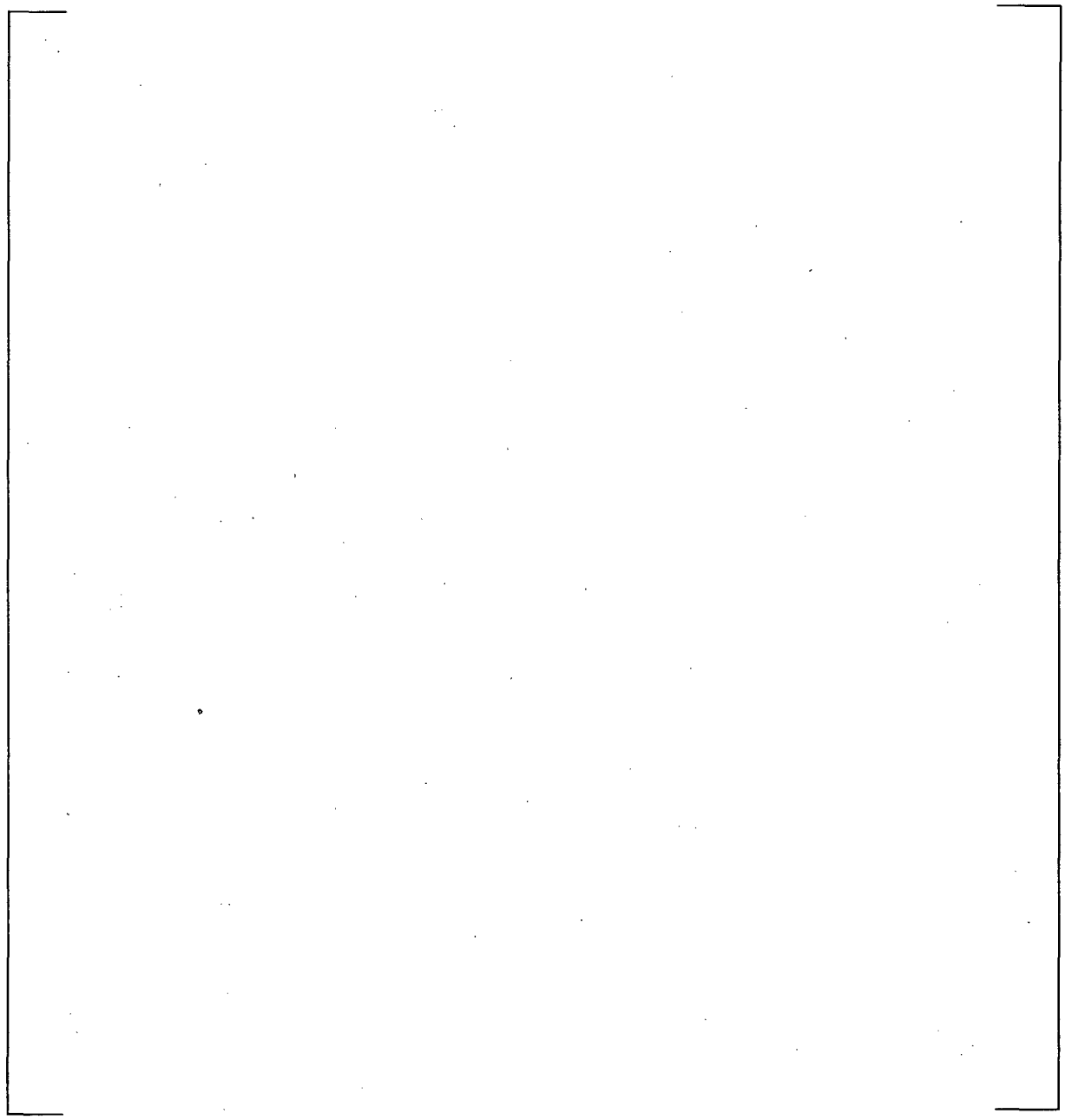

Figure 5-2 Finite Element Model of Model F Tubesheet Region

HOT LEG RESULTS

a,c,e

Figure 5-3 Contact Pressures for NOp at Vogtle 1 & 2, T_{hot} = 603.8°F, P_{sec} = 901 psig

a,c,e

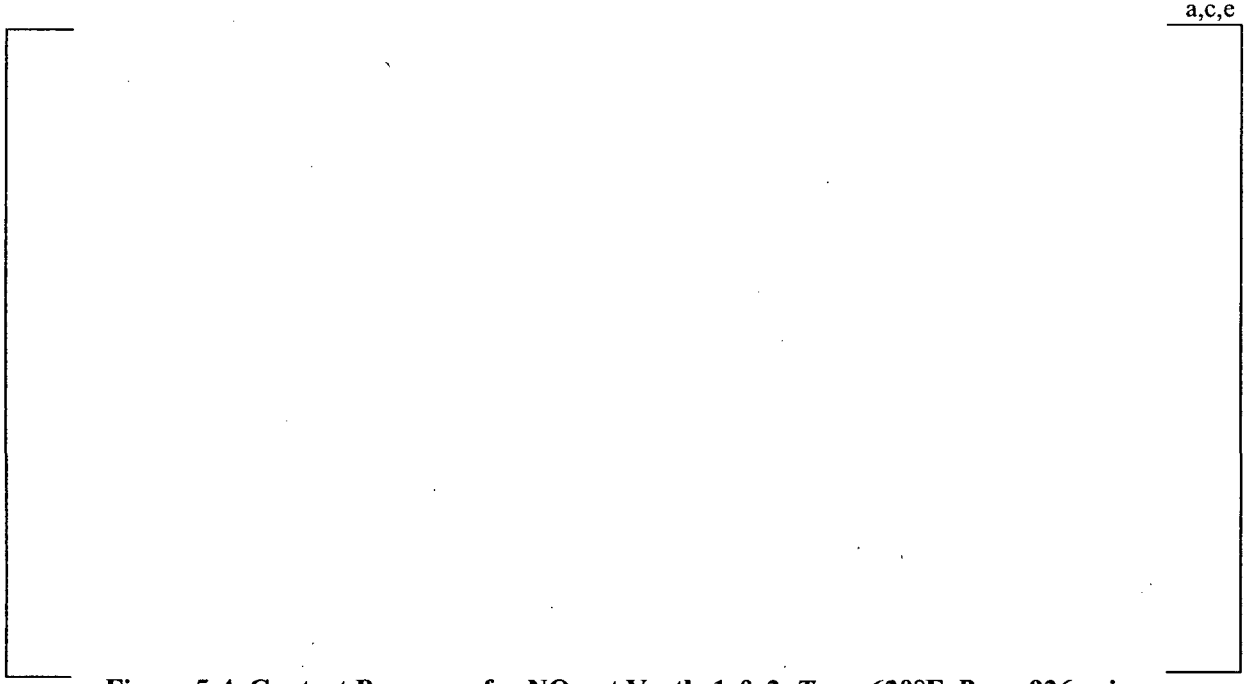

Figure 5-4 Contact Pressures for NOp at Vogtle 1 & 2, T_{hot} = 620°F, P_{sec} = 926 psig

a,c,e

Figure 5-5 Contact Pressures for SLB Faulted Condition at Vogtle 1 & 2

a,c,e

Figure 5-6 Contact Pressures for FLB Condition at Vogtle 1 & 2, T_{hot} = 603.8°F

a,c,e

Figure 5-7 Contact Pressures for FLB Condition at Vogtle 1 & 2, T_{hot} = 620°F

a,c,e

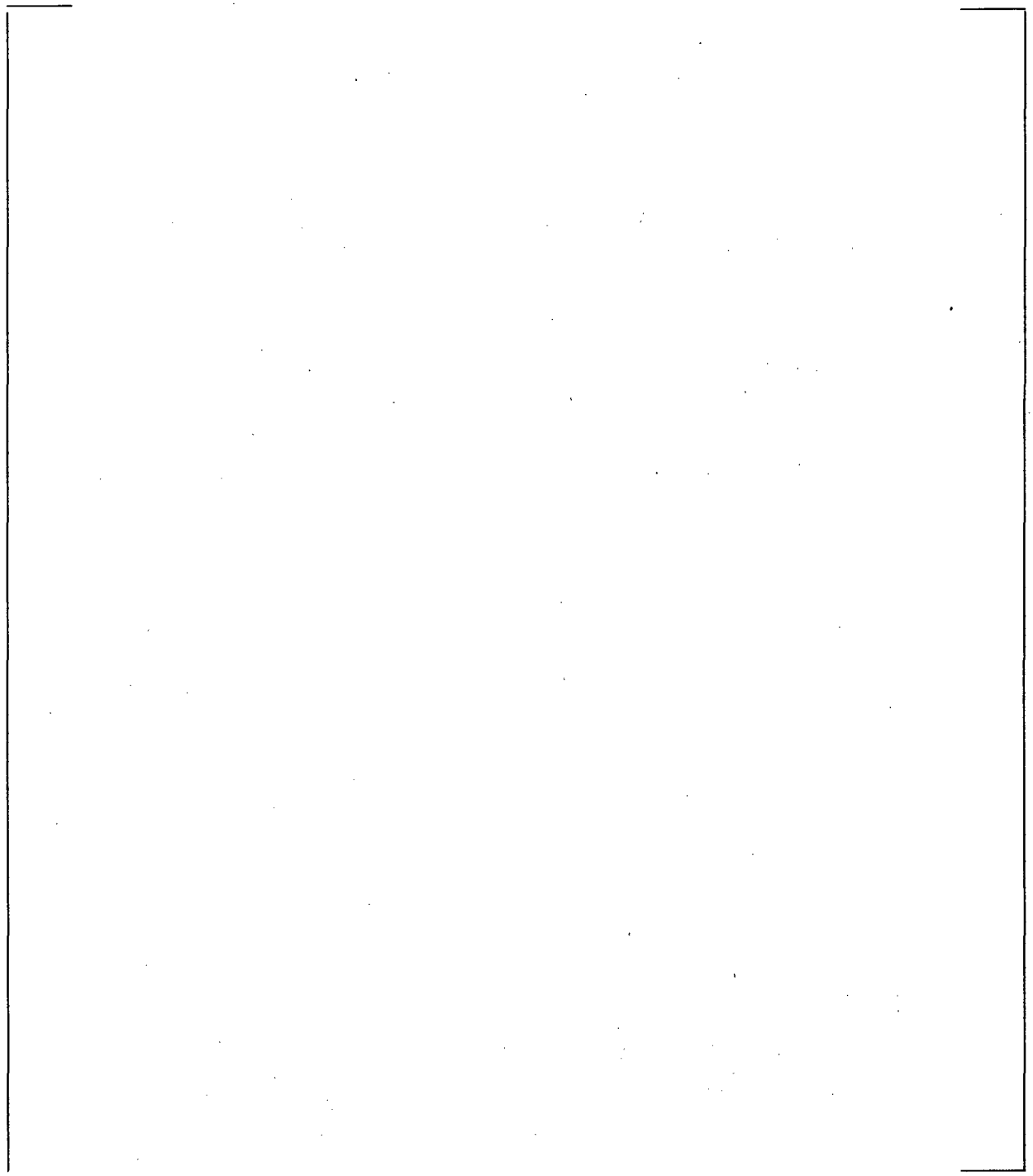

Figure 5-8 Sketch of Divider Plate, Channel Head and Tubesheet with Potential Cracking Areas Highlighted

COLD LEG RESULTS

a,c,e

Figure 5-3a Contact Pressures for NOp at Vogtle 1 & 2, T_{hot} = 603.8°F, P_{sec} = 901 psig

a,c,e

Figure 5-4a Contact Pressures for NOp at Vogtle 1 & 2, T_{hot} = 620°F, P_{sec} = 926 psig

a.c.e

Figure 5-5a Contact Pressures for SLB Faulted Condition at Vogtle 1 & 2

a.c.e

Figure 5-6a Contact Pressures for FLB Condition at Vogtle 1 & 2, T_{hot} = 603.8°F

a,c,e

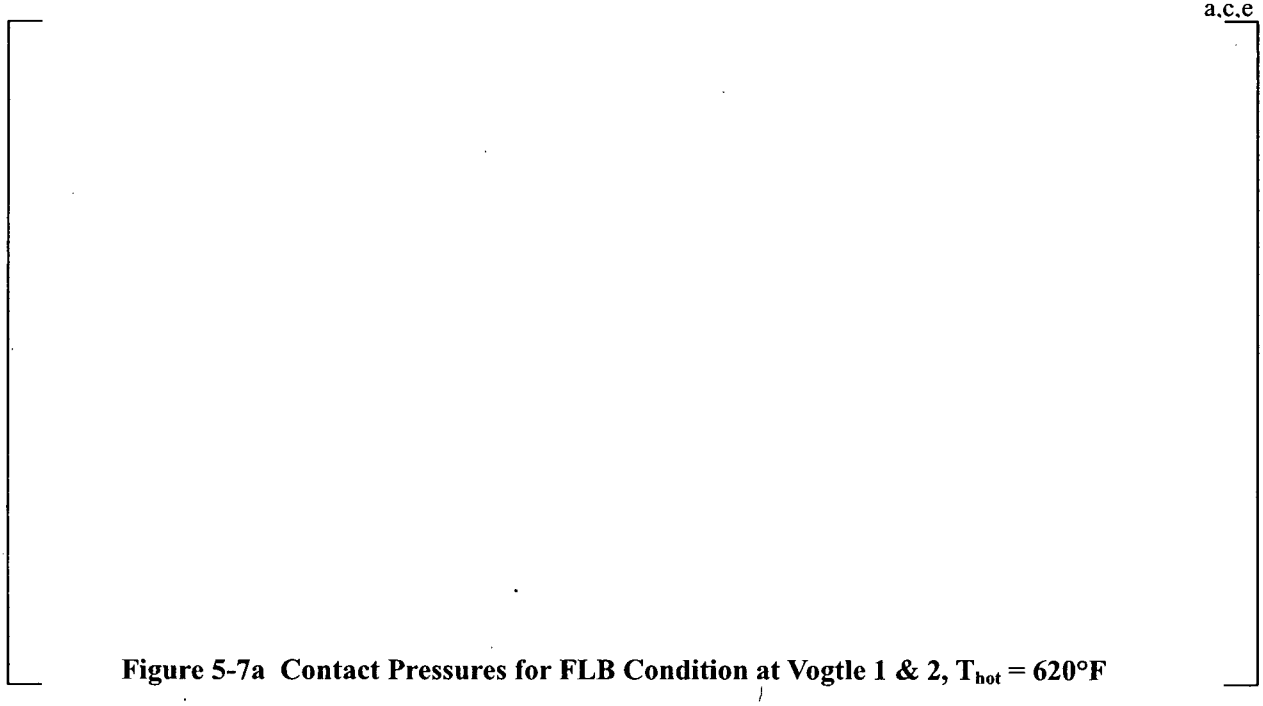

Figure 5-7a Contact Pressures for FLB Condition at Vogtle 1 & 2, T_{hot} = 620°F

6 LEAK RATE ANALYSIS OF CRACKED TUBE-TO-TUBESHEET JOINTS

This section of the report presents a discussion of the leak rate expectations from axial and circumferential cracking confined to the tube-to-tubesheet joint region, including the tack expansion region, the tube-to-tubesheet welds and areas where degradation could potentially occur, due to bulges and overexpansions. Although the welds are not part of the tube per the technical specifications, consideration is given in deference to the discussions of the NRC staff in Information Notice 2005-09 and Generic Letter 2004-01, and References 2 and 6, respectively. It is noted that the methods discussed below support a permanent change to the Vogtle 1 & 2 Technical Specification to require inspection and plugging of the top 17 inches, and exclude the bottom of the tubes on the HL side. With regard to the inherent conservatism embodied in the application of any predictive methods it is noted that the presence of cracking was not confirmed because removal of a tube section was not performed at Catawba 2 or Vogtle 1.

6.1 THE BELLWETHER PRINCIPLE FOR NORMAL OPERATION TO STEAM LINE BREAK LEAK RATES

From an engineering expectation standpoint, if there is no meaningful primary-to-secondary leakage during normal operation, there should likewise be no meaningful leakage during postulated accident conditions from indications located approximately below the mid-plane of the tubesheet. The rationale for this is based on consideration of the deflection of the tubesheet with attendant dilation and diminution (expansion and contraction) of the tubesheet holes. In effect, the leakage flow area depends on the contact pressure between the tube and tubesheet and would be expected to decrease during postulated accident conditions below some distance from the top of the tubesheet. The primary-to-secondary pressure difference during normal operation is on the order of 1200 to 1400 psi, while during a postulated accident, e.g., steam line and feed line break, is on the order of 2560 to 2650 psi.[4] Above the neutral plane of the tubesheet the tube holes tend to experience a dilation due to pressure-induced bow of the tubesheet. This means that the contact pressure between the tubes and the tubesheet would diminish above the neutral plane in the central region of the tubesheet at the same time as the driving potential would increase. Therefore, if there was leakage through the tube-to-tubesheet crevice during normal operation from a through-wall tube indication, that leak rate could be expected to increase during postulated accident conditions.

As noted, the tube holes diminish in size below the neutral plane of the tubesheet because of the upward bending and the contact pressure between the tube and the tubesheet increases. When the differential pressure increases during a postulated faulted event, the increased bow of the tubesheet leads to an increase in the tube-to-tubesheet contact pressure, increasing the resistance to flow. Thus, while the dilation of the tube holes above the neutral plane of the tubesheet presents additional analytical problems in estimating the leak rate for indications above the neutral plane, the diminution of the holes below the neutral plane presents definitive statements to be made with regard to the trend of the leak rate, hence, the

4 The differential pressure could be on the order of 2405 psi if it is demonstrated that the power operated relief valves will be functional.

bellwether principle. Independent consideration of the effect of the tube-to-tubesheet contact pressure leads to similar conclusions with regard to the opening area of the cracks in the tubes, thus further restricting the leak rate beyond that through the interface between the tube and the tubesheet.

The concept of normal operation being a bellwether for the postulated accident leak rate for indications above the neutral plane of the tubesheet is supported by a complex model of the leak rate phenomenon. This is not necessarily the case for cracks considered to be present below the neutral plane of the tubesheet because a diminution of the holes takes place during postulated accident conditions below the neutral plane relative to normal operation. For example, for the hot leg at a radius of a little more than 30.19 inches from the center of the SG and 10.5 inches from the TTS, the contact pressure during normal operation is calculated to be about 312.34 to 361.78 psi[5], (see the second contact pressure column in Table 5-6 and Table 5-7, respectively), while the contact pressure during a postulated SLB would be on the order of 747.08 psi, Table 5-8, and during a postulated FLB would be on the order of 966.99 to 1017.82 psi at the neutral plane of the tubesheet, Table 5-9 and Table 5-10, respectively.

Note: The radii specified in the heading of the tables are the maximum values for the respective zones analyzed, hence the contact pressures in the center column correspond to the radius specified for the left column, etc. The far left column lists the contact pressure values for a radius of 4.02 inches, but is used to a radius of 12 inches, etc. Also, the values tabulated do not include the calculated residual preload from the tube installation, which is not necessary for this comparison.

The analytical model for the flow through the crevice, the Darcy equation for flow through porous media, indicates that flow would be expected to be proportional to the differential pressure. Thus, a doubling of the leak rate could be predicted if the change in contact pressure between the tube and the tubesheet were ignored. Examination of the correlation on Figure 7-19 (for the combined Model F and Model D5 data) indicates that the crevice resistance to flow per unit length (the loss coefficient) would increase during a postulated SLB event.

The leak rate from a crack located within the tubesheet is governed by the crack opening area, the resistance to flow through the crack, and the resistance to flow provided by the tube-to-tubesheet joint. The path through the tube-to-tubesheet joint is also frequently referred to as a crevice, but is not to be confused with the crevice left at the top of the tubesheet from the expansion process. The presence of the joint makes the flow from cracks within the tubesheet much different from the flow to be expected from cracks outside of the tubesheet. The tubesheet prevents outward deflection of the flanks of cracks. This is a more significant effect for axial than for circumferential cracks, and is a significant contributor to the opening area presented to the flow. The restriction provided by the tubesheet greatly restrains crack opening in the direction perpendicular to the flanks regardless of the orientation of the cracks. The net effect is a large, almost complete restriction of the leak rate when the tube cracks are within the tubesheet.

The leak path through the crack and the crevice is tortuous. The flow must go through many turns within the crack in order to pass through the tube wall, even though the tube wall thickness is relatively small. The flow within the crevice must constantly change direction in order to follow a path that is formed

5 The column headed 48.61 inches includes the range of $30.19 < R \leq 48.61$ inches.

between the points of hard contact between the tube and the tubesheet as a result of the differential thermal expansion and the internal pressure in the tube. It is likely that there is both mechanical dispersion and molecular diffusion taking place. The net result is that the flow is best described as primary-to-secondary weepage. At its base, the expression used to predict the leak rate from tube cracks through the tube-to-tubesheet crevice is the Darcy expression for flow rate, Q, through porous media, i.e.,

$$Q = \frac{1}{K \mu} \frac{dP}{dz} \tag{6-1}$$

where μ is the viscosity of the fluid, P is the driving pressure, z is the physical dimension in the direction of the flow, and K is the "loss coefficient" which can also be termed the flow resistance if the other terms are taken together as the driving potential. The loss coefficient is found from a series of experimental tests involving the geometry of the particular tube-to-tubesheet crevice being analyzed, including factors such as surface finish, and then applied to the cracked tube situation.

If the leak rate during normal operation was 0.05 gpm (about 75 gpd), the postulated accident condition leak rate would be on the order of 0.1 gpm if only the change in differential pressure were considered; however, the estimate would be reduced if the increase in contact pressure between the tube and the tubesheet were to be included during a postulated steam line break event. An examination of the contact pressures as a function of depth in the tubesheet from the analyses of the tubesheet as reported in Table 5-6 through Table 5-10 shows that the bellwether principle applies to a significant extent to all indications below the neutral plane of the tubesheet, and may apply to somewhat higher elevations (Reference 33). At the central plane of the tubesheet (hot leg), the increase in contact pressure shown on Figure 6-4 is more on the order of 400 psi relative to that during NOp for all tubes regardless of radius. Still, the fact that the contact pressure increases means that the SLB leak rate would be expected to be bounded by no more than a factor of two relative to normal operation. The flow resistance would be expected to increase at a rate greater than that of the contact pressure (see Section 7.2 for further explanation) and the increase in driving pressure would be mostly offset by the increase in the resistance of the joint.

The numerical results from the finite element analyses are presented on Figure 6-1 at the bottom of the tubesheet (Reference 33). Background information on the finite element model is provided in Appendix A, Response to Wolf Creek NRC RAI 16. A comparison of the contact pressure during postulated SLB conditions relative to that during NOp is also provided for depths of 16.9, 12.6, 10.5, 8.25, and 6.0 inches below the top of the tubesheet (hot leg). The observations are discussed in what follows:

- Near the bottom of the tubesheet, Figure 6-1, the contact pressure increases by 1500 psi near the center of the tubesheet, exhibits no change at a radius of about 56 inches, and diminishes by 250 psi at the extreme periphery, a little less than 60 inches from the center.

- At 16.9 inches below the top of the tubesheet (about 4.13 inches from the bottom of the tubesheet) the contact pressure increases by about 1100 psi at the center to a minimum of about 300 psi at a radius of 56 inches, Figure 6-2. The contact pressure during a SLB is everywhere greater than that during NOp. The influence of the channel head and shell at the periphery causes the deformation to become non-uniform near the periphery.

- At a depth of 12.6 inches, the contact pressure increase ranges from a maximum of 700 psi near the center of the tubesheet to 500 psi at a radius of almost 55 inches as shown on Figure 6-3.

- At roughly the neutral surface, about 10.5 inches, Figure 6-4, the contact pressure during SLB is uniformly greater than that during normal operation by about 400 psi.

- At a depth of 8.25 inches from the TTS, Figure 6-5, the contact pressure increases by about 200 psi near the center of the TS to a maximum increase of 400 psi near the periphery.

- At a depth of about 6 inches from the TTS, Figure 6-6, the contact pressure is nearly equivalent at the center of the TS and increases by 400 psi near the periphery.

With respect to assessing potential SLB leakage from the tubesheet region below 17 inches below the top of the tubesheet, the absolute value of the contact pressure is not as important as the change in contact pressure because the parameter of interest in applying the B* criteria is the relative leak rate between NOp and SLB conditions. The analysis results indicate that there is an axial location within the tubesheet as a function of radius from the center where the contact pressure is invariant between NOp and SLB. The analysis results discussed in the next section include a plot of the invariant elevation for the Vogtle 1 & 2 SGs (Figure 7-11). The elevation of the invariant contact pressure would decrease near the TTS in the central region. Thus, it would not be sufficient to simply use an arbitrary depth value and suppose that the leak rate would be relatively unchanged even if the pressure potential difference were the same without further analysis. However, the fact that the contact pressure generally increases below that elevation indicates that the leak rate would be relatively unaffected for indications a little deeper into the tubesheet.

The leak rate from any indication is determined by the total resistance of the crevice from the elevation of the indication to the top of the tubesheet in series with the resistance of the crack itself, which is also expected to increase with contact pressure (the effect of hoop compression on axial cracks would overwhelm the effect of the fluid pressure on the flanks). A comparison of the curves on Figure 6-5 relative to those on Figure 6-4 indicates that the contact pressure increases during a postulated SLB for a length of at least 2.25 inches upward from the neutral plane for all tubes.

The trend is consistent at radii where the contact pressure decreases, or the increase is not as great near the bottom of the tubesheet. The increase at higher elevations would be expected to compensate. For example, the contact pressures on Figure 6-1 near the bottom of the tubesheet show a decrease beyond a radius of 56 inches; however, the increase at 8.4 inches above the bottom, Figure 6-2 is significant. For the outboard tubes, the increase in contact pressure extends all the way to the top of the tubesheet.

A comparison of the curves at the various elevations leads to the conclusion that for a length of 9 inches upward from an elevation of about 4.1 inches from the bottom of the tubesheet, there is always an increase in the contact pressure when going from normal operation conditions to postulated SLB conditions.

Noting that the density of the number of tubes populating the tubesheet increases with the square of the radius, the number of tubes for which the contact pressure is greater during a SLB than during NOp at the

H* depth from the TTS is far greater than the number for which the contact pressure decreases, i.e., 96% of the tubes are at a radius greater than 12 inches from the center of the tubesheet.

The cold leg results are presented in Figures 6-1a through 6-6a.

6.2 LIGAMENT TEARING DISCUSSION

6.2.1 Circumferential Cracking Discussion

One of the concerns that must be addressed in dealing with cracks in SG tubes is the potential for ligament tearing to occur during a postulated accident when the differential pressure is significantly greater than during normal operation. While this is accounted for in the strength evaluations that demonstrate a resistance to pullout in excess of $3 \cdot \Delta P$ for normal operation and $1.4 \cdot \Delta P$ for postulated accident conditions, the potential for ligament tearing to significantly affect the leak rate predictions needs to be accounted for.

Ligament tearing considerations for circumferential tube cracks that are located below the H* depths within the tubesheet are significantly different from those for potential cracks at other locations. The reason for this is that H* has been determined using a factor of safety of three relative to the normal operating pressure differential and 1.4 relative to the most severe accident condition pressure differential. Therefore, the internal pressure end-cap loads which normally lead to an axial stress in the tube are not transmitted below about 1/3 of the H* depth. This means that the only source of stress acting to extend the crack is the primary pressure acting on the flanks of the crack. Since the tube is captured within the tubesheet, there are additional forces acting to resist the opening of the crack. The contact pressure between the tube and tubesheet results in a friction-induced shear stress acting opposite to the direction of the crack opening. Moreover, the pressure on the flanks is compressive on the tube material adjacent to the plane of the crack, hence a Poisson's ratio radial expansion of the tube wall in the immediate vicinity of the crack plane is induced, increasing the contact pressure and also acting to restrain the opening of the crack. In addition, the differential thermal expansion of the tube is greater than that of the carbon steel tubesheet, thereby inducing a compressive stress in the tube below the H* length.

A scoping evaluation of the [

]^{a,c,e}

[

]^{a,c,e}

In summary, considering the worst-case scenario, the likelihood of ligament tearing from radial circumferential cracks resulting from an accident pressure increase is small since at most, only 9% of the cross-sectional area is needed to maintain tube integrity. Also, since the crack face area will be less than the total cross-sectional area used above, the difference in the force applied as a result of normal operating and accident condition pressures will be less than the 35 lbs associated with the above numbers. Therefore, the potential for ligament tearing is considered to be a secondary effect of essentially negligible probability and should not affect the results and conclusions reported for the H* evaluation. The leak rate model does not include provisions for predicting ligament tearing and subsequent leakage, and increasing the complexity of the model to attempt to account for ligament tearing has been demonstrated to be not necessary (Reference 27).

6.2.2 Axial Cracking Discussion

Axial ligament tearing may occur during a postulated accident when the differential pressure across the tube wall is significantly greater than during normal operation. Ligament tearing is accounted for in the strength evaluations that demonstrate a resistance to pullout in excess of 3.ΔP for normal operation and 1.4.ΔP for postulated accident conditions.

The tube area required to resist tearing due to an axially oriented crack can be calculated using traditional mechanics. It is conservative, in this case, to neglect the forces that would act to keep a crack closed and compress the flanks in the ligament so that tensile tearing would become unlikely. This includes the far field axial stress on the tube cross-section generated by internal pressure end-cap loads which would act to close the ligament and any cracks above the H* depth. The axial orientation of the damage in the tube means that the required area of the tube cross-section to resist tearing and damage should be based on the local strength of the material around the crack. This is in contrast to the typical method used to compare what percent of the area is required to resist ligament tearing in circumferentially damaged tubes based on the amount of force applied to the damaged tube cross-section.

The allowable ratio of the applied stress on a tube cross-section to the limiting stress the tube cross section can support may be defined as:

$$n = \sigma_{APPLIED} / \sigma_{LIMIT} \quad (1)$$

where $\sigma_{APPLIED}$ is the stress applied to the cross-section under either the normal operating condition or a steam line break and σ_{LIMIT} is either the ASME code minimum tensile yield stress of the tube material (used to predict yield in the ligament) or the ASME code minimum ultimate tensile strength of the tube (used to predict rupture and tearing of the ligament). The significant properties of the tube cross section are defined as:

$$A_{INITIAL} = \pi\left(r_o^2 - r_i^2\right) \tag{2}$$

$$A_{MIN} = \pi\left(r_o^2 - r_{\min,i}^2\right) \tag{3}$$

$$t = r_o - r_i \tag{4}$$

$$R_M = \frac{r_o + r_i}{2} \tag{5}$$

where $A_{INITIAL}$ is the cross sectional area of the tube in the undamaged state, A_{MIN} is the minimum cross sectional area required to resist ligament tearing, t is the thickness of the tube wall, R_M is the mean radius of the tube, r_o is the outer radius, r_i is the initial inner tube radius and $r_{min,i}$ is the minimum inner radius of the tube in the damaged configuration that can still resist ligament tearing.

In the case of an axial crack, the largest local stress contributing to the damage in the tube is the hoop stress acting on the tube due to the internal pressure. The hoop stress acting on the tube cross section is calculated using the following relationship:

$$\sigma_{HOOP} = \frac{\mathrm{Pr}}{t} = \frac{PR_M}{t} = \frac{SP_{LIMIT}R_M}{t} \tag{6}$$

Where S is the given safety factor used in the analysis for conservatism and P_{LIMIT} is the limiting internal pressure that will initiate tearing in the tube. The limiting state in the tube material where the ligament will still hold occurs when the applied loading is equal to the allowable loading that the damaged cross section can bear, or when $n = 1$, as shown below.

$$n = 1 = \frac{\sigma_{APPLIED}}{\sigma_{LIMIT}} \rightarrow \sigma_{LIMIT} = \sigma_{APPLIED} \tag{7}$$

The applied stress can be written as:

$$\sigma_{APPLIED} = \frac{F_{LIMIT}}{A_{MIN}} \tag{8}$$

$$F_{LIMIT} = \sigma_{HOOP}A_{INITIAL} \tag{9}$$

where F_{LIMIT} is the force applied to the cross section by the limiting internal pressure. Substitution of Equations 7 and 9 into Equation 8, and rearranging to solve for A_{MIN}, gives:

$$\sigma_{LIMIT} = \frac{\sigma_{HOOP}}{A_{MIN}}A_{INITIAL}$$

$$\sigma_{LIMIT} A_{MIN} = \sigma_{HOOP} A_{INITIAL} \rightarrow A_{MIN} = \frac{\sigma_{HOOP} A_{INITIAL}}{\sigma_{LIMIT}} \tag{10}$$

Substitution of the definitions for t, R_M, σ_{HOOP} and $A_{INITIAL}$ into the equation for A_{MIN} yields

$$A_{MIN} = \left(\frac{r_o + r_i}{2}\right)\left(\frac{1}{r_o - r_i}\right)\frac{SP_{LIMIT}}{\sigma_{LIMIT}}\pi\left(r_o^2 - r_i^2\right) \tag{11}$$

Substitution of Equation 3 into 11 and using the difference of squares identity to rearrange and solve for the minimum inside radius in the damaged tube gives the final result.

a,c,e

[ ] (12)

The results shown in the table below were obtained using the ASME Code minimum material properties (Reference 27) and the physical parameters of the Model F steam generator tubes as stated in the "Thick Cylinder Equations Parameters" table provided at the end of Section 5.1.2.1. The results from Equation 12 were compared to the method used to calculate the required thickness to resist ligament tearing due to circumferential cracking (Reference 27) and the method described in the EPRI Tube Integrity Theory Manual (Reference 28) and Reference 29. [

]^{a,c,e}

a,c,e

[ ]

The results of the axial ligament tearing calculations detailed above are [

]^{a,c,e}

Considering the worst-case scenario, the likelihood of ligament tearing from axial cracks resulting from an accident pressure increase is [

]^{a,c,e} Therefore, the potential for axial ligament tearing is considered to be a secondary

effect of essentially negligible probability and should not affect the results and conclusions reported for the H* evaluation. The leak rate model does not include provisions for predicting ligament tearing and subsequent leakage. Increasing the complexity of the model to attempt to account for axial or circumferential ligament tearing is not considered necessary.

6.3 REVIEW FOR LEAK RATE SUSCEPTIBILITY TO TUBE SLIPPAGE

The impacts to the tube-to-tubesheet joint due to tube slippage are addressed in Appendix A, Response to Wolf Creek NRC RAI Question 8 and Question 9.

HOT LEG RESULTS

a,c,e

Figure 6-1 Change in Contact Pressure at 20.0 Inches Below the TTS

a,c,e

Figure 6-2 Change in Contact Pressure at 16.9 Inches Below the TTS

a,c,e

Figure 6-3 Change in Contact Pressure at 12.6 Inches Below the TTS

a,c,e

Figure 6-4 Change in Contact Pressure at 10.5 Inches Below the TTS

a,c,e

Figure 6-5 Change in Contact Pressure at 8.25 Inches Below the TTS

a,c,e

Figure 6-6 Change in Contact Pressure at 6.0 Inches Below the TTS

COLD LEG RESULTS

a,c,e

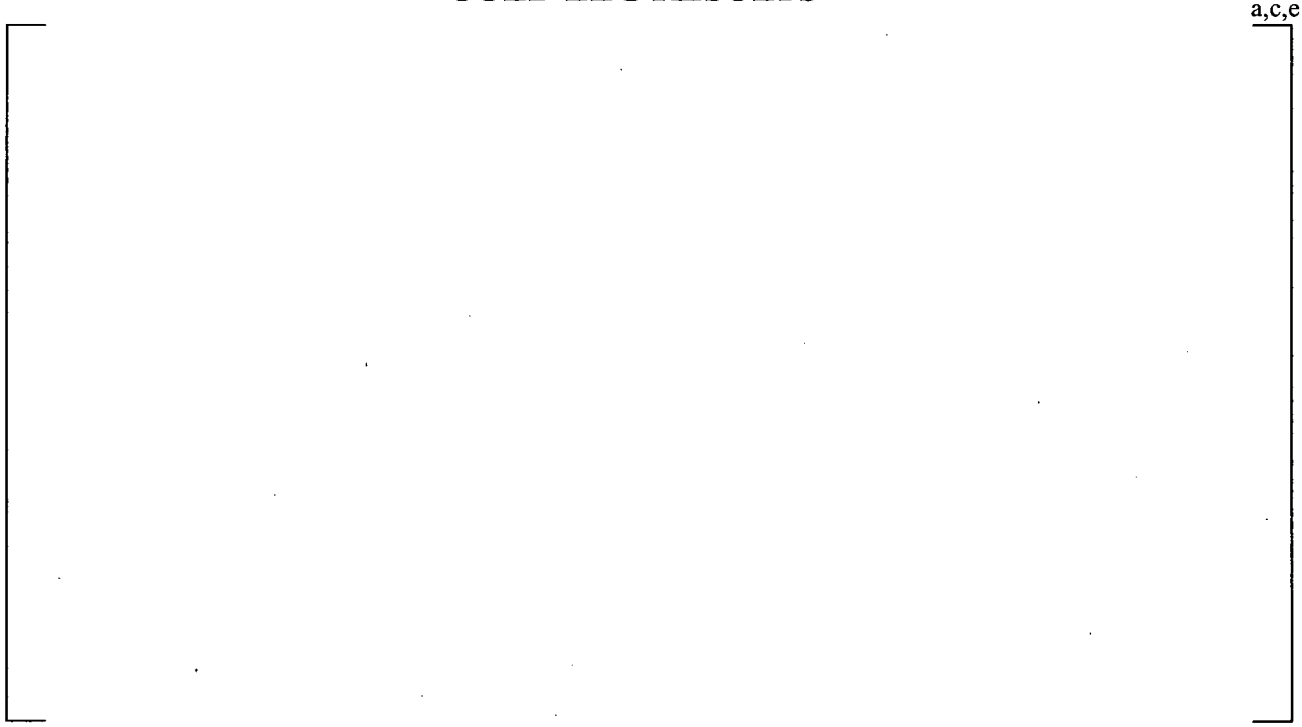

Figure 6-1a Change in Contact Pressure at 20.0 Inches Below the TTS

a,c,e

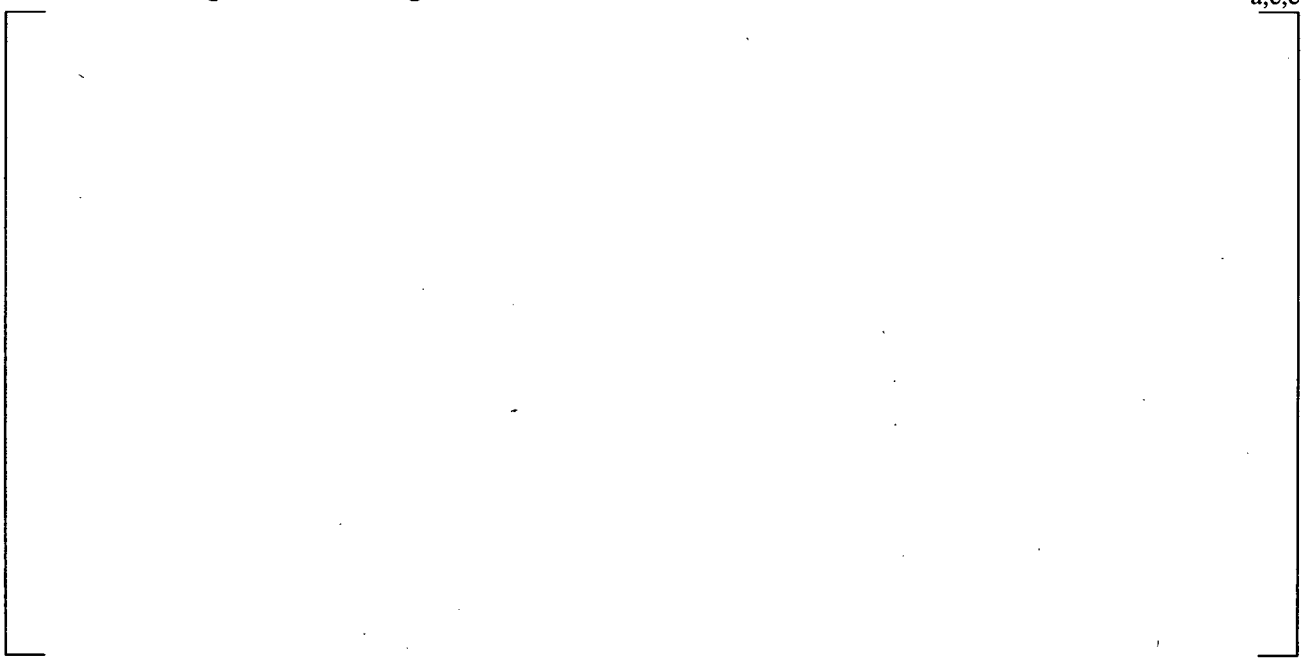

Figure 6-2a Change in Contact Pressure at 16.9 Inches Below the TTS

a,c,e

Figure 6-3a Change in Contact Pressure at 12.6 Inches Below the TTS

a,c,e

Figure 6-4a Change in Contact Pressure at 10.5 Inches Below the TTS

a,c,e

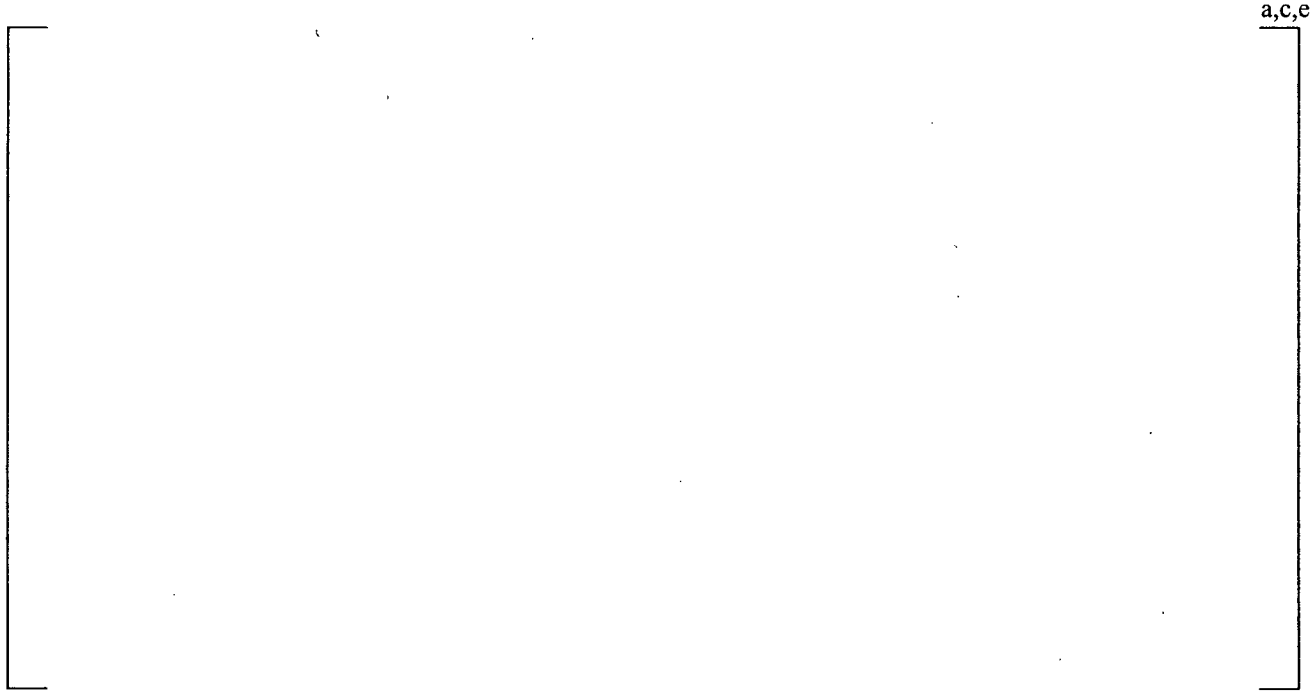

Figure 6-5a Change in Contact Pressure at 8.25 Inches Below the TTS

a,c,e

Figure 6-6a Change in Contact Pressure at 6.0 Inches Below the TTS

7 DETERMINATION OF THE B* DISTANCE

B* is the length of engagement in the tubesheet needed for the leak rate during a postulated steam line break (SLB) event to be bounded by a specified multiple of the leak rate during normal operation (NOp). The rationale for the determination of B* is that there are changes during a SLB relative to NOp that lead to the expectation of an increase in the leak rate and other changes that lead to the expectation of a higher resistance to leakage. The determination of B* is based on analyzing the contributing factors and making an estimate of the change in leak rate that would be expected. The factors that lead to an expectation of an increase in the leak rate are as follows:

1. An increase in the primary-to-secondary differential pressure induced force on the water inside a postulated tube crack and the tube-to-tubesheet interface.

2. A decrease in the tube-to-tubesheet contact pressure above the neutral plane of the tubesheet resulting from dilation of the tubesheet holes in response to an increase in the bending deformation from the primary-to-secondary pressure difference increase. This does not apply to the periphery of the tubesheet where the opposite effect occurs.

3. A decrease in the tube-to-tubesheet contact pressure associated with the higher coefficient of thermal expansion of the tube material relative to that of the tubesheet if the temperature of the tubesheet decreases.

The factors that lead to an expectation of a decrease in the leak rate are:

1. The increase in primary pressure within the tube expands the tube into tighter contact with the tubesheet, resulting in an increase of the resistance of the material interface to flow between the tube and the tubesheet.

2. An increase in the tube-to-tubesheet contact pressure below the neutral plane of the tubesheet resulting from diminution of the tubesheet holes in response to the increase in the bending deformation from the primary-to-secondary pressure difference increase. Again, the effect is opposite for most tubes on the periphery of the tubesheet.

3. An increase in the resistance to flow associated with an increase in the viscosity of the water in the crevice if the temperature of the tubesheet decreases.

The basis for the determination of B* is the consideration of each of the above effects using results from finite element analyses of the tubesheet (Reference 33) and results from leak rate testing of the tube-to-tubesheet interface. The analyses and testing are described Section 4 of this report. In summary, the leak rate is characterized by the Darcy equation for flow through a porous medium, an equation of the same form as the Hagen-Poiseuille equation for fully developed flow. The resistance to flow was developed from test data as a function of the contact pressure between the tube and the tubesheet in accord with expectations. The finite element analysis results provide calculated results for the contact pressure as a function of tube location and depth into the tubesheet based on the NOp and postulated SLB pressure and temperature conditions of the plant.

The following are discussed: background information giving a qualitative overview supporting the development of B*, flow through a crevice formulation, tube-to-tubesheet contact pressure variation, the determination of the B* distance, and conclusions regarding the B* values.

7.1 BACKGROUND INFORMATION

A natural question regarding the development and application of the B* criterion is whether or not numerical studies were performed to verify that the reduction in leak rate resistance above the neutral surface of the tubesheet associated with tubesheet bowing was adequately bounded by the increase in resistance below the neutral surface. The following discussion is intended to provide technical insight into the behavior of the leak rate from through-wall tube indications within the tubesheet by presenting:

1. the theoretical detail that is the basis for the observations from the test data and extrapolation of the test data for leak rate as function of joint length as expressed as the flow loss coefficient, and,

2. the explanation as to why the leak rate at normal operating conditions provides a bellwether for and can be used to establish a bounding value for the leak rate during steam line break conditions.

For most of the tube locations in the tubesheet, the bow is convex upwards (like a dome). Background information on the finite element model is provided in Appendix A, Response to Wolf Creek NRC RAI 16. The tube-to-tubesheet contact pressure is an increasing linear function of the depth from the top of the tubesheet, thus, for any specified location within the tubesheet the contact pressure increases below and decreases above that location. The resistance to leakage through the tube-to-tubesheet interface is an increasing function of the contact pressure between the tube and the tubesheet (see Figure 7-19). The bellwether principle is based on considering the leak rate during a postulated steam line break (SLB) event relative to that during normal operating conditions (NOp). The primary-to-secondary differential pressure during a SLB event is greater than that during NOp so that bowing of the tubesheet increases (see Figure 7-6) with an associated change in the slope of the contact pressure versus depth relation as a function of tube location (see Figure 7-7). For all tubes, except for the small percentage of tubes that are located on the periphery, the slope increases. For tubes on the periphery the slope increases in an absolute sense since there is an inflection point near the periphery. Regardless, the evaluation applies because increasing the contact pressure has a greater influence on the leak rate than decreasing the contact pressure. Supporting technical description regarding Figure 7-19 is provided in Appendix A, Response to Wolf Creek NRC RAI 11.

Numerical studies were not initially performed because the subject was considered to be adequately addressed based on a qualitative evaluation as follows:

1. In the limiting case of no dependence of the leak rate loss coefficient, i.e., the resistance per unit length, on the contact pressure, the leak rate during NOp and postulated SLB would be a function of the length of the crevice and pressure difference only. Using the Darcy equation, the leak rate is a direct function of the differential pressure and the inverse of the crevice length. Since the length remains the same and the driving pressure increases by a factor of about 2, that is, 1300 psi to 2560 psi, the leak rate change is bounded by a similar factor. Any other theoretical dependence of leak rate on pressure difference, e.g., the square root of the pressure difference via the

Bernoulli equation, results in a reduction of the bounding factor relative to the result obtained using the Darcy equation.

2. The test data have demonstrated that the resistance per unit length is a monotonically increasing, non-linear function of the contact pressure with a positive second derivative. The deflection of the TS in combination with the increase in internal pressure results in the change in the contact pressure being zero between NOp and SLB at some depth below the TTS that is above the neutral surface of the tubesheet. The net contact pressure decreases above and increases below that depth, which is a function of location within the tube bundle. Using this elevation as a reference, the increase in resistance per unit length below the zero-change location must always be more than the absolute value of the decrease in resistance per unit length above the zero-change elevation. Thus, the average resistance in going from NOp to SLB must increase and the average leak rate must decrease. This is independent of the individual leak rates involved and only depends on the trend. The latter observation is apparent by inspection of the figure relating loss coefficient to contact pressure in all submittals on the subject of leak rate through tube-to-tubesheet crevices, in this report for example. See Figure 7-19.

There are alternate approaches to proving the above statements from the observations regarding the leak rate from test specimens. The analysis in this report to determine the B* distance is inherently conservative due to the overestimate of the tubesheet deflection because the SG divider plate–to-stub runner weld is assumed to be non-functional.

7.2 FLOW THROUGH A CREVICE (DARCY'S EQUATION)

The equation that is solved for flow through a crevice is Darcy's model for flow through a porous media, that is, the volumetric flow, Q, is a function of the differential driving pressure, ΔP, and the respective inverse values of the viscosity, μ, the loss coefficient, K, and the length of the path, L, as,

$$Q = \frac{1}{\mu K}\frac{\Delta P}{L} \tag{7-1}$$

The driving pressure is based on the upstream minus the downstream values, else a negative sign would be needed in front of the equation. The viscosity is a function of the temperature and pressure of the fluid. The Darcy equation is also of the same form as the Hagen-Poiseuille flow equation for fully developed, laminar, axial flow in an annular gap, i.e.,

$$Q = \frac{1}{\mu\frac{6}{\pi R a^3}}\frac{\Delta P}{L} \tag{7-2}$$

Here, R is the average radius of the gap and α is a characteristic or effective gap dimension for the rough tube-to-tubesheet interface, expected to be very small, on the order of $4 \cdot 10^{-5}$ inch. Thus, the loss coefficient would be expected to be proportional to the inverse of the cube of the effective gap. The

Hagen-Poiseuille form of the leak rate equation gives insight into the relationship between the average resistance, characterized by the loss coefficient, K, and the contact pressure, i.e.,

$$K = \frac{6}{\pi R a^3} \quad (7\text{-}3)$$

If the characteristic gap were proportional to the contact pressure between the tube and the tubesheet, doubling the pressure would increase the leak resistance by a factor of 8, although this is not necessarily expected to be the case because of the complex nature of the interface. In addition, it would not be unexpected that a plot of the ln(K) versus the contact pressure would approximate a straight line. For the rough tube-to-tubesheet interface, the length of the tortuous path can also be considered to be characterized as being effective because the flow does not necessarily have a straight path to follow to the TTS (top of the tubesheet). Approximation of the path as the legs of an equilateral triangle would essentially double the distance traveled from the throughwall location to the TTS. Hence, the use of the loss coefficient integrates the accounting of the effective gap and effective length.

The electrical analogy for the flow considers Q as the current flow and ΔP as the potential, hence the quantity μKL is the resistance to flow, R. Since K is a function of the contact pressure, P_c, the resistance is a function of the location within the tubesheet. The total resistance can be found as the average value of the quantity μK, the resistance per unit length, multiplied by L, or by integrating the incremental resistance, $dR = \mu K\, dL$ over the length L, i.e.,

$$R = \mu \bar{K}\left(L_2 - L_1\right) = \int_{L_1}^{L_2} \mu K\, dL \quad (7\text{-}4)$$

where both μ and K could be functions of location L. The viscosity is a very weak function of the pressure of the water in the crevice and can be considered to be constant for a given plant condition with negligible error, Figure 7-13. However, the viscosity is a strong function of the temperature of the water in the crevice, Figure 7-14, and the tubesheet temperature for the condition being analyzed must be considered. A decrease in the temperature can lead to a significant increase in flow resistance.

7.3 TUBE-TO-TUBESHEET CONTACT PRESSURE VARIATION

Six tubesheet radial locations for which the contact pressure as a function of depth was determined were used in calculating the length of sound tubing below the TTS required to resist the NOp and SLB axial loads, i.e., the H* depth. The intercept, b_0, and slope, b_1, parameters for the calculation of the contact pressure as a function of length, L, into the tubesheet for the six radial locations are listed in Table 7-1. The relationships are always in linear first order form,

$$P_c = b_0 + b_1 L \quad (7\text{-}5)$$

where the coefficients b_0 and b_1 vary as a function of the radial location of the tube in the tubesheet. This is simply a consequence of the fact that in the linear elastic stress analysis, no yielding occurs. A comparison of the FEA results with first order, linear representations is provided on Figure 7-5 for NOp and SLB conditions at a radius of 34 inches from the center of the tubesheet.

Further calculations examined the relationship between the intercept and slope of the prediction equations as a function of tube location radius. It was found that second order polynomial expressions can be used to describe the parameters almost exactly, i.e., with negligible error. A plot of the operating contact pressures, which do not include the residual contact pressure from the hydraulic expansion process, is provided on Figure 7-6 for each location during NOp and Figure 7-7 provides similar information during the postulated SLB event. The polynomial coefficients that were used to determine the values of the intercept and slope, i.e., b_0 and b_1, for any given radius, R, from the center of the tubesheet for NOp conditions are illustrated on Figure 7-8. Here, the following relationships are depicted where the g and h values were determined from the regression analyses (recall that R in the following two equations represents radius),

Normal Operation

$$b_o = g_0 + g_1 R + g_2 R^2 \quad \text{(Intercept)}$$
$$b_1 = h_0 + h_1 R + h_2 R^2 \quad \text{(Slope)} \qquad (7\text{-}6)$$

The coefficients, u and v, of a similar set of expressions were calculated for determining the contact pressure at all locations within the tubesheet during a SLB event, i.e.,

SLB Conditions

$$b_o = u_0 + u_1 R + u_2 R^2 \quad \text{(Intercept)}$$
$$b_1 = v_0 + v_1 R + v_2 R^2 \quad \text{(Slope)} \qquad (7\text{-}7)$$

The polynomial coefficients that were used to determine the values of the intercept and slope for use in calculating the contact pressure during a SLB are illustrated on Figure 7-9. A comparison of the coefficients for the two conditions is provided on Figure 7-10.

7.4 DETERMINATION OF THE B* DISTANCE

A logarithmic-linear (log-linear) regression and an uncertainty analysis were performed for the combined Model D5 and Model F SG data. Figure 7-19 provides a plot of the loss coefficient versus contact pressure with the linear regression trendline for the combined data represented as a thick, solid line. The regression trendline is represented by the log-linear relation,

$$\ln(K) = b_0 + b_1 P_c \qquad (1)$$

where:

b_0 = the ln(K) intercept of the log-linear regression trendline, and,
b_1 = the slope of the log-linear regression trendline.
P_c = contact pressure

In conclusion, the log-linear fit to the Model D5 loss coefficient data follow a relation of the form,

$$K = e^{b_0 + b_1 P_c}, \tag{2}$$

where the absolute leak rates per se are not used in the determination of the 6.81 inch B* distance (hot leg) and the confidence curve on the chart is provided for information only. Since the 6.81 inch B* distance criteria is based on the ratio of the SLB leak rate to the NOp leak rate, it is not significantly sensitive to changes in the correlation slope or intercept.

Originally test results from Model F specimens that were not prepared to the test specifications (e.g., expansion pressures for the tubes were below [ ]^{a,c,e}) were removed from consideration. Whereas with the Model D data, test results that did not seem logical, such as a result of no leakage, were removed from consideration. The net effect on the data population of the Model F and Model D results was:

1. To decrease the variability of the Model D data and exclude the higher loss coefficient results.
2. To increase the variability of the Model F data and exclude the low loss coefficient results.

These test results have since been added back into the database. As a result, 7 additional data points were added back into the Model D5 test results and a total of 27 additional data points were added to the Model F database. The leak loss coefficients calculated for the zero leakage test results are based on an assumed detection threshold for measurement of leakage of 1 x 10^{-7} gpm. The flow constant used to generate the loss coefficients added to the database assumed that flashing occurred in the crevice in Figure 7-17.

See Figure 7-15 for a plot of the combined Model D and Model F total data set. In this context, the term "total" means that all available data for each type of specimen was used in the regression analysis (equations were not provided on Figure 7-16) and no test data were excluded. The test assumptions include: flashing in the crevice, no change in pressure differential calculations due to crevice pressure, the Model F results scaled to compare to Model D results on the basis of tube diameter and all contact pressures calculated using the same theory of elasticity model.

Figure 7-16 shows that the average loss coefficient for the Model D is an order of magnitude higher than the average loss coefficient for the Model F (when flashing is assumed in the crevice). The combined loss coefficient fit curve splits the difference between the Model F and Model D data.

When all of the data from both sets of experiments are included, and the contact pressures during the applied pressure differentials are re-calculated to reflect the results of the White Paper (Reference 21), the means of the regression fits of the two populations become very similar. Furthermore, the 95% confidence limit fit of the total set of the Model F and Model D data still results in a correlation between loss coefficient and contact pressure with a positive slope. See Figure 7-17 for a plot of the log normal linear regression model results using the total Model F and Model D data set and incorporating the results of the crevice pressure study reported in the White Paper (no flashing is assumed in the crevice). See Figure 7-18 for a plot of the 95% confidence limit log normal linear regression model results using the total Model F and Model D data set and incorporating the results of the crevice pressure study reported in the White Paper.

The Model F data is more variable than the Model D and skewed toward the upper end of the data population. The Model D data is less variable than the Model F and clustered around the lower end of the data population. The conclusions from the analysis of the combined data set still support a positive relationship between loss coefficient and contact pressure. Furthermore, using the most conservative loss coefficient versus contact pressure model, shown in Figure 7-18 as the 95% confidence limit fit of the combined data sets, does not change the conclusions of the B* analysis. Figure 7-19 shows the regression analysis results for the Model F and Model D5 data that is used in the development of the B* distances in this report.

The total set of available Model F and Model D data is used to create Figure 7-15 and Figure 7-19. The data used to generate Figure 7-15 is the same as the data used in Figure 7-19, however, different assumptions are used in each Figure. In Figure 7-15, the original analysis assumptions are used to develop the relationship between contact pressure and loss coefficient. The original assumptions include flashing in the crevice and the assumption of secondary side pressure in the crevice for the calculation of the pressure drop across the tube wall. The results shown in Figure 7-19 use different assumptions in the contact pressure and loss coefficient relationship in order to be consistent with the conclusions in Reference 21. The assumptions used in Figure 7-19 include: modifying the pressure in the crevice as a function of the applied primary side pressure, assuming no flashing in the crevice, and, calculating the contact pressure using the theory of elasticity model with the results of Reference 22.

The effect of considering no relationship, or a zero slope model, between contact pressure and loss coefficient was also considered in this analysis. Two constant loss coefficient values were compared in this analysis:

1. The lowest possible value from the 95% confidence fit of the Model D data, k = [ ]^{a,c,e}

2. The mean of the total combined Model D and Model F data set, assuming flashing in the crevice, k = [ ]^{a,c,e}

Assuming a constant value for the loss coefficient negates any benefit from loss coefficient data and forces the leak rate resistance to be calculated based on the effect of the tubesheet bow and potential flow area in the crevice. The net effect of assuming a constant loss coefficient value, and reduced contact pressure, is to increase the maximum B* depth by approximately 0.50 inch. If the lower loss coefficient value is assumed to be constant, then the maximum B* depth increases by slightly more than 0.50 inch. If the mean loss coefficient value is assumed to be constant, then the maximum B* depth increases by slightly less than 0.50 inch (Reference 30).

As noted above, the results from multiple leak rate testing programs indicate that the logarithm of the loss coefficient is a linear function of the contact pressure, i.e.,

$$\ln K = a_0 + a_1 P_c, \tag{7-8}$$

where the coefficients, a_0 and a_1 of the linear relation are found from a regression analysis of the test data; both coefficients are greater than zero. Simply put, the loss coefficient is greater than zero at the

point where the contact pressure is zero and the loss coefficient increases with increasing contact pressure. Thus,

$$K = e^{a_0 + a_1 P_c}, \tag{7-9}$$

and the loss coefficient is an exponential function of the contact pressure. Combining Equation 7-9 for the loss coefficient as a function of the contact pressure with Equation 7-5 for the contact pressure as a function of length yields,

$$K = e^{a_0 + a_1 (b_0 + b_1 L)} = e^{c_0 + c_1 L} \tag{7-10}$$

where L is reckoned downward from the lower of the top of the tubesheet or the bottom of the expansion transition and the joined coefficients are given by $c_0 = a_0 + a_1 b_0$ and $c_1 = a_1 b_1$. Away from the periphery of the tubesheet, b_1 is greater than zero, hence c_1 is also greater than zero and the loss coefficient increases with depth into the tubesheet. Alternatively, the relation also means that near the periphery of the tubesheet the resistance to flow increases above any elevation when the tubesheet bow convex downward. Since the B* distance into the tubesheet is based on finding the depth for which the resistance to leak during SLB is the same as that during NOp, the meaningful radial region of the tubesheet is away from the periphery, that is, where the resistance to leakage decreases near the top of the tubesheet. Another point to note from the above expression is that in the region of interest the second derivative of the loss coefficient with respect to depth is positive. This means that the resistance per unit length is always increasing with depth into the tubesheet. One consequence of the relation is that the decrease in resistance for a specified distance above any reference point is balanced by the increase in resistance over a shorter distance below that reference point. The coefficients for the contact pressure as a function of location are given by Equations 7-6 and 7-7 for NOp and SLB, respectively.

The B* distance is designated by L_B in the following equations and is the depth at which the resistance to leak during SLB is the same as that during NOp (See Figures 7-3 and 7-4). Note that the product of the viscosity and the loss coefficient is the resistance per unit length for any location in the tubesheet. The resistance to leak, R, as a function of the viscosity, μ, average loss coefficient, $\overline{K}$, and length of the leak path from some uppermost location, L_0, to L_B for any condition is given by,

$$R = \mu \overline{K} \left(L_B - L_0 \right) = \int_{L_0}^{L_B} e^{c_0 + c_1 L} dL \tag{7-11}$$

The limits of the integration define the range over which there is a contact pressure between the tube and the tubesheet that is greater than zero, i.e., ignoring any resistance to flow above that elevation. The lower limit is the lower of the TTS, the BET (bottom of the expansion transition), or the point where the contact pressure is zero. Carrying out the integration,

$$R = \mu \frac{e^{c_0}}{c_1} \left[e^{c_1 L_B} - e^{c_1 L_0} \right] \tag{7-12}$$

The equation can be used directly when the point of zero contact pressure between the tube and the tubesheet is at or below the TTS or BET, whichever is lower.

In order to account for the condition wherein L_0 is < 0, i.e., at or above the TTS or BET, whichever is lower, the equation is written as,

$$R = \mu \frac{e^{c_0}}{c_1}\left[e^{c_1 L_B} - \text{if}\left(L_0 > 0, e^{c_1 L_0}, 1\right)\right] \tag{7-13}$$

Here, the first argument of the "if" statement is the condition to be tested, the second argument is the value used if the condition is true, and the third argument is used if the condition is false, that is, when zero contact pressure is predicted above the TTS or BET (See Figure 7-3). For normal operation the resistance to leakage is given by,

$$R_N = \mu_N \frac{e^{c_{0N}}}{c_{1N}}\left[e^{c_{1N} L_B} - \text{if}\left(L_{0N} > 0, e^{c_{1N} L_{0N}}, 1\right)\right] \tag{7-14}$$

and for SLB by,

$$R_S = \mu_S \frac{e^{c_{0S}}}{c_{1S}}\left[e^{c_{1S} L_B} - \text{if}\left(L_{0S} > 0, e^{c_{1S} L_{0S}}, 1\right)\right] \tag{7-15}$$

The B* distance is such that the resistance during SLB is the same as that during NOp, limiting the leak rate to be no more than a factor of two times that during normal operation, thus the solution is obtained for the value of L_B that makes $R_S = R_N$.

For the Vogtle 1 & 2 SGs (hot leg) the value of B* varies from a maximum of 6.81 inches at a radius of 2 inches in the tube bundle, to 6.44 inches at a radius of 32 inches, and less than 1 inch at a radius of 45 inches. Thereafter, the integrated leak resistance is always greater during a SLB event than during NOp. A plot of the calculated B* values is provided on Figure 7-7. Here, any values less than 1 inch were truncated to 1 inch. For example, the top of the tubes at the extreme periphery of the tubesheet are in compression during NOp because of contraction of the tube holes due to convex downward bending. The level of compression increases during a SLB event because the magnitude of the convex bending increases. Thus, any leak rate during NOp would bound the leak rate during SLB. While the driving pressure would increase by a factor of up to 2, the contact pressure between the tube and the tubesheet would increase toward the top of the tubesheet. The hot leg B* results are plotted in Figure 7-7 and Figure 9-1.

For the Vogtle 1 & 2 SGs (cold leg) the value of B* varies from a maximum of 8.50 inches at a radius of 2 inches in the tube bundle, to approximately 8 inches at a radius of 32 inches, and to 6.75 inch at a radius of 38 inches. Thereafter, the integrated leak resistance is always greater during a SLB event than

during NOp. A plot of the calculated B* values is provided on Figure 9-2. Here, any values less than 1 inch were truncated to 1 inch because of contraction of the tube holes due to convex downward bending at the extreme periphery. For example, the top of the tubes at the extreme periphery of the tubesheet are in compression during NOp because of contraction of the tube holes due to convex downward bending. The level of compression increases during a SLB event because the magnitude of the convex bending increases. Thus, any leak rate during NOp would bound the leak rate during SLB. While the driving pressure would increase by a factor of up to 2, the contact pressure between the tube and the tubesheet would increase toward the top of the tubesheet. The cold leg B* results are plotted in Figures 7-5a through 7-14a and Figure 9-2.

7.5 REVIEW OF B* DEPTH SUSCEPTIBILITY TO TUBE SLIPPAGE

The impacts to this B* analysis due to tube slippage are addressed in Appendix A, Response to Wolf Creek NRC RAI Question 9.

7.6 CONCLUSIONS RELATIVE TO B*

The resistance equations above can be used to show that the resistance is always bounded by the region through the thickness of the tubesheet where the contact pressure increases relative to the region where the contact pressure decreases. This simply means that the leak rate resistance increases during a SLB event relative to that during normal operation for similar lengths about a reference depth from the TTS, for example, B*. The resistance equations were used to calculate B* as the distance from the TTS for which the resistance during a postulated SLB event is the same as that during NOp. This means that the leak rate during SLB from any and all indications below B* will be bounded by a multiple of the leak rate during NOp based on the relative driving pressure for the two conditions. The differential pressure ratio during a SLB at Vogtle 1 & 2 is 1.92 to 1.96 for the cases described in Section 5.1.3, times that during NOp depending on the operating conditions considered, e.g., differences in plugging level. Hence, the leak rate during a postulated SLB event would be expected to be no more than 2 times the leak rate being experienced during normal operation. Moreover, the B* analysis did not take into consideration the effect of the increase in the contact pressure below the B* elevation on the leak rate through postulated tube cracks within the tubesheet. For axial cracks, the flanks would be compressed and the leak rate through the cracks themselves would be expected to decrease. For circumferential cracks the resistance to flank displacement in the axial direction would be expected to negate the effect of the slight increase in pressure on the crack flanks. In conclusion, the use of a factor of 2 for driving pressure increase is conservative for the Vogtle Unit 1 steam generators.

Table 7-1 First Order Equation Coefficients for the Variation of Contact Pressures Through Tubesheet (Hot Leg Only)

a,c,e

Table 7-2 Summary Table Leak Rate Required Engagement Lengths

a,c,e

Zone	Leak Resistance Ratio R_{SLB} / R_{NOp} (1, 2)	Engagement from TTS (inches)	
		Hot Leg	Cold Leg

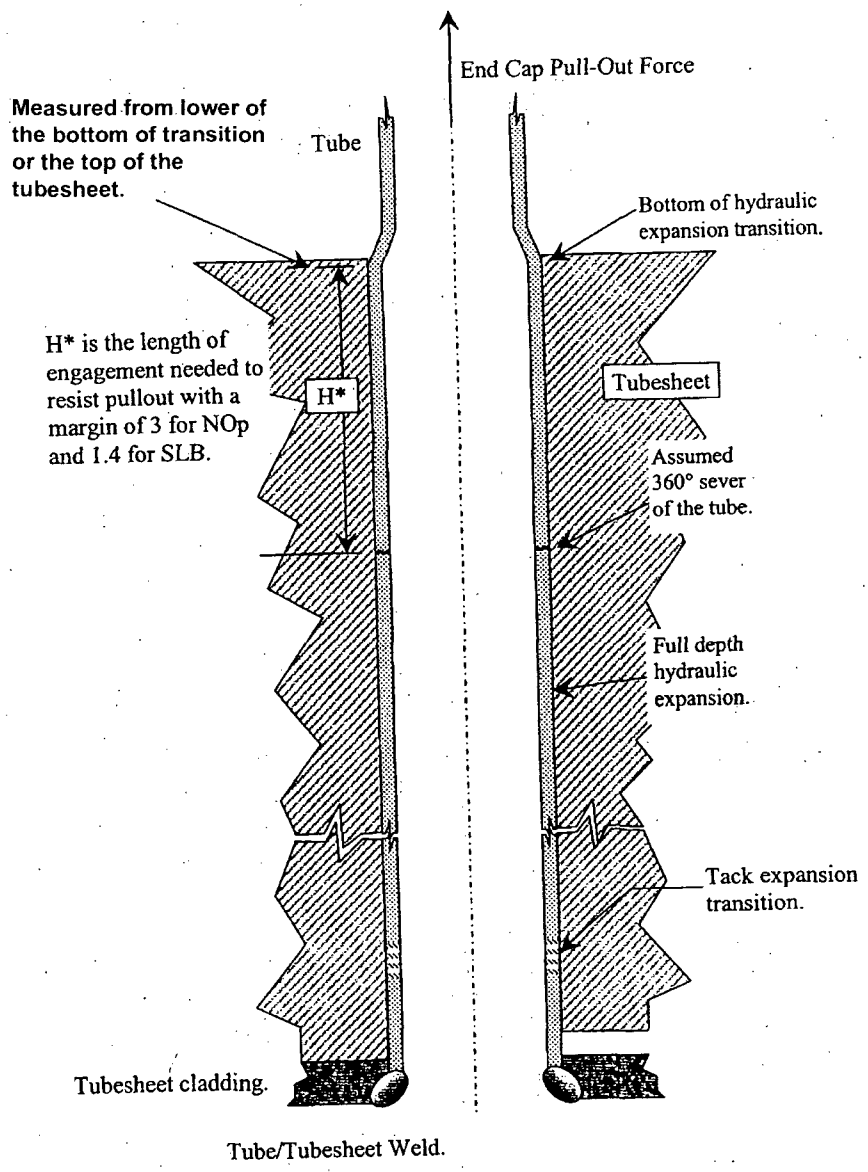

Figure 7-1 Determination of H*

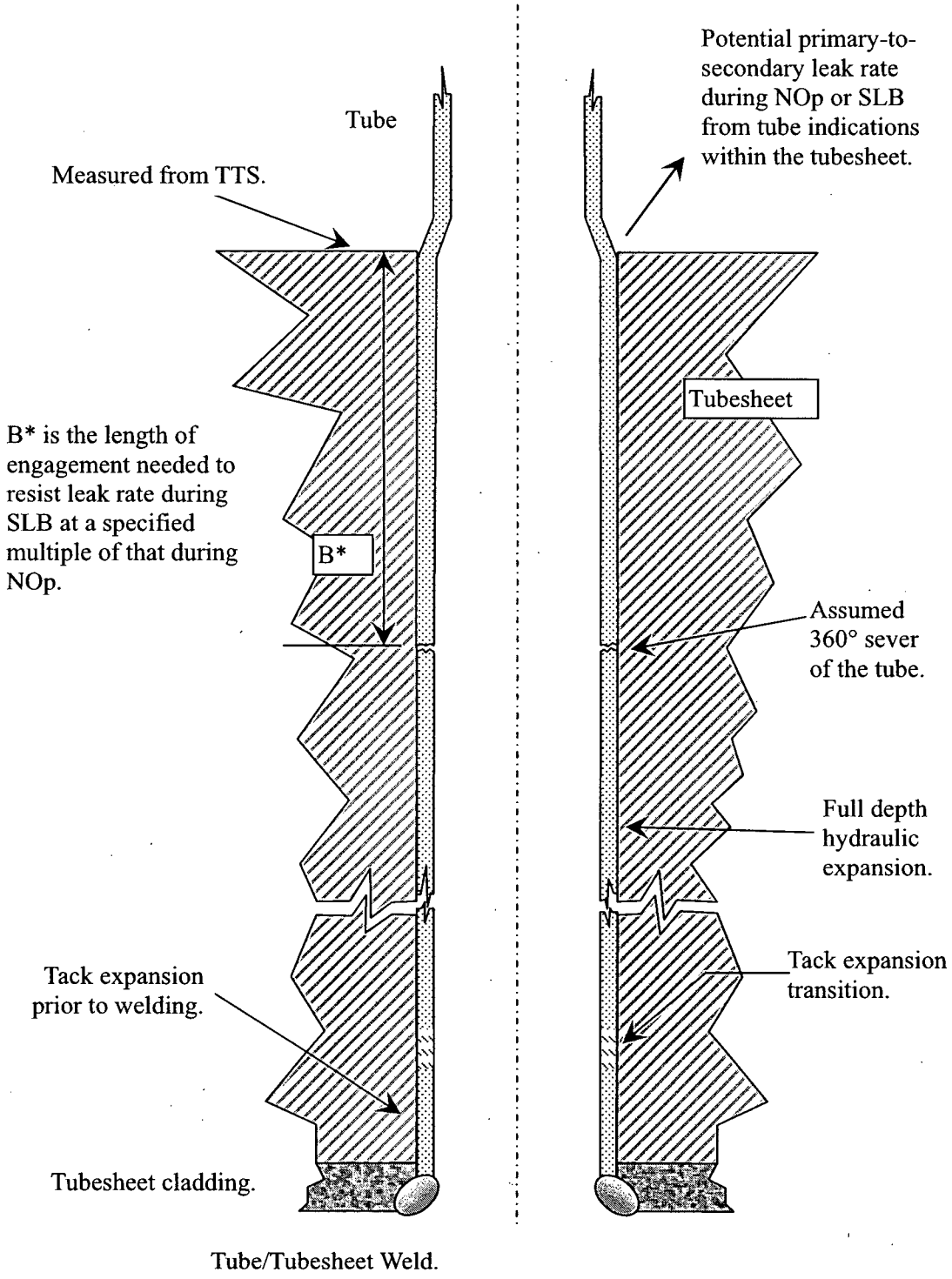

Figure 7-2 Determination of B*

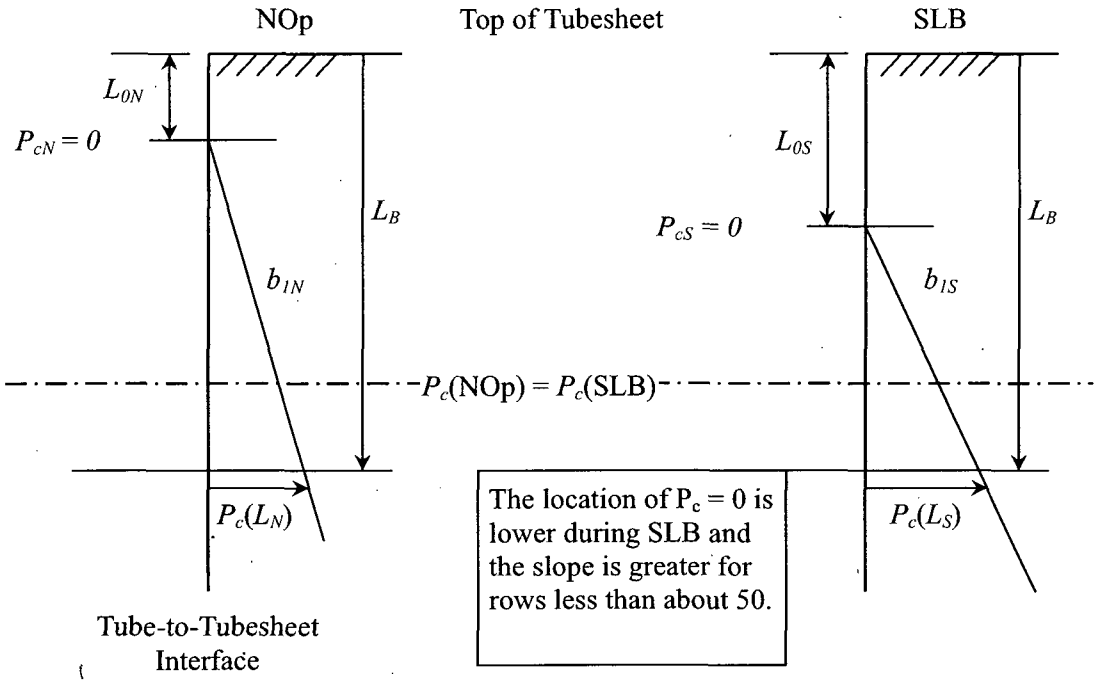

L_{ON} = Distance from the top of the tubesheet (inches) where 0 contact pressure ($P_{cN} = 0$) occurs during normal operating conditions at a defined radius.

L_{OS} = Distance from the top of the tubesheet (inches) where 0 contact pressure ($P_{cS} = 0$) occurs during a postulated steam line break at a defined radius.

$P_c(L_N)$ = Contact pressure as a function of elevation in the tubesheet during normal operating conditions at a defined radius.

$P_c(L_S)$ = Contact pressure as a function of elevation in the tubesheet during a postulated steam line break at a defined radius.

b_{1N} = Slope of contact pressure line as a function of elevation in the tubesheet during normal operating conditions at a defined radius.

b_{1S} = Slope of contact pressure line as a function of elevation in the tubesheet during a postulated steam line break at a defined radius.

L_B = B* distance.

Figure 7-3 Concepts for the Determination of B*

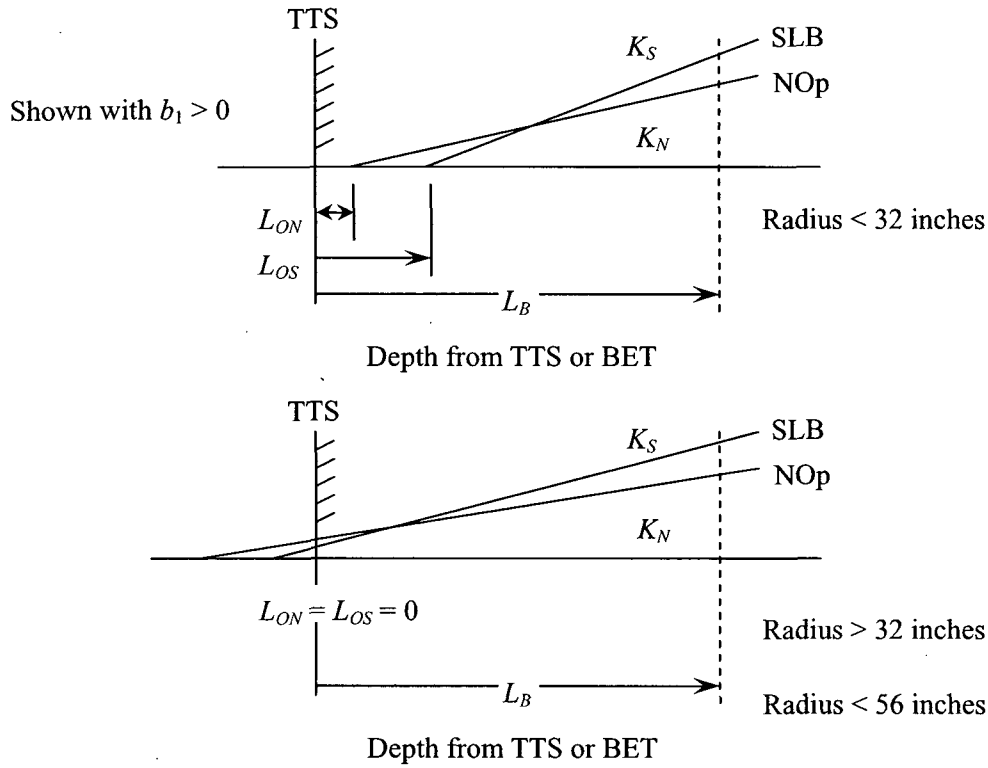

L_{ON} = Distance from the top of the tubesheet (inches) where 0 contact pressure ($P_{cN} = 0$) occurs during normal operating conditions at a defined radius.

L_{OS} = Distance from the top of the tubesheet (inches) where 0 contact pressure ($P_{cS} = 0$) occurs during a postulated steam line break at a defined radius.

L_B = B* distance.

K_N = Loss coefficient during normal operating conditions is a log-linear function of contact pressure.

K_S = Loss coefficient during steam line break conditions is also a log-linear function of contact pressure.

Figure 7-4 Schematic for the Determination of B* Parameters

HOT LEG RESULTS

a,c,e

Figure 7-5 First Order Linear Representation of Contact Pressure (based on Table 7-1)

a,c,e

Figure 7-6 Contact Pressure During Normal Operation (Model F)

a,c,e

Figure 7-7 Contact Pressure During SLB (2560 psi at 297°F)

a,c,e

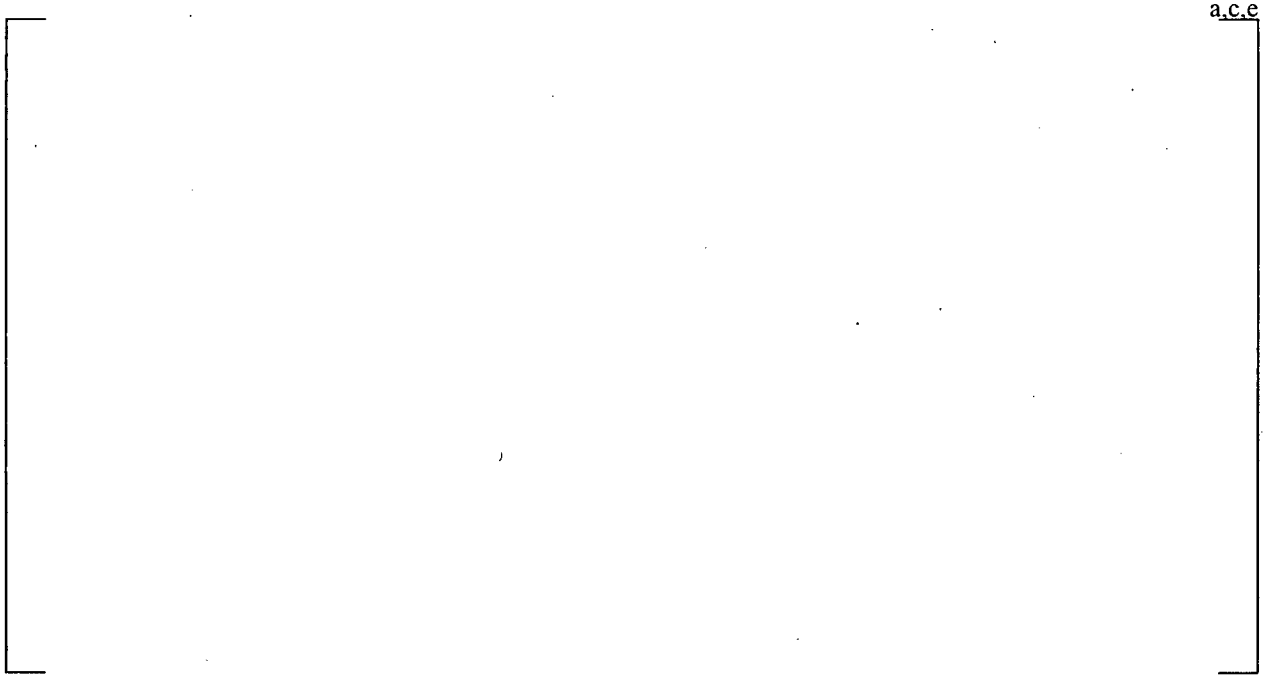

Figure 7-8 NOp Contact Pressure vs. Depth Coefficients by Radius

a,c,e

Figure 7-9 SLB Contact Pressure vs. Depth Coefficients by Radius

a,c,e

Figure 7-10 Comparison of Contact Pressure Coefficients for NOp & SLB Conditions

a,c,e

Figure 7-11 Elevation Below the TTS for Invariant Contact Pressure

a,c,e

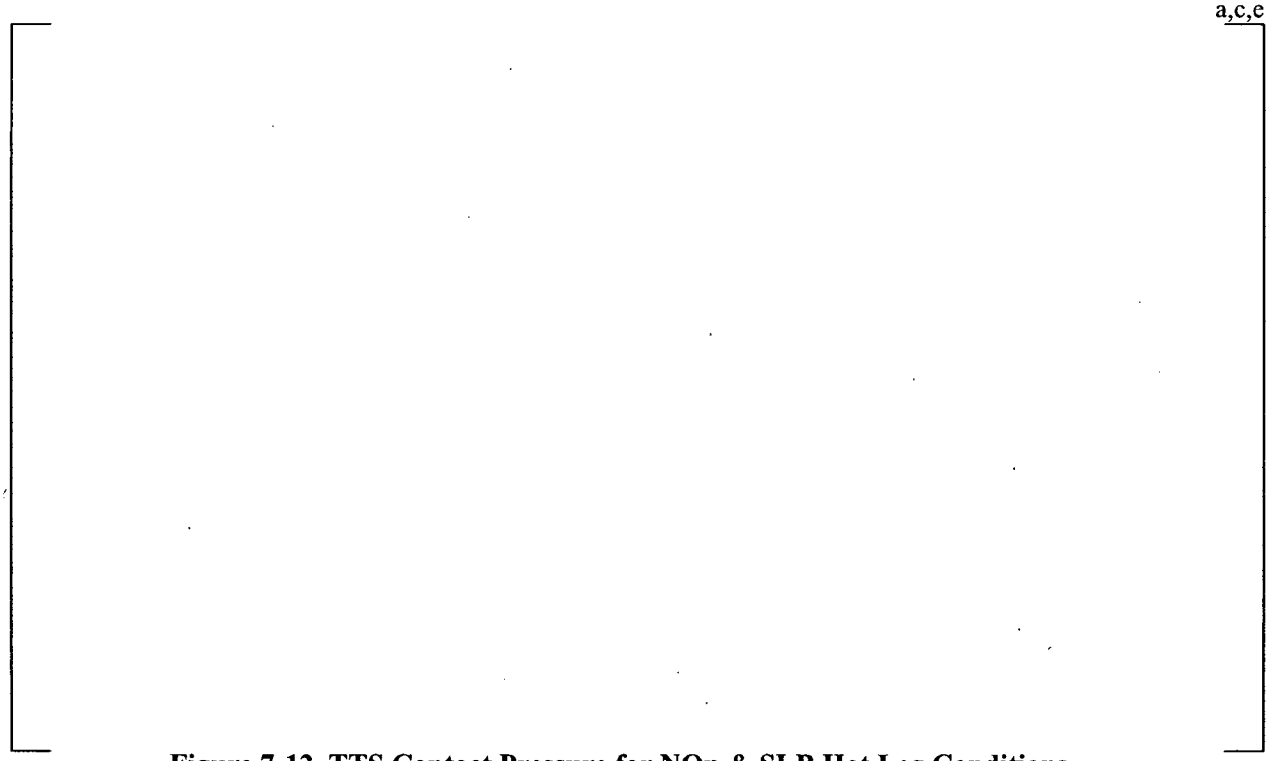

Figure 7-12 TTS Contact Pressure for NOp & SLB Hot Leg Conditions

a,c,e

Figure 7-13 Viscosity of Water as a Function of Pressure

a,c,e

Figure 7-14 Viscosity of Water at 2560 psi as a Function of Temperature

COLD LEG RESULTS

a,c,e

Figure 7-5a First Order Linear Representation of Contact Pressure (Cold Leg)

a,c,e

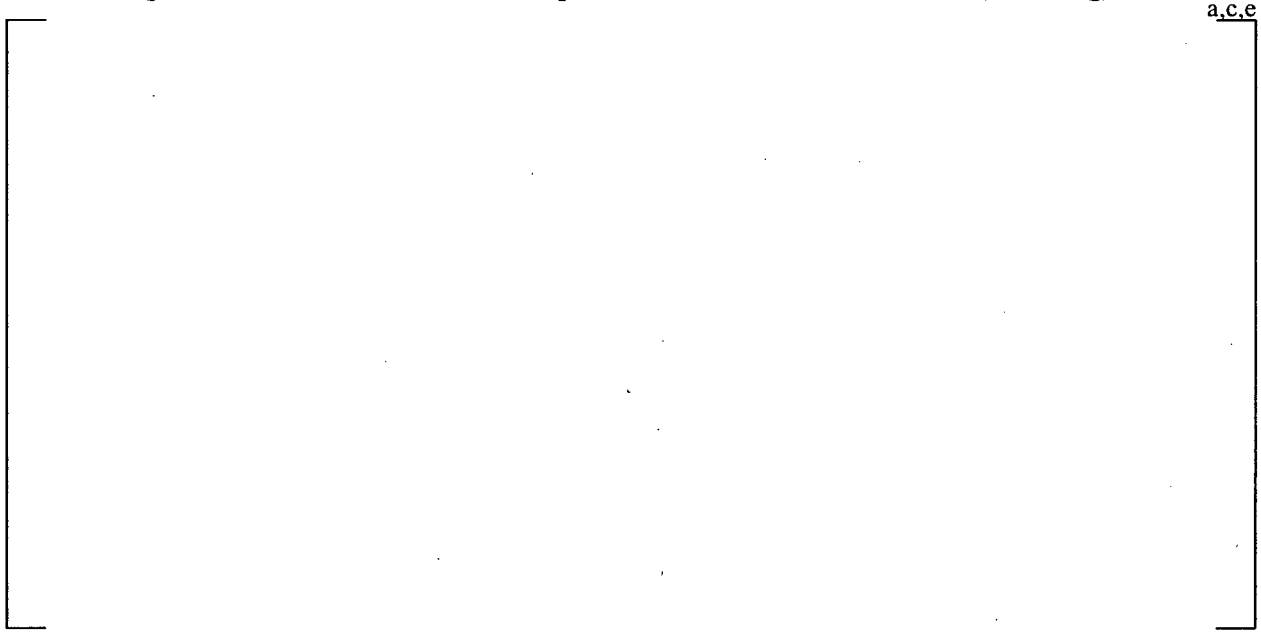

Figure 7-6a Contact Pressure During Normal Operation (Model F)

a,c,e

Figure 7-7a Contact Pressure During SLB (2560 psi at 297°F)

a,c,e

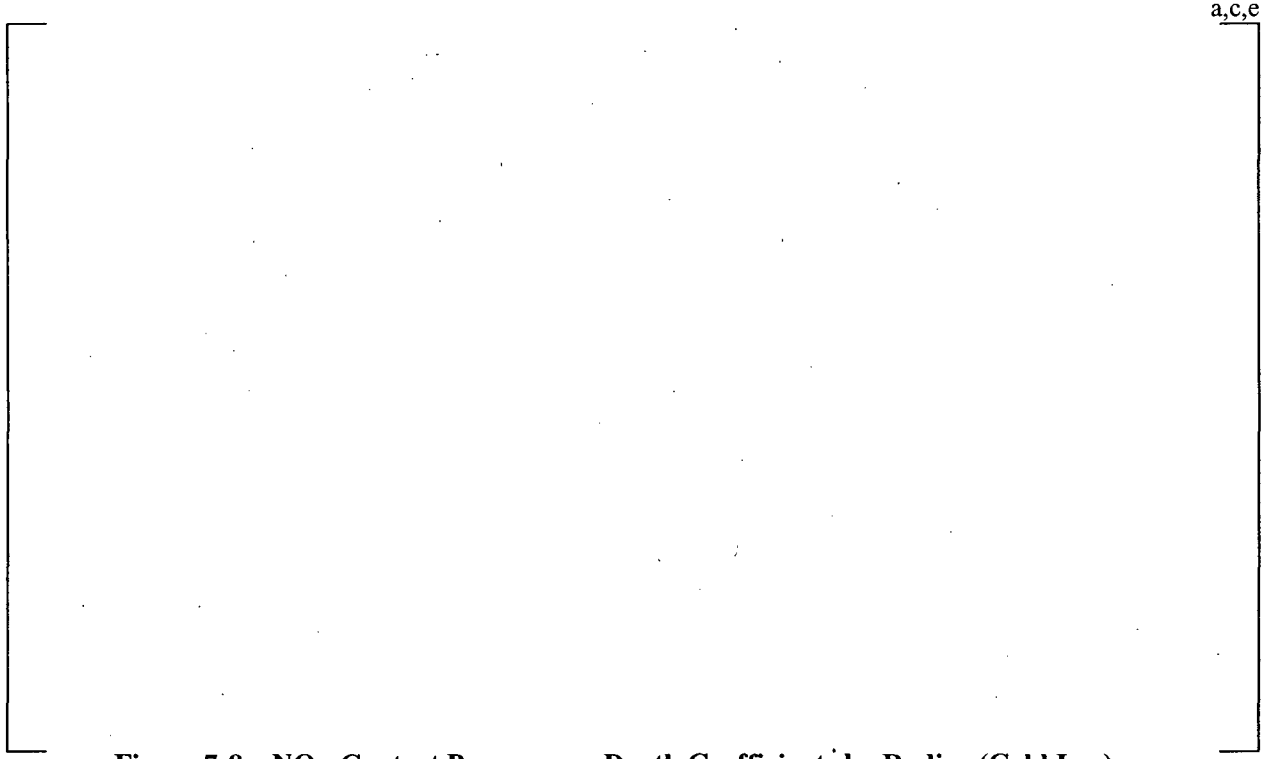

Figure 7-8a NOp Contact Pressure vs. Depth Coefficients by Radius (Cold Leg)

a,c,e

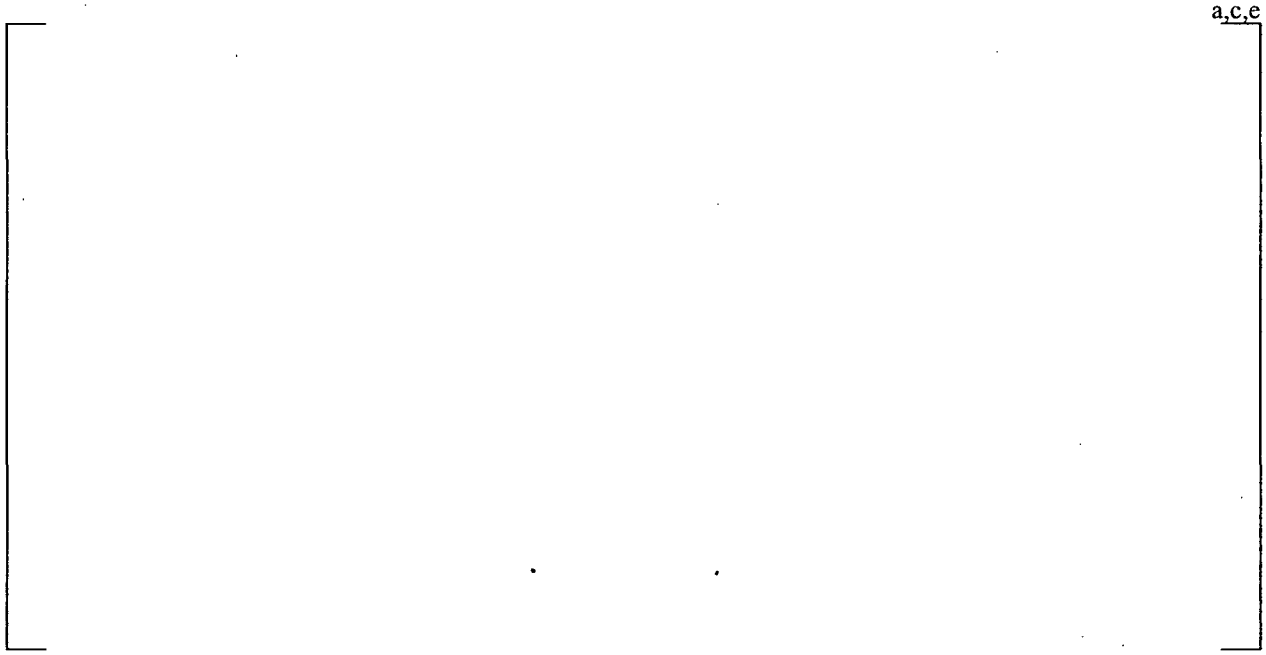

Figure 7-9a SLB Contact Pressure vs. Depth Coefficients by Radius (Cold Leg)

a,c,e

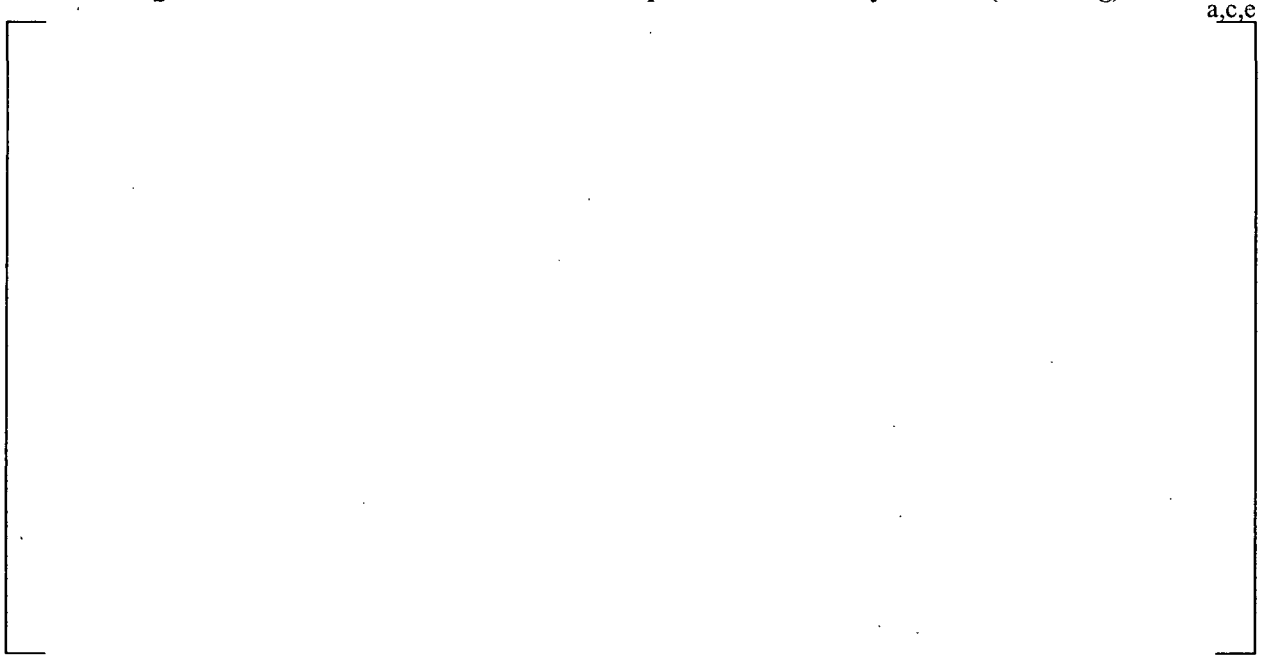

Figure 7-10a Comparison of Contact Pressure Coefficients for NOp & SLB Conditions

a,c,e

Figure 7-11a Elevation Below the TTS for Invariant Contact Pressure

a,c,e

Figure 7-12a TTS Contact Pressure for NOp & SLB Cold Leg Conditions

a,c,e

Figure 7-13a Viscosity of Water as a Function of Pressure

a,c,e

Figure 7-14a Viscosity of Water at 2560 psi as a Function of Temperature

a,c,e

Figure 7-15 Plot of Model D and Model F Total Data Set for 70°F and 600°F (with flashing in the crevice assumed)

a,c,e

Figure 7-16 Total Data Set Fit Using Original Assumptions (Flashing assumed, no crevice pressure modifications)

a,c,e

Figure 7-17 No Flashing in the Crevice, Crevice Pressure Varied Based on Applied ΔP, Scaled Total Data Set Results

a,c,e

Figure 7-18 95% Confidence Limit Results for Varied Crevice Pressure, Total Data Set and No Flashing in the Crevice

a,c,e

[ ]a,c,e

Figure 7-19 Plot of Model D and Model F Total Data Set for 70°F and 600°F with Regression Analysis Results

8 HISTORICAL DISCUSSION ON NRC STAFF ONE-CYCLE B* APPROVALS FOR BRAIDWOOD 2 & VOGTLE 2

8.1 JOINT STRUCTURAL INTEGRITY DISCUSSION

In Section 3.1, "Joint Structural Integrity," of Reference 31, the NRC staff stated that the analyses that were performed by Westinghouse that led to the determination of the required engagement distances were not reviewed in detail and more qualitative arguments were used by the NRC staff for one time approval of the applicable 17 inch tube joint length. The qualitative arguments are stated below.

- The NRC staff estimates, based on the Westinghouse pullout tests, that the radial contact pressure produced by the hydraulic expansion and differential radial thermal expansion is such to require an engagement distance of 8.6 inches to ensure the appropriate safety margins against pullout based on no-slip. This estimate is a mean minus one standard deviation estimate based on 6 pull out tests. This estimate ignores the effect on needed engagement distance from internal primary pressure in the tube and tubesheet bore dilations associated with the tubesheet bow. The NRC staff notes, from a tube pullout standpoint, the use of a 0.25 inch displacement criterion is conservative. Allowing slippage of about 0.2 to 0.3 inches decreases the necessary engagement distance to 5.1 inches, again ignoring the effect on needed engagement distance from internal primary pressure in the tube and tubesheet bore dilations associated with tubesheet bow.

- The internal primary pressure inside the tube under normal operating and accident conditions also acts to tighten the joint relative to unpressurized conditions, thus reducing the necessary engagement distance.

- Tubesheet bore dilations caused by the tubesheet bow under primary-to-secondary pressure can increase or decrease contact pressure depending on tube location within the bundle and the location along the length of the tube in the tubesheet region. Basically, the tubesheet acts as a flat, circular plate under an upward-acting net pressure load. The tubesheet is supported axially around its periphery with a partial restraint against tubesheet rotation provided by the steam generator shell and the channel head. [

  ]^{a,c,e} Over most of the tubesheet away from the periphery, the bending moment resulting from the applied primary-to-secondary pressure load can be expected to put the tubesheet in tension at the top and compression at the bottom. Thus, the resulting distortion of the tubesheet bore (tubesheet bore dilation) tends to be such as to loosen the tube-to-tubesheet joint at the top of the tubesheet and to tighten the joint at the bottom of the tubesheet. The amount of dilation and resulting change in joint contact pressure would be expected to vary in a linear fashion from the top to the bottom of a tubesheet. Given the neutral plane to be at approximately the mid-point of the tubesheet thickness, tubesheet bore dilation effects would be expected to further tighten the joint from 10.5 inches below the TTS to 17 inches below the TTS which would be the lower limit of the proposed tubesheet region inspection zone. Combined with the effects of the tube joint tightening associated with the radial differential thermal expansion and primary pressure inside the tube, contact pressure over at least a 6.5 inch distance should be considerably higher than the contact pressure simulated in the above

mentioned pullout tests. A similar logic applied to the periphery of the tubesheet leads the staff to conclude that at the top 10.5 inches of the tubesheet region, contact pressure over at least a 6.5 inch distance should be considerably higher than the contact pressure simulated in the above mentioned pull out tests. Thus, the staff concludes that the proposed 17-inch engagement distance (or inspection zone) is acceptable to ensure the structural integrity of the tubesheet joint.

The NRC qualitative arguments are further supported on a more quantitative basis based on a study completed for the Model F steam generators for another plant. Moreover, similar statements were made in Reference 32 in approving a similar amendment for a plant with Model D5 SGs.

8.1.1 Discussion of Interference Loads

There are four source terms that must be considered relative to the determination of the interface pressure between the tube and the tubesheet. These are,

1. the initial preload from the installation of the tube,
2. internal pressure in the tube that is transmitted from the ID to the OD,
3. thermal expansion of the tube relative to the tubesheet, and
4. bowing of the tubesheet that results in dilation of the tubesheet holes.

The initial preload results from the plastic deformation of the tube material relative to that of the tubesheet. The material on the inside diameter experiences more plastic deformation than the material on the outside and, thus has a deformed diameter which is incrementally greater. Equilibrium of the hoop forces and moments in the tube means that the OD is maintained in a state of hoop tension at a diameter greater than a stress-free state. The model for the determination of the initial contact pressure between the tube and the tubesheet, P_c, is illustrated on Figure 8-1 for the elements of the unit cell and on Figure 8-2 for the analysis schematic. Both the tube and the tubesheet behave as elastic springs after the expansion process is applied. The normal stress on the tube must be equal in magnitude to the normal stress on the tubesheet and the sum of the elastic springback values experienced by each must sum to the total interference.

As long as the tube and the tubesheet remain in contact, the radial normal stresses must be in equilibrium. Thus, the problem of solving for the location of the interface and the contact pressure is determinate. The elements considered in the analysis are illustrated on Figure 8-2 for all operating and postulated accident conditions; the centerline of the tube and tubesheet hole are to the left in the figure. Each source of deformation of the tube outside surface starting from the installed equilibrium condition can be visualized starting from the top left side of the figure. The sources of deformation of the tubesheet inside surface can be visualized starting from the lower left side of the figure. As illustrated in Figure 8-3, although not to scale, the tube material has a coefficient of thermal expansion that is greater than that of the tubesheet. The radial flexibility[6], f, of the tube relative to that of the tubesheet determines how much of the pressure is actually transmitted to the interface between the tube and the tubesheet. Positive radial deformation of the tube in response to an internal pressure is found as the product of the pressure, Pp, and the tube flexibility associated with an internal pressure, discussed in the next section. Thus, the tube gets tighter in

6 Flexibility is the ratio of deformation to load and is the inverse of the stiffness.

the tubesheet hole as the temperature of the tube and tubesheet increase. The deformation of the tube in response to an external or secondary pressure, P_s, is the product of the pressure times the flexibility associated with an external pressure. The normal operation contact pressure, P_N, is found from compatibility and equilibrium considerations. The deformation of the tubesheet hole in response to an internal pressure, P_s, is found as the product of the pressure and the flexibility of the tubesheet associated with an internal pressure. The opening or closing of the tubesheet hole, δr_i, resulting from bow induced by the primary-to-secondary pressure difference is in addition to the deformations associated with temperature and internal pressure. Once the tube has been installed, the deformations of the tube and tubesheet associated thermal expansion, internal pressure, and tubesheet bow remain linearly elastic.

Because of the potential for a crack to be present and the potential for the joint to be leaking, the pressure in the crevice is assumed to vary linearly from the primary pressure at the crack elevation to the secondary pressure at the top of the tubesheet. If the joint is not leaking, it would be expected that there was no significant fluid pressure in the crevice. The pressure assumption is considered to be conservative because it ignores the pressure drop through the crack. The leak path through the crevice is not normally around the entire circumference of the tube. In addition, the leak path is believed to be between contacting microscopic asperities between the tube and the tubesheet, thus the pressure in the crevice would not be acting over the entire surface area of the tube and tubesheet. In any event, pressure in the crevice is always assumed to be present for the analysis.

There is no bow induced increase in the diameter of the holes during normal operation or postulated accident conditions below the mid span elevation within the tubesheet, hence most analyses concentrate on locations near the top of the tubesheet. The tubesheet bow deformation under postulated accident conditions will increase because of the larger pressure difference between the bottom and top of the tubesheet. The components remain elastic and the compatibility and equilibrium equations from the theory of elasticity remain applicable. Below the mid-span elevation within the tubesheet, the tubesheet holes will contract. The edges of the tubesheet are not totally free to rotate and there is some suppression of the contraction near the outside radius. This also means that the dilation at the top of the tubesheet is also suppressed near the outside radius of the tubesheet. The maximum hole dilations occur near the center of the tubesheet.

The application of the theory of elasticity means that the individual elements of the analysis can be treated as interchangeable if appropriate considerations are made. The thermal expansion of the tube can be thought of as the result of some equivalent internal pressure by ignoring Poisson effects, or that tubesheet bow could be analytically treated as an increase in temperature of the tubesheet while ignoring associated changes in material properties.

8.1.2 Flexibility Discussion

Recall that the flexibility, f, is defined as the ratio of deflection relative to applied force; it is the inverse of stiffness which is commonly used to relate force to deformation. There are four flexibility terms associated with the radial deformation of a cylindrical member depending on the surface to which the loading is applied and the surface for which the deformation is being calculated, e.g., for transmitted internal pressure one is interested in the radial deformation of the OD of the tube and the ID of the tubesheet. The deformation of the OD of the tube in response to external pressure is also of interest. The

geometry of the tube-to-tubesheet interface is illustrated on Figure 8-3. The flexibility of the tubesheet, designated herein by the subscript c, in response to an internal pressure, P_{ci}, is found as,

[a,c,e]

Tubesheet (8-1)

where:

r_{ci} = inside radius of the tubesheet and outside radius of the tube,
r_{co} = outside radius of the tubesheet hole unit cell,
E_c = the elastic modulus of the carbon steel tubesheet material, and
υ = Poisson's ratio for the tubesheet material.

Here, the subscripts on the flexibility stand for the component, c for tubesheet (and later t of tube), the surface being considered, i for inside or o for outside, and the surface being loaded, again, i for inside and o for outside. The superscript designates whether the cylinder is open, o, or closed, c, of interest in dealing with the end-cap load from pressure in the tube. The former case is a state of plane stress and the latter is not since a closed cylinder has an end-cap load. The flexibility of the tube in response to the application of an external pressure, P_{ro}, e.g., the contact pressure within the tubesheet, is,

[a,c,e]

Open Tube (8-2)

Poisson's ratio is the same for the tube and the tubesheet. When the external pressure can act on the end of the tube,

[a,c,e]

Closed Tube (8-3)

where E_t is the elastic modulus of the tube material. The flexibility of the tube in response to an external pressure is different when the secondary side pressure is present because that pressure also acts to compress the tube in the axial direction giving rise to a Poisson expansion effect, resisting the radial compression due to the pressure.

Finally, the flexibility of the outside radius of the tube in response to an internal pressure, P_{ti}, is,

a,c,e

[ ]

Closed Tube (8-4)

where r_{ti} is the internal radius of the tube and the tube is assumed to be closed. For an open tube the term in parentheses in the numerator is simply 2. A closed tube expands less due to Poisson contraction associated with the end-cap load from the internal pressure. A summary of the applicable flexibilities is provided in Table 8-1. Note that during normal operation there is an end-cap load on the tube from the secondary pressure but not from that associated with the fluid in the crevice if the joint is leaking. Both flexibilities would then be involved in calculating the radial deformation of the outside of the tube. Only the open tube flexibility is used with the pressure in the crevice for postulated accident conditions.

When the inside of the tube is pressurized, P_{ti}, some of the pressure is absorbed by the deformation of the tube within the tubesheet and some of the pressure is transmitted to the OD of the tube, P_{to}, as a contact pressure with the ID of the tubesheet. The magnitude of the transmitted pressure is found by considering the relative flexibilities of the tube and the tubesheet as,

a,c,e

[ ]

(8-5)

Note that the tube flexibility in response to the contact pressure is for an open tube because there is no end-cap load associated with the contact pressure. The denominator of the fraction is also referred to as the interaction coefficient between the tube and the tubesheet. About 85 to 90% of the pressure internal to the tube is transmitted through the tube in Westinghouse designed SGs. However, the contact pressure is not increased by that amount because the TS acts as a spring and the interface moves radially outward in response to the increase in pressure. The net increase in contact pressure is on the order of 67 to 74% of the increase in the internal pressure, depending on the constraint conditions. For example, the contact pressure between the tube and the tubesheet is increased by about 1970 psi during normal operation relative to ambient conditions. Likewise, the increase in contact pressure associated with SLB conditions is about 2250 psi relative to ambient conditions.

When the temperature increases from ambient conditions to operating conditions, the differential thermal expansion of the tube relative to the tubesheet increases the contact pressure between the tube and the tubesheet. The mismatch in expansion between the tube and the tubesheet, δ, is given by,

$$\delta = \left(\alpha_t \, \Delta T_t - \alpha_c \, \Delta T_c\right) r_{to}$$

Thermal Mismatch (8-6)

where:

α_t, α_c = thermal expansion coefficient for the tube and tubesheet, respectively,

ΔT_t, ΔT_c = the change in temperature from ambient conditions for the tube and tubesheet, respectively.

During normal operation the temperature of the tube and tubesheet are effectively identical to within a very short distance from the top of the tubesheet and the individual changes in temperature can usually be replaced by ΔT_t, thus,

$$\delta = (\alpha_t - \alpha_c)\Delta T_t \, r_{to} \tag{8-7}$$

The change in contact pressure due to the increase in temperature relative to ambient conditions, P_T, is given by,

a,c,e

[ ] (8-8)

Likewise, the same equation can be used to calculate the reduction in contact pressure resulting from a postulated reduction in the temperature of the tube during a postulated SLB event.

The net contact pressure, P_C, between the tube and the tubesheet during operation or accident conditions is given by,

Net Contact Pressure

$$P_C = P_0 + P_P + P_T - P_B \tag{8-9}$$

where P_B is the loss of contact pressure due to dilation of the tubesheet holes, P_0 is the installation preload, P_P is the pressure-induced load, and P_T is the thermal-induced contact load. There is one additional term that could be considered as increasing the contact pressure. When the temperature increases, the tube expands more in the axial direction than the tubesheet. This is resisted by the frictional interface between the tube and the tubesheet and a compressive stress is induced in the tube. This in turn results in a Poisson expansion of the tube radius, increasing the interface pressure. The effect is not considered to be significant and is essentially ignored by the analysis.

8.1.3 Analysis

From the preceding discussions, it is apparent that the contact pressure during normal operation can be found by equating the total deformation of the outside radius of the tube, r_{to}, to the total deformation of the inside radius of the tubesheet hole, r_{ci}, where the net deformation of the outside of the tube, δ_{to}, is given by,

Tube Deformation

$$\delta_{to} = \alpha_t \Delta T_t r_{to} + P_p f^c_{toi} + P_s f^c_{too} + P_N f^o_{too} \tag{8-10}$$

and the net deformation of the tubesheet hole, δ_{ci}, is given by,

TS Deformation

$$\delta_{ci} = \alpha_c \Delta T_c r_{ci} + P_s f^o_{cii} + \delta r_i + P_N f^o_{cii} . \tag{8-11}$$

The inclusion of the P_N terms assures compatibility and the two net deformations must be equal. It can usually be assumed that the secondary fluid pressure does not penetrate the tubesheet hole and the terms involving P_s may be ignored. All of the terms except for the final contact pressure, P_N, are known and the tubesheet bow term, δ_{ri}, is found from the finite element model analysis of the tubesheet. The total contact pressure during operation is then found as P_N plus P_c, the installation contact pressure. For postulated SLB conditions, the solution is obtained from,

$$\alpha_t \Delta T_t r_{to} + P_p f^c_{toi} + P_N f^o_{too} = \alpha_c \Delta T_c r_{ci} + \delta r_i + P_N f^o_{cii} , \tag{8-12}$$

or, the total contact pressure during a postulated SLB event is given by,

SLB Contact Pressure

$$P_T = P_c + \frac{\alpha_t \Delta T_t r_{to} - \alpha_c \Delta T_c r_{ci} + P_p f^c_{toi} - \delta r_i}{f^o_{cii} - f^o_{too}} , \tag{8-13}$$

where $r_{to} = r_{ci}$. A similar expression with more terms is used to obtain the contact pressure during normal operation. The denominator of the above equation is referred to as the tube-to-tubesheet influence coefficient because it relates deformations associated with the interfacing components to the interface pressure. The influence coefficient for Westinghouse Model F SG tubes is calculated using the information tabulated in Table 8-1 as $3.33 \cdot 10^{-6}$ psi/inch.

By taking partial derivatives with respect to the various terms on the right, the rate of change of the contact pressure as a function of changes in those parameters can be easily calculated. For example, the rate of change of the contact pressure with the internal pressure in the tube is simply,

$$\frac{\Delta P_N}{\Delta P_p} = \frac{f^c_{toi}}{f^o_{cii} - f^o_{too}} . \tag{8-14}$$

Thus, the rate of change of contact pressure with internal pressure in the tube is 0.564 psi/psi. Likewise, the rate of change of the contact pressure with change in the tube temperature or tubesheet temperature is given by,

$$\frac{\Delta P_N}{\Delta T_t} = \frac{\alpha_t r_{to}}{f^o_{cii} - f^o_{too}} \text{ and } \frac{\Delta P_N}{\Delta T_c} = -\frac{\alpha_c r_{ci}}{f^o_{cii} - f^o_{too}}, \tag{8-15}$$

respectively. Again using the values in Table 8-1, the rate of change of contact pressure with tube temperature is 18.3 psi/°F if there is no increase in tubesheet temperature. The corresponding change with an increase in tubesheet temperature without an increase in tube temperature is –17.36 psi/°F, leaving a net increase in contact pressure of 0.94 psi/°F with a uniform increase in temperature of the tube and the tubesheet.

Finally, the rate of change of contact pressure with tubesheet bow is calculated as,

$$\frac{\Delta P_N}{\Delta \delta r_{ci}} = \frac{1}{f^o_{cii} - f^o_{too}}. \tag{8-16}$$

The effect of the dilation associated with the tubesheet bow can be calculated using the information tabulated in Table 8-1. For each 0.1 mil of diameter dilation the interface pressure is reduced on the order of 380 psi. A summary of all of the contact pressure influence factors is provided in Table 8-1. A summary of tubesheet bow induced hole dilation values is provided in Table 8-2.

8.1.4 Conclusions

Although the study conducted by Westinghouse was completed for another Model F SG, the results listed in Table 8-2 indicate that the effect of the tubesheet bow can result in a significant average decrease in the contact pressure during postulated accident conditions above the neutral plane. However, for the most severe case in one plant, in tube R18C77, the diametral change at the worst case location is less than 0.2 mils at the H* depth during postulated accident conditions. This same type of result would be expected to be the case for the Model F SGs at the Vogtle 1 & 2 Electric Generating Plant. Below the neutral plane, tubesheet bow is shown not to result in any tube dilation, thus supporting the NRC staff conclusion that:

> "Given the neutral axis to be at approximately the mid-point of the tubesheet thickness (i.e., 10.5 inches below the TTS to 17 inches below the TTS), tubesheet bore dilation effects would be expected to further tighten the joint from 10 inches below the TTS to 17 inches below the TTS which would be the lower limit of the proposed tubesheet region inspection zone. Combined with the effects of the tube joint tightening associated with the radial differential thermal expansion and primary pressure inside the tube, contact pressure over at least a 6.5 inch distance [from 17 inches below the TTS] should be considerably higher than the contact pressure simulated in the above mentioned pullout tests."

8.2 JOINT LEAKAGE INTEGRITY DISCUSSION

As noted in Sections 3.2 and 4.2, "Joint Leakage Integrity," References 31 and 32, the NRC staff reviewed the qualitative arguments developed by Westinghouse regarding the conservatism of the conclusion that a minimum 17 inch engagement length ensures that leakage during a main steam line break (MSLB) will not exceed two times the observed leakage during normal operation. The NRC staff reviewed the qualitative arguments developed by Westinghouse regarding the conservatism of the "bellwether approach," but the NRC staff's depth of review did not permit it to credit Westinghouse's insights from leak test data that leak flow resistance is more sensitive to changes in joint contact pressure as contact pressure increases due to the log normal nature of the relationship. The staff was still able to conclude that there should be no significant reduction in leakage resistance when going from normal operating to accident conditions.

The basis for the Westinghouse conclusion that flow resistance varies as a log normal linear function of joint contact pressure is provided in detail below. The data from the worst case tube in a comparative study analytically supports the determination that there is at least an 8 inch zone in the upper 17 inches of the tubesheet where there is an increase in joint contact pressure due to a higher primary pressure inside the tube and changes in tubesheet bore dilation along the length of the tubes. The NRC concurred (Reference 31) that the factor of 2 increase in leak rate as an upper bound by Westinghouse is reasonable given the stated premise that the flow resistance between the tube and the tubesheet remains unchanged between normal operating and accident pressure differential. The NRC staff noted in Reference 31 that the assumed linear relationship between leak rate and differential pressure is conservative relative to alternative models such as the Bernoulli or orifice models, which assume the leak rate to be proportional to the square root of the differential pressure.

The comparative study supported the NRC staff conclusion that, "considering the higher pressure loading when going from normal operating to accident conditions, Westinghouse estimates that contact pressures, and, thus, leak flow resistance, always increases over at least an 8 inch distance above 17 inches below the top of the tubesheet appears reasonable to the NRC Staff."

Table 8-1 Typical Radial Flexibilities Times Elastic Modulus (in/psi) a,c,e

Table 8-2 Example Contact Pressure Influence Factors for Model F & Model D5 SG Tubes at 600°F a,c,e

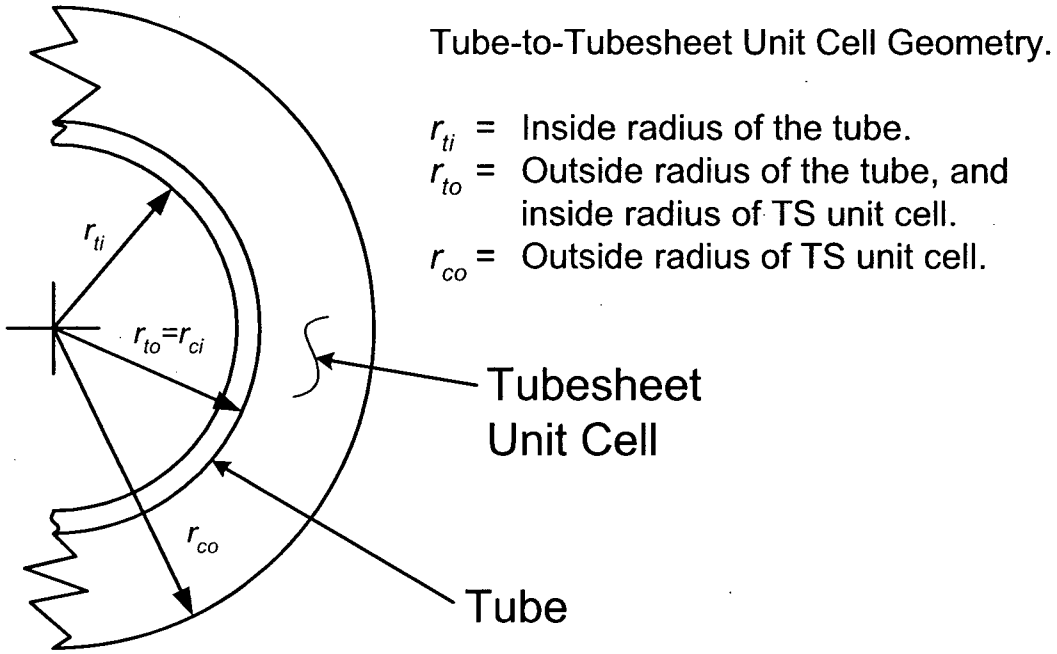

Figure 8-1 Geometry of the Tube-to-Tubesheet Interface

a,c,e

Figure 8-2 Model for Initial Contact Pressure

a,c,e

Figure 8-3 Determination of Contact Pressure, Normal or Accident Operation
(As illustrated, the bow does not result in a loss of contact; however, there are situations where the bow is sufficient to result in a loss of contact between the tube and the tubesheet at the top of the tubesheet).

9 CONCLUSIONS

9.1 ANALYSIS

The evaluation of Section 5 of this report provides a technical basis for assuring that the structural performance criteria of NEI 97-06 are inherently met for degradation of any extent below the H* depth identified in Table 5-12, i.e., depths ranging from 7.24 to 13.38 inches (Hot Leg Only) below the TTS (including allowance of 0.3 inches to account for the hydraulic expansion transition) selected to be bounding for all tubes in all zones (Reference 33). The corresponding evaluation presented in Section 7 provides a technical basis for bounding the potential leak rate from non-detected indications in the tube region below about 6.81 inches from the top of the tubesheet as no more than twice the leak rate during normal operation Reference 33). The evaluation is independent of the magnitude of any degradation that might occur because it is based solely on the resistance of the interface between the tube and the tubesheet. In other words, the tube may be nonexistent below the H* depth. The conclusion is general in that the depths determined are for the most severely affected region of the tubesheet, the central region. The conclusions also apply to any postulated indications in the tack expansion region and in the tube-to-tubesheet welds, although the level of conservatism would be significantly more.

A graphical summary of the findings are presented on Figure 9-1. Figure 9-1 was determined consistent with methods and assumptions used in Wolf Creek NRC RAI #2, as provided in Appendix A. Figure 9-1 is representative of Case No. 89 from Wolf Creek NRC RAI # 2. The depths associated with H*[7] and B* are presented relative to the left ordinate while the leak rates are presented relative to the right ordinate as a function of radial location from the center of the tubesheet.

- The H* depths are bounding relative to a B* for equal leak rate resistance during NOp and SLB. This means that if the structural limits, H*, are satisfied, the leakage limit, B*, will also be satisfied.

- Using the H* values of Table 5-12 results in leak rate per tube increasing on average by less than a factor of 1.92 in Zone D. This is the case because the ratio of SLB to NOp pressure differential is 2560/1334 (1.92) and the distance of 13.38 inches exceeds the B* distance of 6.81 inches.

The conclusions to be drawn from the performed analyses are that:

1. There is no structural integrity concern associated with tube or tube weld cracking of any extent provided it occurs below the H* distance as reported in Section 5 of this report. The pullout resistance of the tubes has been demonstrated for axial forces associated with 3 times the normal operating differential pressure and 1.4 times differential pressure associated with the most severe postulated accident.

2. Contact forces during postulated LOCA events are sufficient to resist axial motion of the tube. Also, if the tube-end welds are not circumferentially cracked, the resistance of the tube-to-

7 The presented H* depths are depicted for individual radii from the center of the tubesheet rather than by zone for comparative purposes.

tubesheet hydraulic joint is not necessary to resist push-out. Moreover, the geometry of any postulated circumferential cracking of the weld would result in a configuration that would resist push-out in the event of a loss of coolant accident. In other words, the crack flanks would not form the cylindrical surface necessary such that there would be no resistance to expulsion of the tube in the downward direction.

3. The leak rate for indications below a B* depth of about 6.81 inches from the top of the tubesheet would be bounded by twice the leak rate that is present during normal operation of the plant regardless of tube location in the bundle. This is initially apparent from comparison of the contact pressures from the finite element analyses over the full range of radii from the center of the tubesheet, and ignores any increase in the leak rate resistance due to the contact pressure changes and associated tightening of the crack flanks. The expectation that this would be the case was confirmed by the detailed analysis of the relative leak rates of Section 7.

4. The H* depth bounds the B* depth for the relocation of the pressure boundary. The B* evaluations were performed utilizing the same operating parameters that were used for the determination of the depths required to meet the structural performance criteria, that is, conservative values for the operating temperature.

In conclusion, a relocation of the pressure boundary to the deeper of the H* or B* values is acceptable from both the structural and leak rate perspective. The prior conclusions rely on the inherent strength and leak rate resistance of the hydraulically expanded tube-to-tubesheet joint, a feature which was not considered or permitted to be considered for the original design of the SG. Thus, omission of the inspection of the tube end region constitutes a reassignment of the pressure boundary to the tube-to-tubesheet interface, which requires NRC staff approval of a license amendment.

The cold leg requirements are greater than the hot leg requirements with regard to leak rate and pullout resistance (See Table 9-1).

It is important to note that all of the evaluations performed considered the tube to be severed at the reassigned pressure boundary location with no resistance to flow from the leak path within the tube itself, i.e., cracks. At the specified depths the crack flanks would be restricted from opening or parting, and may be held tighter, thus reducing the accident condition leak to below that anticipated herein.

With regards to the preparation of a significant hazards determination, the results of the testing and analyses demonstrate that the relocation of the pressure boundary to a depth based on the more conservative of either H* or B* does not lead to an increase in the probability or consequences of the postulated limiting accident conditions because the margins inherent in the original design basis are maintained and the expected leak rate during the postulated accident is not expected to increase beyond the plant-specific limit. In addition, the relocation of the pressure boundary does not create the potential for a new or departure from the previously evaluated accident events. Finally, since the margins inherent in the original design bases are maintained, no significant reduction in the margin of safety would be expected.

The zone specific inspection depths which are justified in this WCAP provide an overall high level of conservatism based on multiple conservative assumptions in the modeling, some of which are additive

inputs (the following items 3, 4, and 5) to the margins from actual material limits. The significant conservative assumptions are summarized in the following numbered paragraphs:

1. The H* and B* values are inherently conservative due to the overestimate of tubesheet deflection, as incorporated into these evaluations with use of the divider plate factor of 0.64. In actuality, tubesheet deflection would be resisted to an even greater extent by (a) the divider plate and welds even if cracked, and (b) the stiffening effect of the tubes being expanded into the tubesheet (detailed discussion on pages 5-3 and 5-12).

2. The evaluations assume that all tubes in all steam generators are separated from the tube end section below the justified inspection region on both hot leg and cold leg sides due to 100% through wall cracks for the 360 degree circumference of the tubes in the bundle (detailed discussion on page 5-1).

3. The holding strength of the tube-to-tubesheet joint when the tube-to-tubesheet end weld is assumed to be not present is based on conservative empirical tube pullout test results. The test results used were only the data obtained at room temperature, which is conservative with respect to tube expansion into the tubesheet at operating temperature resulting in increased pullout force (detailed discussion in Appendix A, response to Wolf Creek NRC RAI #1).

4. The crevice pressure interpretation in the White Paper (Reference 21) is conservative and focuses on the limiting operating conditions and how to apply them to result in the greatest impact on contact pressure (detailed discussion on page 5-11 and Appendix B of this report).

5. The determination for the H* and B* lengths for each zone are conservatively chosen to bound all tubes in the zone and are based on a conservative sensitivity study (detailed in the Vogtle Units 1 and 2 Response to Wolf Creek NRC RAI No. 2 included in Appendix A of this report).

9.2 EXAMPLE APPLICATION FOR VOGTLE 1 & 2

This document provides a technical justification for limiting the RPC inspection in the tubesheet expansion region to less than the full depth of the tubesheet (21.03 in). The justification includes two necessary parts to satisfy both the structural requirements and the leakage requirements under normal operating conditions and under limiting accident conditions:

- H* addresses the structural requirements. H* defines the minimum length of engagement required for hydraulically expanded tubes to prevent tube pullout from the tubesheet under limiting accident conditions. The principal loads acting to pull a tube from the tubesheet are end-cap loads resulting from the primary-to-secondary pressure differentials. H* varies with radial position from the tubesheet centerline due to tubesheet bow resulting from the primary-to-secondary pressure differential. The bow increases during accident conditions due to a greater pressure differential across the tubesheet. Increased tubesheet bow causes tube-hole bore dilation above the neutral axis resulting in reduced interface loads between the tube and the tubesheet. Tubesheet bending varies with the radial distance from the centerline of the tubesheet as dictated by the structural constraints of the tubesheet, e.g., shell and support ring on the OD and divider plate [if assumed functional] at the centerline.

- B* addresses leakage requirements. As defined in this document, B* is the distance from the top of the tubesheet where the leakage flow resistance at SLB conditions equals the leakage flow resistance at normal operating conditions. B* is the length of engagement in the tubesheet needed for the leak rate during a postulated SLB event to be bounded by a specified multiple of the leak rate during normal operation. This definition of B* is useful in that the accident leakage will be equal to the ratio of the accident pressure differential to the normal operating pressure differential times the normal operating leakage. In effect, the normal operating leakage becomes a "bellwether" for the accident leakage; therefore, if normal operating leakage is within acceptable limits, accident-induced leakage will also be within acceptable limits.

The Technical Specification allowable normal operating leak rate for Vogtle Units 1 & 2 is 150 gpd (0.1 gpm) in accord with NEI 97-06 and TSTF-449, References 7 and 34 respectively, and the allowable accident-induced leak rate is 0.35 gpm total in the affected SG. The SLB differential pressure is a factor of 2, or less, greater than the NOp differential pressure depending on the plugging status of the SGs at Vogtle Units 1 and 2. The accident-induced primary-to-secondary differential pressure is never more than a factor of 2 greater than the normal primary-to-secondary operating differential pressure. Therefore, if the current NOp leakage is at its limiting value, 0.1 gpm, the accident-induced leakage will not exceed 0.2 gpm, a factor of 1.96, or greater, less than its allowable value if the bounding values of H* and B* are applied. Recall that this does not include consideration of the reduction in flow associated with an increase in viscosity as the temperature decreases.

A summary of the H* and B* required engagement depths is provided in Table 9-1. The following observations can be made from the information in the table and on Figure 9-1 for the hot leg and on Figure 9-2 for the cold leg relative to example application:

1. Using the maximum hot leg H* depth of 13.38 inches as a governing inspection depth would be sufficient to address all hot leg considerations for both structural and leak rate integrity. The H* value of 13.38 inches assumes that the divider plate-to-stub runner weld is non-functional in the Vogtle Unit 1 and 2 steam generators.

2. The H* distances are limiting over the B* distances at every radial location in the Vogtle 1 & 2 steam generators.

3. An inspection plan that accounts for the change in H* distance as a function of radius appears to be worthwhile.

9.3 PLANNED VOGTLE APPROACH FOR TUBESHEET REGION ALTERNATE REPAIR CRITERIA

This WCAP provides justification for eliminating the inspection and plugging requirements for the tube ends on the hot leg side in the Vogtle steam generator tubing. The WCAP justification establishes the required lengths to meet the structural and leakage criteria as described with the lengths being determined using the H* and B* analyses. The planned Vogtle approach is to bound the H* and B* analyses with inspection and plugging requirements to a depth of 17 inches into the tubesheet, as measured from the top of the tubesheet for the hot leg side of the tube bundle only. The planned Vogtle approach does not

adversely affect compliance with the H* and B* requirements and other associated conclusions as described in Sections 9.1 and 9.2.

Additional conservative margin from that described in Items 1 through 5 in Section 9.1 above results from the approach planned for Vogtle 1 & 2 of extending the inspection requirements down to a depth of 17 inches from the top of the HL tubesheet. The significant assumptions and associated conservative margins are summarized in the following paragraphs:

1. There is additional increase in contact pressure below the zone specific B* depths which is not accounted for in the B* analyses. The B* analyses did not take credit for the increase in contact pressure on the leak rate through the postulated tube cracks within the tubesheet below the B* depth (detailed discussion on page 6-4, graphical representation of extra margin across the tubesheet is provided in Figure 9-1 and Figure 9-2).

2. The planned approach for Vogtle 1 & 2 provides additional margin of safety because inspection and plugging requirements will continue to apply to the tube extent between the depths justified in the WCAP and the 17 inch depth into the HL tubesheet.

3. The B* depths assure that accident leakage will remain within 2 times any operating leakage which is occurring from within the tubesheet region. With inspection and plugging requirements to a 17" depth on the HL side, any leakage from below the required depth of 17" must leak through a tortuous path of a total length which significantly exceeds the B* depth (graphical representation of extra margin across the tubesheet is provided in Figure 9-1 and Figure 9-2).

4. The integration of Items 1-3 above is addressed in this paragraph. With the inspection and plugging requirements being applicable to a depth of 17 inches from the top of the tubesheet on the hot leg side, tube integrity to the 17 inch depth is assured. Any accident leakage from below the 17" depth must go through a greater distance tortuous leak path with tube-to-tubesheet contact pressures higher than those assumed in the WCAP justification. Given that by definition, the B* depth ensures that accident leakage coming from the tubesheet region will remain within 2 times any operating leakage, the depth difference between the B* depth and the 17 inch depth will result in an overall significantly greater leakage resistance than that modeled in the B* analyses, therefore leakage potential will be less with the requirements being applicable to a depth of 17 inches.

Table 9-1 Calculated H* & B* Depths by Radial Zone

Location		H* Depths		B* Depths	
Zone	Radius	Hot Leg	Cold Leg	Hot Leg	Cold Leg

a,c,e

a,c,e

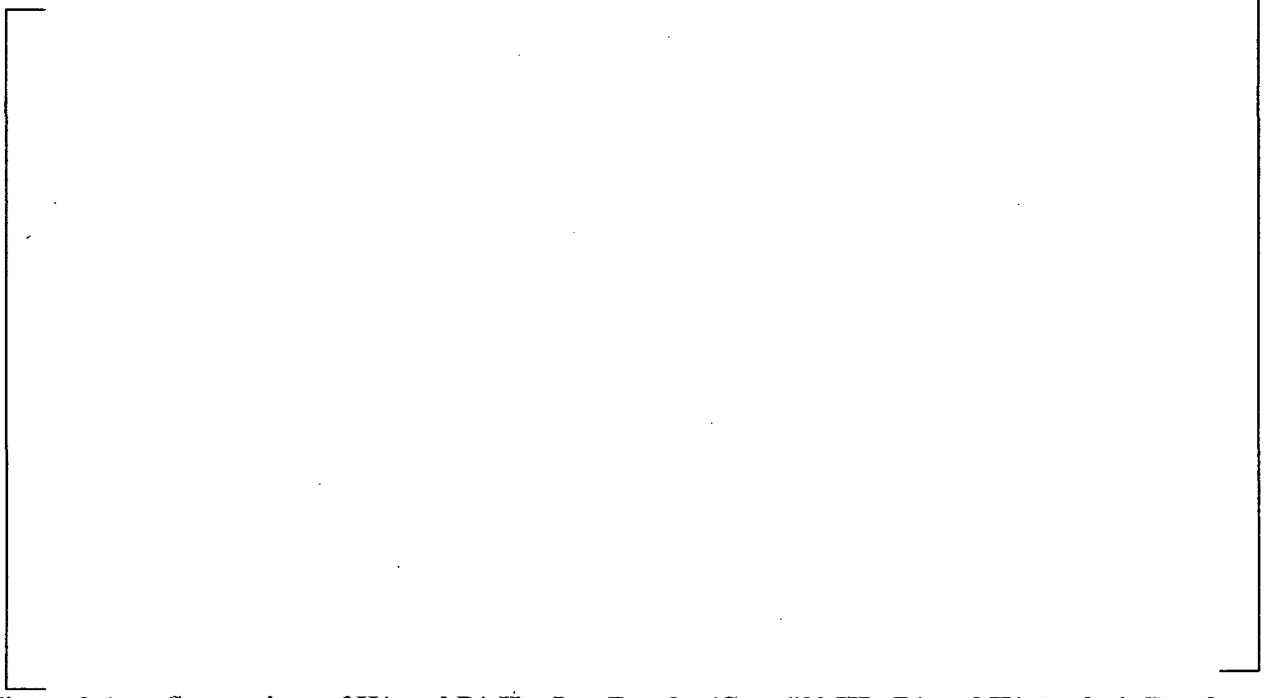

Figure 9-1 Comparison of H* and B* Hot Leg Results (Case #89 HL, B* and H* Analysis Results for Model F Hot Leg Stacked Input Case. [

]^{a,c,e})

a,c,e

[

Figure 9-2 Comparison of H* and B* Cold Leg Results (Case #89 CL, B* and H* Analysis Results for Model F Hot Leg Stacked Input Case. [

]^{a,c,e})

10 REFERENCES

1. OE19662 (Restricted & Confidential), "Steam Generators (Catawba Nuclear Power Station)," Institute of Nuclear Power Operations (INPO), Atlanta, GA, USA, December 13, 2004.

2. IN 2005-09, "Indications in Thermally Treated Alloy 600 Steam Generator Tubes and Tube-to-Tubesheet Welds," United States Nuclear Regulatory Commission, Washington, DC, April 7, 2005.

3. SGMP-IL-05-01, "Catawba Unit 2 Tubesheet Degradation Issues," EPRI, Palo Alto, CA, March 4, 2005.

4. OE20339, "Vogtle Unit 1 Steam Generator Tube Crack Indications," Institute of Nuclear Power Operations (INPO), Atlanta, GA, USA, April 4, 2005.

5. ASME Boiler and Pressure Vessel Code, Section III, "Nuclear Power Plant Components," American Society of Mechanical Engineers, New York, New York, 1971, Summer 1972 Addenda.

6. GL 2004-01, "Requirements for Steam Generator Tube Inspections," United States Nuclear Regulatory Commission, Washington, DC, August 30, 2004.

7. NEI 97-06, Rev. 2, "Steam Generator Program Guidelines," Nuclear Energy Institute, Washington, DC, May 2005 (issued for use by NEI on September 2, 2005 and confirmed by the NRC staff as complying with TSTF-449 on October 3, 2005). Implementation is mandatory by March 2, 2006.

8. PCWG-05-49, "Vogtle Units 1 & 2 (GAE/GBE): Approval of Category III (for Contract) PCWG Parameters to Support a 2% Measurement Uncertainty Recapture (MUR) Uprate," November 18, 2005.

9. WCAP-14871 (Proprietary), "Vogtle Electric Generating Plant (VEGP) Steam Generator Tube-to-Tubesheet Joint Evaluation," Westinghouse Electric, Pittsburgh, PA, May 1997.

10. WCAP-16145 (Proprietary), "Justification for the Partial-Length Rotating Pancake Coil (RPC) Inspection of the Tube Joints of the Vogtle Units 1 & 2 Model F Steam Generators," Westinghouse Electric Company LLC, Pittsburgh, PA, October 2003.

11. NCE-88-271 (Proprietary), "Assessment of Tube-to-Tubesheet Joint Manufacturing Processes for Sizewell B Steam Generators Using Alloy 690 Tubing," Westinghouse Electric, Pittsburgh, PA, November 1988.

12. WNET-180 (Proprietary), Volume 11, "Model F Steam Generator Stress Report," Westinghouse Electric, Pittsburgh, PA, September 1980.

13. WCAP-15932-P (Proprietary), Rev. 1, "Improved Justification of Partial-Length RPC Inspection of the Tube Joints of Model F Steam Generators of Ameren-UR Callaway Plant," Westinghouse Electric Company LLC, Pittsburgh, PA, May 2003.

14. ASME Boiler and Pressure Vessel Code Section III, "Rules for Construction of Nuclear Power Plant Components," 1989 Edition, The American Society of Mechanical Engineers, New York, NY.

15. Porowski, J. S. and O'Donnell, W. J., "Elastic Design Methods for Perforated Plates," Transactions of the ASME Journal of Engineering for Power, Vol. 100, p. 356, 1978.

16. Slot, T., "Stress Analysis of Thick Perforated Plates," PhD Thesis, Technomic Publishing Co., Westport, CN 1972.

17. Computer Program WECAN/Plus, "User's Manual," 2nd Edition, Revision D, Westinghouse Government Services LLC, Cheswick, PA, May 1, 2000.

18. SM-98-102 (Proprietary), Rev. 2, "Tube/Tubesheet Contact Pressures for Yonggwang 2," Westinghouse Electric, Pittsburgh, PA, November 1998.

19. STD-TP-1997-7951, Rev. 1, "Vogtle-1 SG 4 Tube-to-Tubesheet Joint Evaluation (Hydraulic Expansion Only to Determine Leakage and Loading Resistance)," Westinghouse Electric, Pittsburgh, PA, May 19, 1997.

20. CN-SGDA-03-99 (Proprietary), "Evaluation of the Tube/Tubesheet Contact Pressures for Wolf Creek, Seabrook, and Vogtle 1&2 Model F Steam Generators," Westinghouse Electric Company LLC, Pittsburgh, PA, September 2003.

21. LTR-SGDA-07-4, Rev. 3 (Proprietary), "Letter Summary of Changes to B* and H* Analysis due to New Crevice Pressure and Divider Plate Data," Westinghouse Electric Company LLC, Pittsburgh, PA, September 24, 2007.

22. Terakowa, T. Imai, A., Yagi, Kazushige, Fukada, Y., Okada, K., "Stiffening Effects of Tubes in Heat Exchanger Tubesheet," Journal of Pressure Vessel Technology Transactions, ASME Vol. 106, No. 3, August 1984.

23. CN-SGDA-02-152 (Proprietary), Rev. 1, "Evaluation of the Tube/Tubesheet Contact Pressures for Callaway Model F Steam Generators," Westinghouse Electric Company LLC, Pittsburgh, PA, March 2003.

24. Drawing 1511E64 (Proprietary), "Steam Generator Model F Tubing and Anti-Vibration Bar Assembly," Westinghouse Electric, Pittsburgh, PA, March 1979.

25. Process Specification 81013 RM (Proprietary), Revision 9, "Hydraulic Tube Expansion," Westinghouse Electric, Pittsburgh, PA, August 1, 1980.

26. CN-SGDA-03-133 (Proprietary), Rev. 0, "Evaluation of the H* Zone Boundaries for Specific Model D-5 and Model F Steam Generators," Westinghouse Electric Company LLC, Pittsburgh, PA, October 2003.

27. CN-SGDA-03-121 (Proprietary), "H* Ligament Tearing for Models F and D5 Steam Generators," Westinghouse Electric Company LLC, Pittsburgh, PA, October 2003.

28. EPRI Tube Integrity Tools Theory Manual, Final Report, May 2006.

29. LTR-SGDA-06-108 (Proprietary), "Data and Analysis Methodology in Support of Axial Ligament Tearing Model," Westinghouse Electric Company LLC, Pittsburgh, PA, June 29, 2006.

30. LTR-CDME-07-74 (Proprietary), "Identification of Wolf Creek Unit 1 Microsoft Excel Spreadsheets and Analysis Tools Supporting LTR-CDME-07-72-P Attachment," Westinghouse Electric Company LLC, Pittsburgh, PA, April 2007.

31. NRC Letter, "Vogtle Electric Generating Plant, Units 1 and 2, RE: Issuance of Amendments Regarding the Steam Generator Tube Surveillance Program (TAC Nos. MC8078 and MC8079)," United States Nuclear Regulatory Commission, Washington, DC, September 21, 2005.

32. NRC Letter, "Braidwood Station, Units 1 and 2 – Issuance of Exigent Amendment Re: Steam Generator (SG) Tube Surveillance Program (TAC No. MC6757)," United States Nuclear Regulatory Commission, Washington, D.C., April 28, 2005.

33. LTR-CDME-07-96, Rev. 3 (Proprietary), "Technical Support and Reference Listing for Vogtle Alternate Repair Criteria Analysis," Westinghouse Electric Company LLC, Pittsburgh, PA, October 2007.

34. TSTF-05-05, "TSTF-449, Revision 4, 'Steam Generator Tube Integrity'," Technical Specifications Task Force, administered by Excel Services Corporation, 11921 Rockville Pike, Rockville, MD, April 14, 2005.

35. STD-DP-1997-8015, Rev. 0, "Data Package for Leak Testing of Vogtle Unit 1 Steam Generator Tube to Tubesheet Joint Per STD-TP-1997-7951, Rev. 1," Westinghouse Electric, Pittsburgh, PA 6/18/97.

36. WCAP-16736-P, "Vogtle Electric Generating Plant Measurement Uncertainty Recapture Power Uprate Program Licensing Report," Westinghouse Electric Company LLC, Pittsburgh, PA February 2007.

37. LTR-CDME-07-72, "Response to NRC Request for Additional Information Relating to LTR-CDME-05-209-P of the Wolf Creek Generating Station (WCGS) Permanent B* License Amendment Request," Westinghouse Electric Company LLC, Pittsburgh, PA April 24, 2007.

38. Divider Plate Cracking in Steam Generators: Results of Phase 1: Analysis of Primary Water Stress Corrosion Cracking and Mechanical Fatigue in the Alloy 600 Stub Runner to Divider Plate Weld Material. EPRI, Palo Alto, CA:2007. 1014982.

39. LTR-CDME-07-198, "Response to NRC Request for Additional Information Relating to LTR-CDME-07-72 P-Attachment and LTR-CDME-05-209-P of the Wolf Creek Generating Station (WCGS) Permanent B* License Amendment Request," September 25, 2007.

40. CN-SGDA-06-28, "Steam Generator Design Pressure Evaluation for Vogtle Units 1 and 2 4.5% Uprate and MUR Uprate," Rev. 0.

41. Regulatory Guide 1.121 (Draft), "Bases for Plugging Degraded PWR Steam Generator Tubes," United States Nuclear Regulatory Commission, Washington, DC, August 1976.

APPENDIX A
RESPONSES TO RECENT NRC RAI RELATED TO H*/B* FOR VOGTLE UNITS 1 AND 2

A.1 BACKGROUND DISCUSSION

Wolf Creek Nuclear Operating Corporation (WCNOC) submitted a license amendment request on February 21, 2006 proposing changes to the Technical Specifications for the Wolf Creek Generating Station. The proposed changes were to revise the Technical Specification to exclude portions of the steam generator tube from the top of the tubesheet in the steam generators from periodic tube inspections based on the application of structural analysis and leak rate evaluation results to re-define the primary-to-secondary pressure boundary. The NRC staff provided an initial Request for Additional Information (RAI) on June 27, 2006. Subsequently, a second NRC staff RAI was received by WCNOC via electronic mail on June 22, 2007. The purpose of this Appendix is to provide responses to the second set of NRC RAI that directly impact the Vogtle Units 1 and 2 H*/B* analysis. Responses to certain NRC RAI were not given when the RAI were judged to represent points of clarification related solely to the WCNOC submittal or points of clarification related to Reference A.1 (which is included as Appendix B to this report). The impact of the first Wolf Creek NRC RAI was already considered in the text of this report.

A.2 NRC RAI RESPONSES

A total of 36 questions were received on the second NRC RAI on the Wolf Creek Generating Station of which 29 were related to the development of the alternate repair criteria. Of these 29 questions, answers to 11 (RAI Question Nos. 1, 2, 4, 5, 8, 9, 10, 11, 16, 17, 18) of the questions pertain directly to Vogtle Units 1 and 2 and responses are provided below.

Wolf Creek NRC RAI No. 1

1. *Reference 1, Enclosure I, Table 6-4 - Are the listed F/L, force per length, values correct? If so, please describe in detail how they were calculated. If not correct, please provide all necessary revisions to the H* analysis results. [For Byron 2, Braidwood 2, and Seabrook, F/L is calculated as follows:*

   F/L = (Pull Force/specimen length) x (net contact pressure/total contact pressure)

   A consistent approach for Wolf Creek (based on allowing 0.25 inch slip) would yield F/L values on the order of 200 pounds per inch (lb/inch) rather than 563 lb/inch as shown in the Table.]

Vogtle Units 1 and 2 Response to Wolf Creek RAI No. 1

There have been two approaches to calculating the F/L value using the empirical test data. The first involves a basic calculation using first principles and the second involves a model based on the theory of elasticity. Although the equation for calculating F/L is not the same as noted in the question, the first principles method yields the same value.

The following response details the two methods that have been used for calculating the ratio F/L. Following the explanation of the methods, F/L is recalculated for Vogtle Units 1 and 2 using the method that is consistent with that used for Byron 2, Braidwood 2, etc. The values provided in Reference A.2 are believed to be correct based on application of the theory of elasticity; however, for consistency with prior

submittals of H*/B*, the recalculation based on first principles was performed, and is now the basis for the technical justification of H*/B* for Vogtle Units 1 and 2.

The pullout force for the Model D5, Model 44F and Model 51F SGs used the following formula to calculate the contact pressure (P_c), based on the first principles approach:

a,c,e

[ )]

(1)

Next, an average value minus one standard deviation value (-1σ) is determined for contact pressure based on the measured pullout force data. The F/L values, in units of lbf/in are calculated using the formula:

a,c,e

[ ]

(2)

The theory of elasticity model was used to calculate the residual contact pressure and the pullout force for the Vogtle Units 1 and 2 Model F steam generators, reflecting the advance in the state of this analysis compared to prior application such as Seabrook, Byron and Braidwood.

Using the theory of elasticity model:

The listed value of 522.3 lb_f/in. is correct.

The values are based on 0.25 inch slip pullout test data and contact pressures that were calculated using the theory of elasticity:

a,c,e

[ ]

a,c,e

[ ]

The value for *Po* is calculated for each test using a coefficient of friction of 0.3.

a,c,e

[ ]

The average *F/L* value is then calculated using the equation:

a,c,e

[ ] (3)

where:

a,c,e

[ ]

The theory of elasticity model was chosen because there is a decrease in the contact pressure between the tube and the tubesheet due to Poisson's contraction of the tube in response to the application of the axial end cap load. Conversely, an increase in the contact pressure would result from the application of an axial load tending to push on the tube; a push load arises from pressure on the crack flanks in operation. (Assuming a 360° throughwall crack.) The decrease in contact pressure results in a radial inward springback of the tubesheet and a radial outward springback of the tube outside radius. Resistance to pullout of the tube is manifested as a shear stress from the contact pressure between the tube and the tubesheet. The pullout resistance incrementally decreases along the interface as the axial load is applied. Not all of the axial load is transmitted downward into the tubesheet because of the resistance provided by the shear stress, thus the Poisson contraction is progressively less with distance into the tubesheet. The complex theory of elasticity model is required to properly describe the complicated relationship between the deformations of the tube and the tubesheet.

The load carrying capability of a joint, F, was calculated by considering a force equilibrium for a short cylindrical element of the tube to establish a differential equation involving axial stress and net contact pressure. Compatibility and force deformation relations were then used to express the contact pressure as a function of depth in the tubesheet resulting in a first order differential equation (DE). When the contact pressure is constant the DE is homogeneous. When the contact pressure is a function of depth into the tubesheet the DE is not homogeneous. By considering the initial contact pressure to be linear (i.e., a constant slope) through the tubesheet, a linear first order DE results.

The theory of elasticity method used to calculate the residual contact pressure and pullout force for the Vogtle Units 1 and 2 Model F SGs is different from the calculation of the residual contact pressure and pullout forces in the Model D5 and Model 44F H*/B* submittals. In order to be consistent with prior H*/B* submittals, the following empirically based approach for determining residual contact pressure and joint pullout force is applied: This approach will be consistent with the calculations described in prior submittals for Model D5 and Model 44F (i.e., the first principles approach) and will bound the empirical data available.

Note that only room temperature data will be used to determine tube resistance to pullout so that temperature effects do not have to be subtracted out from the test data. This is conservative because the value of mean – 1 σ bounds essentially all of the data points as shown in Figures A-1, A-2 and A-3, below.

The room temperature F/L values are calculated by taking the pullout force for each specimen test result and dividing it by the expansion length. The following data will be used to derive the Vogtle Units 1 and 2 Model F steam generator tube joint resistance to pullout (F/L) and residual contact pressure values (Source: Test Numbers 1 through 8 of Table 4-5 of this report):

a.c.e

Test No.	Specimen No.	Expansion Length (in.)	Pull Force (lbf/in)	Contact Pressure[1] (psi)	F/L (lbf/in)[2]

The resulting force per length number for the Vogtle Units 1 and 2 Model F steam generators is the mean minus one standard deviation value for force per unit length and is [ ]^{a,c,e} This number is conservative and remains below all of the room temperature pullout data. See Figure A-1 below.

a.c.e

Figure A-1 Tube Pullout Force Plot – Model F SGs

A comparison of the pullout forces per length values for all Model D5, 44F, and F steam generators using this same methodology is provided in the table below:

a,c,e

Room Temperature Tube Pullout Force (F/L) Values		
Model Steam Generator	**Original Pullout Force Value (lbf/in)**	**Revised Pullout Force value (Lbf/in)**

The revised joint pullout force value of [ ]^{a,c,e} for the Vogtle Units 1 and 2 steam generators will be factored into the response to NRC RAI question number 2. Similar plots of the room temperature pullout data are provided below for the Model D5 and 44F steam generators in Figures A-2 and A-3 for information only.

a,c,e

Figure A-2 Tube Pullout Force Plot – Model D5 SGs

a,c,e

Figure A-3 Tube Pullout Force Plot – Model 44F Data

It is important to note that the use of room temperature only data does not significantly change the previous values for pullout force used for the Model D5 and Model 44F for which both room temperature and elevated temperature data were considered.

Wolf Creek NRC RAI No. 2

2. *Reference 2, Enclosure I, Response to RAI questions 1 and 2 - provides the sensitivity of contact pressure to many of the material and geometric parameters used in the analyses. The response provides only a qualitative assessment of these sensitivities to support the conclusion that the values assumed in the H* analyses support a conservative calculation of H*. For example, the sensitivity study showed that contact pressure is sensitive to the yield strength of the tubing. The response states that the yield strength of the tubing used in the pullout test specimens was higher than the documented mean yield strength for prototypical tubing material, but did not indicate to what extent the yield strength of the test material bounds the range of prototypic yield strength variability. Thus, the staff has no basis to agree or disagree with the conclusion that test specimen contact pressures are conservatively low. The steam generators contain up to 5620 tubes, and it needs to be demonstrated that the computed H* distances are conservative for all the tubes, not simply the average tubes or 95% of the tubes. Please provide a quantitative assessment demonstrating that the assumed values of the material and geometric parameters support a conservative H* analysis for all tubes. This assessment should consider thermal expansion coefficient (TEC) for the tube and tubesheet in addition to the parameters included in the Reference 2 response.*

Vogtle Units 1 and 2 Response to Wolf Creek NRC RAI No. 2

The following sources of potential variability were identified and the impact on H*/B* distances of varying these parameters has been quantified (Reference A.3):

a,c,e

[

]

Only six (6) of these must be addressed numerically in the uncertainty study for H*/B*, and only five (5) of these affect the residual contact pressure for hydraulic expansion. The remaining three variables (Hydraulic Expansion Pressure, Strain Hardening, Tube Outer Diameter) are inherently modeled in the analysis process and do not require independent variation and are discussed below. The greatest potential quantitative impacts on the H*/B* distances are the result of tolerances in [

]a,c,e

Analysis Approach

Three approaches were considered for combining the uncertainties associated with determining the H*/B* distances. The three approaches considered are defined in Reference A.4 and they are:

Arithmetic strategy
Simplified statistical strategy
Monte Carlo strategy

Only the arithmetic strategy and simplified statistical methods were used to combine the uncertainties for the sensitivity study discussed below. This is the case because the arithmetic approach to combining uncertainties is expected to provide conservative results relative to both the simplified statistical and the Monte Carlo approaches. Moreover, the simplified statistical and Monte Carlo results typically provide similar results when it is assumed that the independent variables are normally distributed (as is the case with the parameters discussed above).

The method discussed below is a modified arithmetic strategy were the parameters were combined using at least a mean plus/minus one standard deviation value, whichever results in the greatest increase in H* distance. The method for combining the uncertainties is defined as a "stacked model" because all of the identified uncertainties are superimposed in a conservative direction.

The simplified statistical method result for combining uncertainties is provided in the discussion below but the explanation of the method for combining the uncertainties is not because the method is entirely consistent with that described in Section 7.3.5.2 of Reference A.4.

The sensitivity study is divided into two parts:

1. An evaluation of those variables which affect the residual contact pressure due to tube expansion. Only five (5) of the nine (9) listed parameters directly affect the residual contact pressure used in the analysis of the Model F tubesheet joint. The applicable parameters do not include the uncertainty in the tube TEC and tubesheet TEC, tube outer diameter and tubesheet hole size.

2. An evaluation of, those variables which affect the contact pressure developed between the tube and the tubesheet during all plant operating conditions.

The uncertainty in all of the parameters above is considered in a sensitivity study. The maximum contribution from hydraulic expansion to tube-to-tubesheet contact pressure is calculated to be [ ]^{a,c,e} This is the mean minus 1σ value based on the equation in the response to RAI No. 1. The contribution of residual contact pressure to tube pullout resistance is small compared to the contribution from differential thermal expansion between the tube and the tubesheet, internal pressure, and tubesheet bow (depending on tube radial location and elevation in the tubesheet).

The steam generator tube integrity acceptance criterion for the sensitivity study is cited on page 20 of the Reference A.5. The conditional probability noted in DG-1074 states that "burst of one or more tubes under postulated accident conditions shall be limited to 1.0E-2." The 1.0E-2 value is 40% of the limiting 0.025 value described in Reference A.5. This value is conservatively used as an acceptable probability for combining uncertainties for the critical parameters identified above to calculate H* and B* distances. For the calculation of the H*/B* distances, this value represents the probability that the performance criteria of Reference A.6 will not be met and, in this application, does not represent the probability of a steam generator tube rupture event. Tube burst is prevented by the constraint provided by the tubesheet, and the probability of tube pullout or excessive leakage during accident conditions will be considerably lower because the analysis for H*/B* already assumes a factor of 3 on the normal operating pressure differential. The calculation of a probability smaller than the acceptance criterion of 1.0E-2 supports the technical specification requirement that all tubes have adequate margin against burst (or tube pullout).

The empirical rule is used to assign a probability to each individual parameter, assuming a normally distributed population, given the mean and standard deviation of the data set. The empirical rule states that for a normal distribution:

68% of the data will fall within 1 standard deviation of the mean.
95% of the data will fall within 2 standard deviations of the mean.
Almost all (99.7%) of the data will fall within 3 standard deviations of the mean.

This translates into a probability of 0.16 of varying from the mean value by +/- one standard deviation. The probability of varying by +/- two standard deviations is 0.025. And, likewise, the probability of varying by 3 standard deviations is 0.0015.

A "stacked" model of the uncertainties is used to determine a limiting combination of H*/B* distances. The model is considered to be a "stacked" model because all of the uncertainties are superimposed simultaneously in a conservative direction (i.e., a direction that results in the greatest H*/B* distances). The combination of uncertainties on the variables that result in an acceptably low probability closest to the acceptance criterion of 0.01 is used. Each of the parameters evaluated are assumed to be independent of each other. This is a valid assumption because no functional relationship exists between component dimensions and material properties, nor among the individual material properties noted above. The probability (Φ) that the "stacked" model H* /B* distances will not meet the performance criteria of Reference A.6 is calculated using the equation:

a,c,e

The parameters considered in the analysis that affect residual contact pressure are addressed below. Figure 6-13 of Reference A.3 presents a normalized sensitivity analysis for various parameters based on an FEA study for hydraulic expansions performed at approximately 40 ksi. This sensitivity study is considered to also apply to the Vogtle Units 1 and 2 SGs whose tube expansions were performed at pressures between 30 ksi and 33 ksi.

In the context of this sensitivity analysis, an increase in the H* or B* distance means that the required inspection depth into the tubesheet, relative to the top of the tubesheet, increases. A decrease in the H* or B* distance means that the required inspection depth into the tubesheet, relative to the top of the tubesheet, decreases. The discussion below describes the effect on the H* and B* analysis from a variation of each parameter. Table A-1 summarizes the discussion and provides a view of relative sensitivities.

These results are based on more than 100 individual sensitivity studies to determine the most limiting parameters and trends in the sensitivity of the H* and B* criteria to variations in the input parameters.

The following lists the parameters in order of greatest to smallest effect on the H* distance.

a,c,e

Similarly, the following lists the parameters in order of greatest to smallest effect on the B* distance.

[ ]^{a,c,e}

The magnitude of the variability of each parameter was altered based on its importance to the H* and B* criteria. The term "greatest effect" in this context means that a variation in that parameter caused a larger difference in the final value of H* or B* than the next lower ordered parameter. For example, varying the [

]^{a,c,e}

Variables not Addressed Independently

As shown in Figure 6-13 in Reference A.3, three other variables can affect residual contact pressure. These are [

]^{a,c,e}

1. The impact of initial radial clearance between the tube and the tubesheet is not directly modeled in the H*/B* analysis but is accounted for by variation of the tube OD and the tubesheet hole ID. Figure 6-13 of Reference A.3 is based on [

]^{a,c,e}

Impact of the Variability of [ ]^{a,c,e}

The uncertainty on [

]^{a,c,e} and ultimate strength properties are evaluated and summarized by tube size and type of heat treatment. Material certifications for thermally treated Inconel 600 steam generator tubing produced by Westinghouse were evaluated to obtain material strength properties. Yield strength (S_y), ultimate strength (S_u) have been analyzed to obtain mean values, standard deviations and lower bound tolerance limit strength properties. The following table is information for 11/16 inch diameter A600TT tubes excerpted from Reference A.9.

a,c,e

[

]

The variation in yield strength can be factored into the H*/B* analysis at room temperature conditions by referring to Figure 6-13 of Reference A.3. It is shown in Figure 6-13 that [

]^{a,c,e}

Impact of the Variation of [ ]^{a,c,e}

Similarly, the variation in [

]^{a,c,e}

[

]a,c,e

Impact of [ ]a,c,e

Based on Reference A.3, dimensional data for [

]a,c,e

Impact of [ ]a,c,e

In solid mechanics, [

]a,c,e

Impact of [ ]a,c,e

A calculation was performed using the [

]a,c,e

The values for the various parameters for the stacked model are included in the table below. The stacked model includes the variability of each parameter and the results of a series of sensitivity studies to determine the worst case, or maximum effect, on the H* and B* analysis. For example, the effect of varying the [ ]a,c,e

[

]^{a,c,e}

The probability (Φ) that the stacked model H*/B* distances will not meet the performance criteria of NEI 97-06, Rev. 2 (Reference A.6) is determined to be:

a,c,e

[

]

= 2.6E-6.

0.01 >> 2.6E-6

This probability compares favorably with the acceptance criterion of 1.0E-2 which is *conservatively* based on the conditional probability of tube burst for one or more tubes under accident conditions.

Table A-1 Stacked Model Parameters and Corresponding Uncertainties

Parameter Varied	Definition of Uncertainty Used	Input Parameter Value	Probability of Occurrence

a,c,e

The revised values for H*/B* using the parameters from the stacked model analysis are provided in Tables A-2 and A-3 below. Table A-2 includes the hot leg results; Table A-3 includes the cold leg results. The combined probability term included in Tables A-2 and A-3 below includes a probability of:

a,c,e

[ ]

The divider plate factor used in each case is taken from EPRI Report 1014982; Divider Plate Cracking in Steam Generators; Phase 1 Report, Reference A.12. The probability associated with each divider plate factor is based on engineering judgment and the relative few divider plate cracking indications reported even after long periods of operation and repeat inspections in the French SGs.

The H*/B* results are plotted in Figures A-4 through A-7 below. Figures A-4 and A-5 provide the hot leg results. Figures A-6 and A-7 provide the cold leg results.

Table A-2 Hot Leg Result Summary for B* and H* Using Stacked Worst Case Property Input Values

[

Case #	TEC Source	Combined Probability	Divider Plate Factor	Max. H* (in.)	Max. B* (in.)

] a,c,e

Table A-3 Cold Leg Result Summary for B* and H* Using Stacked Worst Case Property Input Values

[

Case #	TEC Source	Combined Probability	Divider Plate Factor	Max. H* (in.)	Max. B* (in.)

] a,c,e

HOT LEG RESULTS

a,c,e

Figure A-4 Case #89, B* and H* Analysis Results for Model F Hot Leg Stacked Input Case.
[

][a,c,e]

a,c,e

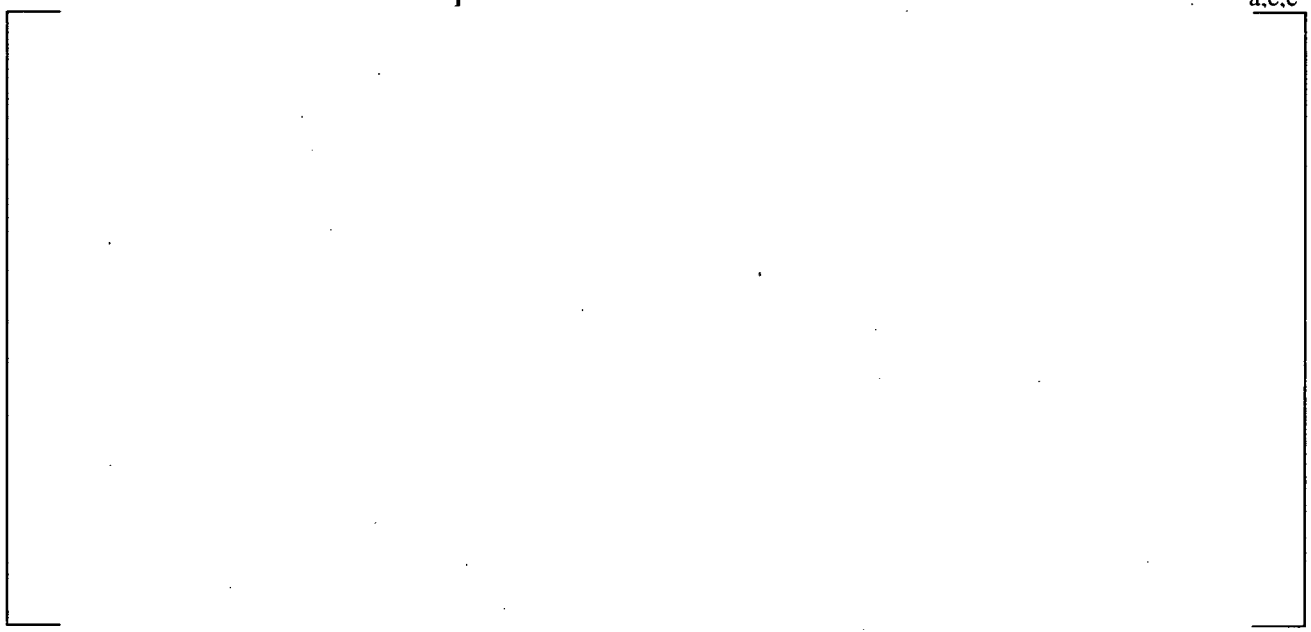

Figure A-5 Case #92, B* and H* Analysis Results for Model F Hot Leg Stacked Input Case.
[

][a,c,e]

COLD LEG RESULTS

a,c,e

[

]

Figure A-6 Case #89, B* and H* Analysis Results for Model F Cold Leg Stacked Input Case.
[

][a,c,e]

a,c,e

Figure A-7 Case #92, B* and H* Analysis Results for Model F Cold Leg Stacked Input Case. [

]a,c,e

The results of the sensitivity study show that the H* distance remains the limiting criterion for establishing the inspection depths in the Vogtle Units 1 and 2 steam generators at every radial location. The cold leg H* distances also continue to be more limiting than the hot leg distances.

For the hot leg, the required H* distance is 13.38 inches from the top of the tubesheet. (Case #89)
For the cold leg, the required H* distance is 14.71 inches from the top of the tubesheet. (Case #89)

These values include the uncertainties associated with the [
]a,c,e identified in Table 1.0 above when stacked in a manner analogous to the arithmetic process outlined in Reference A.4. As an alternative method for checking the validity of the "stacked model" results, a simplified statistical process analogous to that described in the EPRI Integrity Assessment Guidelines was applied and a similar result was obtained for the combined uncertainties. This alternative check included the limiting and more conservative definitions of variability in each parameter defined above, as opposed to the 1.645σ recommended in the EPRI Steam Generator Integrity Guidelines.

The combined uncertainties, all biased in a direction to increase the H* distance, with conservative assignment of standard deviation from their means, results in a whole bundle probability of 2.6E-6 of not meeting the structural and leakage performance criteria specified in NEI 97-06, Revision 2.

The maximum H* distances are based on using a divider plate factor of 0.64 versus a divider plate factor of 1.0. It has been shown that, without the divider plate to stub runner weld present, the tube plate

vertical deflection is still limited to 36% less than if the divider plate was not present at all, Reference A.12 In other words, most of the structural benefit of the divider plate is derived from the welds to the channelhead, and not from the weld to the tubesheet (stub runner). No degradation has been reported in the welds between the divider plate and the bowl, in contrast to the reports of degradation in the weld between the divider plate and the stub runner.

The results discussed in this response are not expected to change in the highly unlikely case that an input parameter takes on an "extreme" value due to some combination of installation artifacts or deviation from mean material properties. This is for two reasons:

1. The variability of the parameters that are most important to the analysis is known and the extreme values have already been considered. For example, the thermal expansion coefficient of the tube and the tubesheet is very important to the results of an H* analysis. However, the ANTER labs data shows that the variability of those parameters is limited to +/- 1.5% with 95% confidence interval. The conclusion, then, from the most recent data means that there will always be a difference between the TEC of the tube and the tubesheet and therefore there will always be differential thermal growth between the tube and the tubesheet. The sensitivity study results presented above include the effects of varying both the ANTER labs properties and the ASME code properties to the extreme limits of the available test data and still show adequate margin with respect to the desired inspection distances into the tubesheet. Note that significant margin exists despite the fact that the other input parameters are also being varied, many to the extreme range of the known data for that property (e.g., Young's Modulus of the tube and the tubesheet). Therefore, extreme values of most of the parameters critical to the H* and B* analysis (i.e., Young's Modulus of the tube, thermal expansion coefficient of the tube and the thermal expansion of the tubesheet) have already been evaluated in the analysis.

   The only critical parameter for which an extreme value has not been evaluated is the yield strength of the tube. The results of varying the tube yield strength to either extremely negative limits or extremely positive limits still provide adequate margin with respect to the desired inspection limits. For example, if the yield strength in the tube approaches a value of zero, the contact between the tube material and the tubesheet material will be nearly perfect. This would dramatically increase the residual contact pressure between the tube and the tubesheet and make it much more difficult for the tube to pull out under the limiting loads. On the other hand, assuming that the yield strength of the tube is triple the highest value (approaching a value of 5σ) the residual contact pressure from installation would tend toward zero. The results of a B*/H* analysis for the Model F SG, with no residual contact pressure from installation, but with mean ASME code material properties and design input values for all other parameters, is a B* of 8.16 inches and an H* of 13.55 inches for the limiting cold leg. Therefore, an extreme variation in tube yield strength is bounded by the analysis results from the "stacked" model cases discussed above.

2. The bellwether concept inherently addresses any postulated effect of an extreme value result. If a tube in the steam generator is postulated to exhibit the worst case value for every parameter that is used in the B*/H* analysis, and those parameter values were beyond those considered in any of the sensitivity studies described here, and the tube is assumed to be still in service, the expected conditions would be such that the tube would leak during normal operating conditions. If the leak

during normal operating conditions is significant, it will be located and plugged. A significant leak would require a gross crack that occurs in a short time (i.e., one operating cycle) or have a prior history of leakage. There is no known mechanism that would cause a complete circumferential throughwall crack in one operating cycle to cause a significant leak, which, in any case, would cause a plant shutdown if it were to occur. Even for the case of a severe circumferential crack, not of 360 degree extent, or a large axial crack, structural integrity of the tube would be maintained by the remaining tube ligaments. Therefore, the postulate of an extreme condition tube is extremely unlikely due to the normal plant leakage monitoring requirements.

It is concluded that the H* and B* inspection criteria conservatively provides significant margin in the tubesheet for all of the tubes in the bundle even if: the extremely unlikely case that a specifically stacked set of material properties variations and dimensional conditions, all biased in a direction to result in greater H* values exist in the steam generator, the divider plate weld to the tubesheet is 100% degraded, and lower bound residual pullout strength and contact pressures are used.

Wolf Creek NRC RAI No. 4

4. *Reference 2, Enclosure I, Response to RAI question 7 - The Model D5 steam generator (SG) pullout data in Table 2 indicate that pullout force increases with temperature for the 3-inch long specimens and decreases with temperature for the 6-inch long specimens. For the 4-inch specimens, pullout force increases with temperature to 400°F and decreases with temperature beyond that point. Discuss the reasons for this apparent discrepancy in trends among the data. Discuss whether the reduction in tube yield strength with temperature might be sufficient for some specimens to limit any increase in contact pressure associated with differential thermal expansion between the tube and tubesheet*

Vogtle Units 1 and 2 Response to Wolf Creek NRC RAI No. 4

The decrease in tube yield strength with increasing temperature is not likely to reduce or limit the contact pressure between the tube and tubesheet. First, the loads and conditions on the limiting section in the tube are not sufficient to cause plastic yielding in the tube. See the response to Wolf Creek RAI No. 5. A decrease in the tube yield strength is likely to increase the contact pressure between the tube and tubesheet up to the point of plastic yielding of the tube material. For example, consider a load state on the tube that would generate a state of plastic yielding in the tube material. In that case, the plastically yielded tube material would flow with no resistance in an isochoric manner (i.e., volume preserving deformation). This kind of deformation would have two effects on the interface between the tube and the tubesheet.

1. The tube material would be able to plastically flow into the crevices and surface peaks and valleys of the tubesheet local to the plastic tube material. This would create a state of near perfect intimate contact between the tube and the tubesheet; thereby preventing any leakage through the crevice and allowing for the dispersal of large amounts of strain energy which would further reduce the possibility of tube pullout.

2. Although the surface of the tubesheet could push back on the plastically yielded tube material, the internal pressure in the tube (the primary pressure of the SG) would keep the tube material in contact with the tubesheet regardless of the tubesheet deformation because there would be no stiffness in the tube material to resist the plastic flow.

In conclusion, it is highly unlikely the tube material in the tubesheet will plastically yield due to the loads and constraints applied to the tube (See RAI No. 5). However, in the event that the tube did plastically yield, the effect would be to increase both the leakage resistance and the pullout resistance of the tube. Therefore, it is more conservative to consider both the tube and the tubesheet material as elastic structures that retain their respective stiffnesses in the event that contact pressures and conditions allow the two material surfaces to deflect away from each other. This more conservative case is the condition that is considered in the H*/B* analysis.

The pullout strength for the Model D5 tubing and the Model 44F H*/ B* submittals is a lower bounding value based on pullout test results from both room temperature and elevated temperature testing. The data plotted in both Figures A-8 and A-9 have had the effects of thermal expansion due to elevated temperature testing subtracted out, thus only the mechanical contribution of the joint are reflected in the figures. As can be seen from Figure A-8 and A-9 provided below, the average minus one standard deviation value for pullout strength essentially bounds the data cloud for both the Model 44F and Model D5 test data. Regardless of the tube size, it can be seen that using the empirically determined mean minus one standard deviation resulting value for pullout strength is a conservative value for the bulk of the data for both the Model D5 and 44F steam generators.

The data plotted in both Figures A-8 and A-9 have had the effects of thermal expansion due to elevated temperature testing subtracted out. It can be seen by Figures A-8 and A-9 that, for the different expansion lengths, the room temperature data does not always result in the lowest pullout strength for the Model D5 and 44F test specimens as well. For the specific example cited by the NRC staff, i.e., the Model F result for Wolf Creek, it can be seen that the Model D5 7-inch expansion length room temperature test specimen results in a higher tube pullout strength than the elevated temperature test results. For the Model 44F steam generator, however, the approximate 7-inch expansion length room temperature test specimen results in a lower tube pullout strength than that for the elevated 400°F test specimen and a comparable pullout strength to the elevated 600°F test result. Therefore, it is concluded that what is interpreted in the question as a data trend reflecting temperature effects is, in reality, normal variability among the different test specimens.

a,c,e

a) elevated temperature data adjusted to remove thermal expansion component

a,c,e

b) Room Temperature Data

Figure A-8 Model D5 Pullout Test Results for Force/inch at 0.25 inch Displacement

a,c,e

a) (elevated temperature data adjusted to remove thermal expansion component)

a,c,e

b) Room Temperature Data

Figure A-9 Model 44F Pullout Test Results for Force/inch at 0.25 inch Displacement

The NRC staff's concern whether a reduction in tube yield strength with increasing temperature might be sufficient for some specimens to limit any increase in contact pressure associated with differential thermal expansion between the tube and tubesheet was considered. As stated in the response to NRC RAI No. 7 in LTR-CDME-07-72, Reference A.7, the data in Table 2.0 is intended to show that for an expansion length as short as 2.95 inches, a significant increase in pullout force occurs at elevated temperatures (e.g., pullout force increases from [ ]^{a,c,e} when temperature increases from 70°F to 600°F, respectively). Therefore, since the test results inherently include the variation of yield strength with temperature, the results indicate that yield strength reduction with temperature does not limit the increase in contact pressure due to thermal expansion.

Wolf Creek NRC RAI No. 5

5. *Following up on question 4 above, is there a possibility that any tubes could be stressed beyond the compressive yield strength (at temperature) of the tube material due to differential thermal expansion, internal pressure, and tubesheet hole dilation for the range of yield strengths in the field? Describe the basis for either yes or no to this question. If yes, how has this been factored into the contact pressures, accumulated pullout resistance load as a function of elevation, and H* in Tables 7-6 through 7-10 and 7-6a through 7-10a of Reference 2, Enclosure I?*

Vogtle Units 1 and 2 Response to Wolf Creek RAI No. 5:

It is not possible for a SG tube with an intact cross section to compressively fail due to the applied pressures calculated in the H* and B* analysis. The basis for this statement is a stress analysis of the tube material using the Tresca yield criteria. The analysis approach and results follow:

The maximum applied contact pressure from Tables 5-6 through 5-10 and Tables 5-6a through 5-10a of this report is 3475.26 psi or approximately 3.5 ksi. The maximum contact pressure occurs in the cold leg, during FLB at the bottom of the tubesheet (21.03 inches below the top of the tubesheet). For 11/16 inch Alloy 600 tubing, the minimum yield strength is 51.4 ksi with a standard deviation of 3.85 ksi at room temperature, Reference A.9 [WCAP-12522]. At a temperature of 650°F the tensile yield stress is 36.77 ksi or 36.8 ksi, Reference A.9 [WCAP-12522]. For a material element at the outside surface of the tube wall (the tube material in contact with the tubesheet wall), assuming the full axial load is applied to the tube despite its location in the tubesheet, the state of stress is equivalent to that of an element in a thin-walled pressure vessel with the third principal stress not equal to zero. Note that the radius used in the following equations is the mean tube radius because the tube is a thin-walled structure.

For the FLB condition, the principal stresses on the tube wall element are:

$$\sigma_1 = \sigma_{XX} = \frac{p_{PRI} r}{t} = \frac{2650 psi \cdot 0.3336 in}{0.0396 in} = 22324.2 psi = 22.3 ksi$$

$$\sigma_2 = \sigma_{YY} = \frac{p_{PRI} r}{2t} = \frac{2650 psi \cdot 0.3336 in}{2 \cdot 0.0396 n} = 11162.1 psi = 11.2 ksi$$

$$\sigma_3 = \sigma_{ZZ} = P_{CONTACT} = -3475.26 psi = -3.5 ksi$$

Applying the Tresca theory, or maximum shear stress yield criteria, gives:

$$\frac{Y}{2} = \tau_{MAX} = \left| \frac{\sigma_1 - \sigma_3}{2} \right|$$

$$Y = 36.8 ksi > \left| 22.3 ksi - (-3.5 ksi) \right| = 25.8 ksi$$

This shows that the tube has a safety factor of at least 1.43 with respect to yielding using the minimum yield strength for Alloy 600 at elevated temperature. At room temperature conditions, the safety factor

increases to nearly 2.0. If the material properties and conditions in the steam generator are varied for a worst case analysis then the maximum contact pressures in the tubesheet will be reduced. Any reduction in contact pressure between the tube and the tubesheet make it even less likely that a tube will yield in compressive failure.

In conclusion, it is not possible for an intact tube to yield in compression under the state of stress created by the transient event with the maximum applied contact pressure.

Wolf Creek RAI No. 8

8. *Reference 1, Enclosure I, Table 6-4 - The listed F/L values are based on allowing 0.25 inch slippage. Reference 1 does not address the potential for limited, but progressive incremental slippage under heatup/cooldown and other operational load cycles. Nor does Reference 1 address the effects of slippage on normal operating leakage and on accident-induced leakage or the ratio of normal operating and accident induced leakage. The response to RAI question 5 in Reference 2, Enclosure I, does not provide any further insight into this issue. That response specifically addressed test results for tubes with a hard roll expansion, and the staff believes that the slippage versus axial load characteristics for such an expansion may be entirely different than for a hydraulic expansion. Discuss and address the potential for progressive incremental slippage under heatup/cooldown and other operational load cycles. In addition, address the potential for slippage under operational and accident conditions to affect the ratio of accident-induced leakage to operational leakage.*

Vogtle Units 1 and 2 Response to RAI No. 8:

Cyclic loading testing was conducted on five tubes, including A600TT tubes, which were hydraulically expanded into a test block (Reference A.3). The tubes were loaded to a given load between [ ]^{a,c,e} The axial position of the primary side end of the tube was measured before loading and after unloading. The direct measurements of the displacement of the primary end of the tubes were in reasonable agreement with displacements recorded from the secondary side by the displacement gage. Figure A-10 below shows the load-displacement curves. Reference A.3 concludes that the tubes underwent rigid body displacement (breakaway) at a [ ]^{a,c,e} relative to the maximum pullout load. Based on the much steeper unloading and reloading curves relative to the initial loading curves (See R12C4 and R12C5), it can be concluded that the tubes did slip at small loads.

There is no effect on the ratio of the normal and accident leakage for a 360° circumferential flaw in the event of relative slippage between the tube and tubesheet interface. If any slippage occurred it would be an indication of a degradation of the frictional interface between the tube and the tubesheet. Degrading this interface and lowering the frictional resistance of the tube portion within the tubesheet would change the necessary pullout load, but not the contact pressure between the tube and the tubesheet. Therefore, the leak resistance coefficient, k, would not be changed and the relationship between the contact pressure and the leak rate coefficient would not be changed. Also, the Bellwether Principle still applies to the situation. Regardless of the friction between the tube and the tubesheet, the increase in leakage is directly proportional to the difference in the primary and secondary side pressures. In the absence of resistance to leakage from the tube-to-tubesheet interface, Darcy's model for axial flow in a porous medium, predicts that any increase in leak rate would be equal to the increase in the differential pressure, which is bounded

by a factor of two (2). Therefore, if the leak rate under normal operating conditions was considered acceptable, the leak rate under accident conditions would also be acceptable and any increase in leakage during an accident would be conservatively bounded by a factor of two (2).

If it is assumed that a tube continues to incrementally slip, the cumulative distance of slippage would result in eventual contact with adjacent (lateral or vertical) tubes. This condition would be detected during normal inspection of the tubes soon after contact had occurred. The nominal spacing between tubes varies from about 0.3 inch at the inner rows to about 0.48 inch at the outer rows. Displacement of a tube by this amount would have no effect on B* since the difference between H* and B* exceeds this value.

Figure A-11 shows the difference between H* and B* for both the hot leg and the cold leg. The minimum difference, approximately 1.75 inches, occurs on the HL at the periphery of the bundle. Since H* bounds B* in all cases, B* will apply at all locations even if the tube is postulated to slip by 1.75 inches.

Peripheral tubes, which may not have adjacent tubes, are discussed in the response to RAI No. 9.

a,c,e

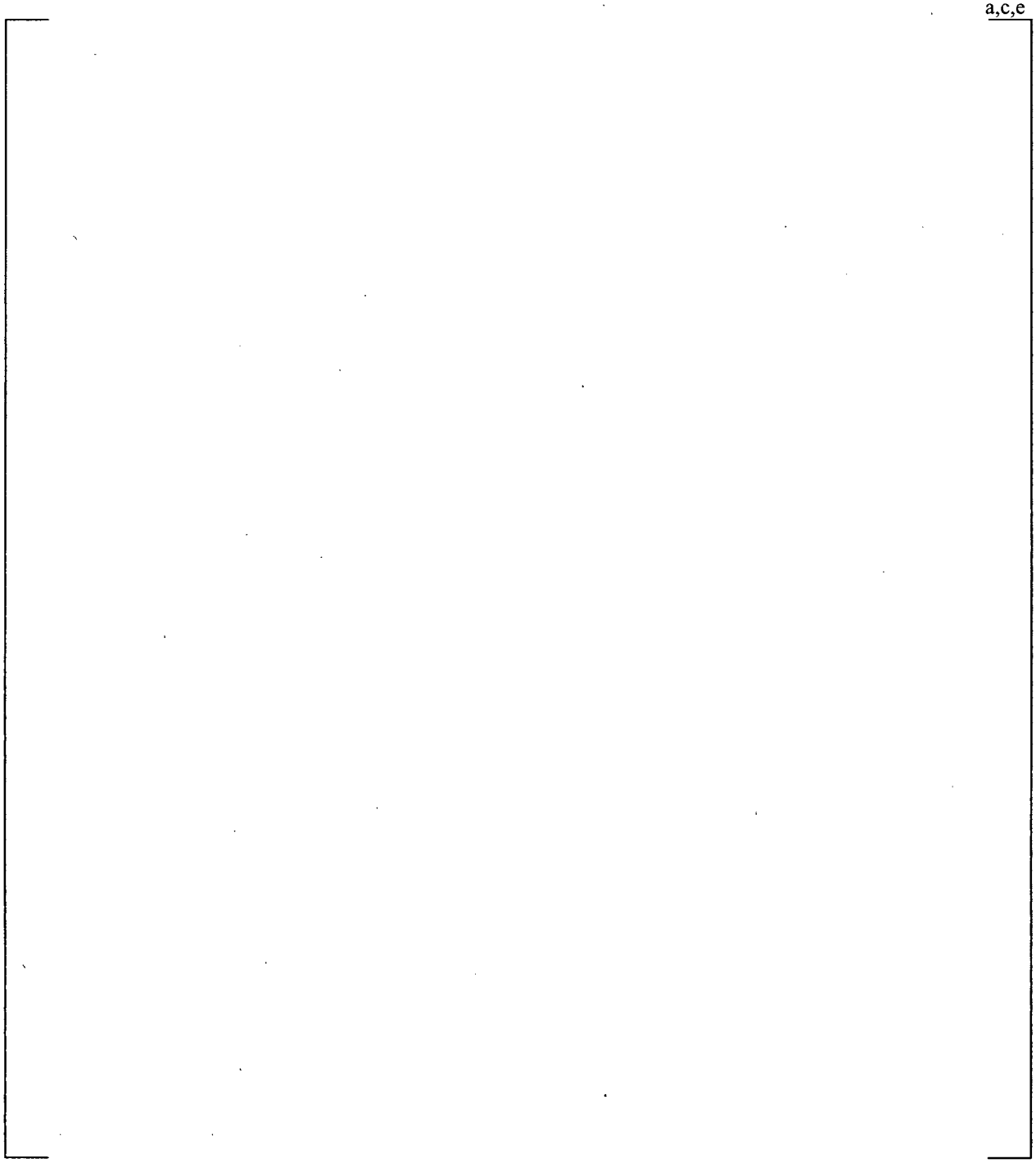

Figure A-10 Load-Unload-Reload Pullout Curves

a,c,e

Figure A-11 Difference Between H* and B*

Wolf Creek RAI No. 9

9. Discuss your plans for revising the proposed technical specification (TS) amendment to monitor the tube expansion transition locations relative to the top of the tubesheet to ensure that the tubes are not undergoing progressive, incremental slippage between inspections.

Vogtle Units 1 and 2 Response to RAI No. 9:

No revisions to the Vogtle Units 1 and 2 Technical Specifications are proposed.

The response to RAI No. 8 concluded that, based on individual pull tests using a test block of tubes expanded in a tubesheet, [ ]^{a,c,e} However, the test conditions were very conservative in that no tubesheet bow was simulated. In an operating SG, the application of tube loads depends on the SG primary side being pressurized, resulting in tube sheet bow. All tubes are constrained from motion by tube hole contraction below the tubesheet mid-plane for the bulk of the tubes or above the mid-plane for the tubes near the periphery of the tubesheet. For any motion to occur, it is tacitly assumed that a 360 degree throughwall circumferential crack exists below H*. If even a small ligament exists, the axial end cap force will be resisted by the tube-end weld at the bottom of the tubesheet. Further, the tests were performed at room temperature. Consequently, the two most significant factors affecting H* were not simulated.

If a 360° throughwall circumferential crack is assumed just below H* and that a tube continues to incrementally slip, the cumulative distance of slippage is limited by eventual contact with adjacent (lateral and/or vertical) tubes after a short distance. The maximum nominal distance between u-bends is 0.482 inch in rows 52 and greater. In smaller radius rows, the axial spacing is incrementally less due to smaller indexing of the tube straight legs. Because of axial constraints provided by the tube bundle, and lateral restraint provided by the presence of the AVBs, the maximum axial displacement of a tube is limited to less than one pitch, 0.980 inch, even if the u-bend of the postulated moving tube moves toward the adjacent column. As noted in RAI No. 8, the minimum margin between H* and B* is 1.75 inches; therefore a postulated extreme displacement such as this would not affect the efficacy of H*/B*.

An extreme displacement condition as described above would result in tube to tube contact well before a significant displacement had been achieved. Tube-to-tube contact would be detected during normal inspection of the tubes soon after contact had occurred. If tube-to-tube contact is detected, normal inspection procedures would require investigating the source of the contact and corrective action would be required.

No significant slippage of tubes has been reported to date in the industry. The requirements of Reference A.13 (EPRI SG Inspection Guidelines) assure that all tubes have been inspected to date at Vogtle Units 1 and 2, both by bobbin and by RPC in the region ±3 inches relative to the top of the tubesheet on the HL. No indications of gross slippage (i.e., the expansion transition moved above the top of the tubesheet) have been observed. This is an indication that either no circumferential separation has occurred in the expansion region or that significant slippage does not occur.

H* bounds B* by a minimum of 1.75 inches at all locations; therefore, leakage is not a concern because of the Bellwether principle. If a tube is found not to leak, regardless of the position of the bottom of the

expansion transition (BET) relative to the top of the tubesheet (assuming motion has occurred), accident induced leakage will also be zero. If a tube is leaking within the performance limits at normal operating conditions, it will also not exceed the accident induced leakage limits. Leakage exceeding the normal operating limits requires shutdown of the plant and elimination of the source of the leakage. Consequently, the difference between H* and B* represents a conservative limit for tube motion, since, at the next inspection, if a flaw is found to exist above H*, the tube will require plugging. Therefore, continued monitoring of the BET at inspections is not necessary because, until significant motion (up to 1.75 inches) of the tube has occurred, there is no potential for accident induced leakage to exceed acceptable values.

A postulated condition of a circumferential separation occurring at H* within one inspection cycle is not a credible event. Since even a small ligament is sufficient to assure axial restraint of the tube, a 360° circumferential sever is required for tube motion to occur. The growth of a crack to a 360° circumferential throughwall condition requires a significant period of time after crack initiation, spanning at least several inspection cycles. If a circumferential crack were to develop at the H* distance, and if it is postulated that the tube experiences incremental motion, normal inspection of the tube to H* would identify the crack well before separation could occur, and the tube would be plugged. The factor of safety against tube pullout under normal operating conditions is approximately 3, and the 3DPNO condition envelopes all accident condition pullout loads.

In summary:

Incremental motion, like that observed in manufacturing testing, is not expected because of the operating constraints in an operating SG. The tests that exhibited slight incremental motion did not simulate the operating conditions (temperature and pressure) that would lead to additional constraint provided by tubesheet bow and the thermal effects.

It is not necessary to monitor tubes for small displacements. Since the Bellwether Principle applies, normal leakage monitoring will determine the need to shut down the plant when primary to secondary leakage is detected. Therefore, excessive accident induced leakage within the tubesheet expansion region can never occur. If a tube is found to be leaking, normal inspections to H* will determine if a flaw exists above H*. In that event, the tube must be plugged. All tubes except the peripheral tubes can be monitored during normal inspections for potential tube to tube contact. If tube to tube contact is observed, the source of the contact will be determined and appropriate action taken to repair the condition.

The minimum difference between H* and B* is approximately 1.75 inches. Therefore, motion of up to 1.75 inches will not affect leakage, and provides a definitive, observable degree of displacement. This extent of motion is not possible in the interior of the bundle; therefore, any concern about displacement should focus principally on the peripheral tubes. For the peripheral tubes, normal bobbin inspection will detect significant displacement since the expansion transition will be reported above the top of the tubesheet.

For all tubes, a circumferential sever is required for any motion to occur. The development of a 360° circumferential crack from crack initiation requires significant time. Normal inspection to H* will identify a circumferential crack within the H* distance if incremental motion is postulated.

Wolf Creek RAI No. 10

10. Reference 1, Enclosure I, Section 7.1.4.2 - This section provides a brief discussion of SLB, feed line break (FLB), and loss-of-coolant accident (LOCA) in terms of which is the most limiting accident in terms of tube pullout potential. Expand this discussion to indicate whether SLB and FLB are the most limiting accidents among the universe of design basis accidents (DBA) (or other faulted conditions in the design basis) in terms of both tube pullout, and the margin between the calculated accident-induced tube leakage for each DBA and the assumed accident-induced tube leakage in the safety analysis for that DBA.

Vogtle Units 1 and 2 Response to RAI No. 10:

The following accidents model primary-to-secondary leakage in the Vogtle Units 1 and 2 USAR:

Section 15.3.3, Reactor Coolant Pump Shaft Seizure (Locked Rotor)
Section 15.4.8, Spectrum of RCCA Ejection Accidents
Section 15.1.5, Steam System Piping Failure
Section 15.2.6 Loss of Non-Emergency AC Power to the Station Auxiliaries (BLACKOUT)

An evaluation of these transients has been conducted to determine the duration of time that the primary-to-secondary pressure differential exceeds the normal operating condition primary-to-secondary pressure differential (Reference A.14). It has been determined that the duration of time that the primary-to-secondary pressure differential exceeds the normal operating pressure differential for a locked rotor [ ]^{a,c,e} and that the SLB event remains the limiting accident. The leakage limit that is defined for the locked rotor event and the control rod ejection event is 1.0 gpm. The leak rate for the locked rotor event and the control rod ejection event can be integrated over one minute to compare to the limit. Since the time above the normal operating pressure differential is less than [ ]^{a,c,e} the time integration should permit an increase in acceptable peak leakage at the peak pressure differential by at least a factor of 2. As the allowable primary to secondary leak rate is limited to 150 gpd (0.1 gpm) in the Vogtle Units 1 and 2 SGs during normal operating conditions, accident induced leakage is expected to remain less than [ ]^{a,c,e} This leakage rate is bounded by the current accident analysis assumption. See Tables A-4 and A-5 and Figures A-12 and A-13 below.

For tube pullout considerations, the limiting load applied to the tube is 3 times the normal operating pressure differential. This value bounds 1.4 times both the SLB and FLB loads.

Vogtle Units 1 and 2 USAR Section 15.2.6, "Loss of Non-Emergency AC Power to the Station Auxiliaries" also models SG primary to secondary leakage. However, based on a review of Reference 14, the maximum primary-to-secondary pressure differential [ ]^{a,c,e} during this upset transient never exceeds the normal operating pressure differential of 1334 psi. Therefore, there is no adverse impact on the existing radiological consequences calculated in the Vogtle Units 1 and 2 USAR with the implementation of the H*/B* criteria.

Table A-4 Primary-to-Secondary Side Pressure Differential Time-Histories for RCP Locked Rotor and Control Rod Ejection Transients (Vogtle Units 1 and 2 Model F Steam Generators) a,c,e

Table A-5 Primary-to-Secondary Side Pressure Differential Time-History for Main Steam Line and Feedwater Line Breaks (Vogtle Untis 1 and 2 Model F Steam Generators) a,c,e

Time sec	Normal Operation ΔP psi	Feedwater Line Beak ΔP psi	Time sec	Steam Line Break ΔP psi

a,c,e

Figure A-12 Plots of the Primary-to-Secondary Side Pressure Differential Time-Histories for RCP Locked Rotor and Control Rod Ejection Transients (Vogtle Units 1 and 2 Model F Steam Generators)

a,c,e

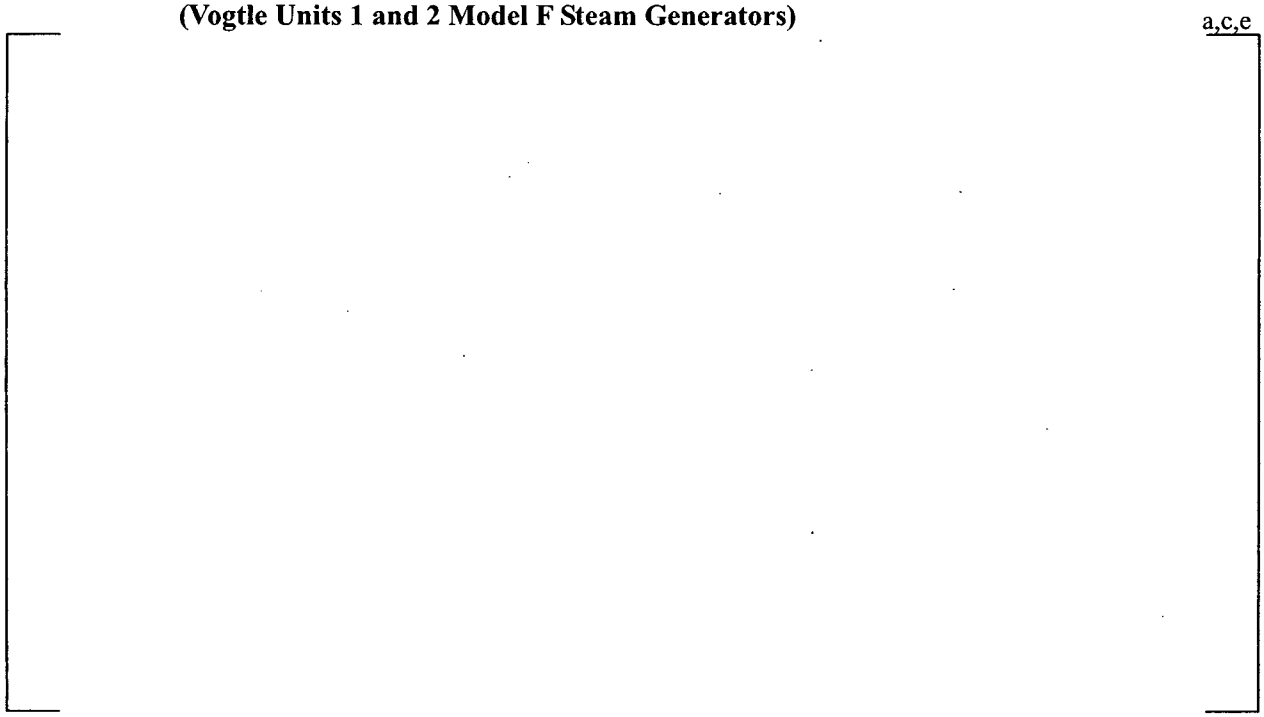

Figure A-13 Plot of the Primary-to-Secondary Side Pressure Differential Time-History for Main Steam Line Break

Wolf Creek RAI No. 11

11. Figure 11 of Reference 2, Enclosure I contains loss coefficient data for Model F SG tubing that was not included in Figure 6-6 of Reference 1, Enclosure 1. This data was for contact pressures ranging from about 1200 psi to about 2000 psi. Why was this data not included in Figure 6-6? Discuss if this is this because of low expansion pressures and if the data that is not included in Figure 6-6 is room temperature data. [If yes, then the NRC staff observes that the room temperature loss coefficients for the Model F specimens are relatively invariant with contact pressure above a contact pressure threshold of around 700 psi. The 600 degree F data is also invariant with contact pressure. Thus, loss coefficient may not be a direct function of contact pressure once a threshold degree of contact pressure is established. The difference in loss coefficient data between the 600°F data and the room temperature may be due to parameter(s) other than contact pressure. This other parameter(s) may not be directly considered in the B analysis.]*

Vogtle Units 1 and 2 Response to RAI No. 11:

The reasons for originally not including the data are discussed in the response to NRC RAI No. 11 in Reference A.7.

The additional data include:

1. Test results from the Model F specimens that were not prepared in accordance with criteria of the test specifications (i.e., the test specification expansion pressure was not achieved).

2. Test results from Model D5 specimens that resulted in no leakage. The Model D5 testing was specifically oriented toward leakage; therefore, since a zero-leak test does not provide usable data for leakage, these tests were not previously reported.

The data that were added includes both room temperature data and elevated temperature data.

The Staff's observations about the leak rate data and the relationship between the loss coefficient and contact pressure for the Model D and Model F tests are noted. However, Westinghouse believes, based on the data, that there is a definable relationship between the loss coefficient of a TS crevice and the contact pressure between the tube and tubesheet. The data available provides the information necessary to define a conservative log-linear relationship between contact pressure and loss coefficient. See Figure A-14 for a plot of the total Model F and Model D data set with a curve of the 95% confidence fit obtained by a log-linear regression of the combined Model D and Model F data sets.

a,c,e

Figure A-14 Plot of Loss Coefficient, k, as a Function of Contact Pressure, P_c.

The results plotted in Figure A-14 illustrate four important characteristics in the Model F and Model D data and the resulting 95% confidence interval fit of the combined data set.

a,c,e

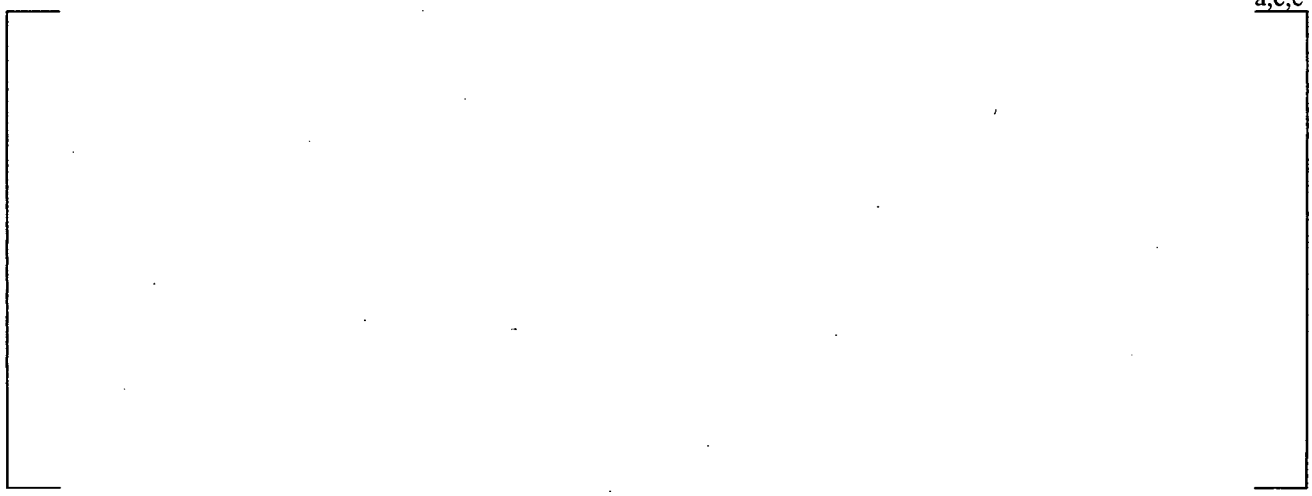

These results indicate that the Model D loss coefficient data is [

]a,c,e

[

]^{a,c,e}

If only the Model D data were used, [

]^{a,c,e}

Therefore, the available test data is considered valid and is applied in a very conservative manner via the Darcy model for axial flow through a porous medium. The Staff has noted in the past that the Darcy model is a more conservative approach than either the Bernoulli model or a converging orifice model. A different model is likely to give a less conservative result compared to the current bounding approach using the fit of the combined data set. In conclusion, using the 95% confidence fit of the combined Model F and Model D data set is an extremely conservative approach which results in a curve that bounds most of the loss coefficient data and maximizes the required B* distance.

Wolf Creek NRC RAI No. 16

16. *Reference 2, Enclosure 1 - Provide a description of the revised finite element model used to support the revised H* calculations in Tables 6-7 through 6-10 and Tables 6-7a through 6-10a. Compare this revised model to the original model which supported the Reference 1 analysis. Explain why the revised model is more realistic than the original model.*

Vogtle Units 1 and 2 Response to RAI No. 16:

Three finite element models were used to justify the contact pressure calculations for H* and B*.

- The first, original, finite element analysis is an axisymmetric model, as shown in Reference A.2 that calculates the radial deflection of the tubesheet under unit load conditions as a function of the tubesheet elevation and radius. For convenience, this model will be called Model O-1.

- The second finite element model is a three-dimensional solid model that calculates the vertical deflection of the tubesheet as a function of tubesheet radius for various load cases assuming different stiffnesses and/or cracking in the divider plate. The output from the second finite element model defines the divider plate factor and was used to check the results from the first. For convenience, this model will be called Model O-2.

- The third finite element model was an improved version of Model O-2, which included changes further discussed below.

The original finite element model (Model O-1), that was used to calculate the tubesheet deflection, was not revised as it does not model the divider plate in the lower SG complex.

The second finite element model (Model O-2), originally used to determine the divider plate factor used in the H*/B* analysis, was revised to become Model O-3. The modifications to the O-2 model include a solid tubelane, the addition of the weldments and connections between the divider plate and the channelhead and tubesheet, non-axisymmetric boundary conditions and variable stiffness in the divider plate material. The revised model, O-3, more accurately reflects the true geometry, loading and material conditions of the tubesheet. Therefore, the revised model, O-3, more completely represents the actual SG configuration than the original FEA analytical model (O-2) did.

The results of a study funded by EPRI (Reference A.12) and data from original design documents from Westinghouse show that the majority of the structural benefit of the divider plate is derived from the divider plate connection to the channelhead. The divider plate factor for the case where the structural credit for the divider plate to tubesheet connection is negated is DP = 0.64. This means that even in the event that the upper 5.00 inches of the divider plate, stub runner and weld material somehow disappears the tubesheet displacements are still reduced by a minimum of 36%.

The results shown in Tables 5-6 through 5-10 and Tables 5-6a through 5-10a of this report are highly conservative because the DP value that should be used based on the available data on cracking indications in the divider plate is DP = 0.64.

The figures and tables included in this report are based on the final models using the stacked worst case and a divider plate factor of 0.64.

Wolf Creek NRC RAI No. 17

17. Reference 2, Enclosure 1, Attachment 1 (The Westinghouse Letter Summary of Changes to B and H*), page 14 - address the status of the divider plate evaluation being performed under EPRI sponsorship, and the schedule for completion of the various topics being addressed in the evaluation. Describe any inspections that have been performed domestically that provide insight on whether the extent and severity of divider plate cracks is bounded by the foreign experience. Discuss the available options for inspecting the divider plates.*

Vogtle Units 1 and 2 Response to RAI No. 17:

The status of the EPRI program is not related to the current B*/H* analysis and any results from the EPRI program will have no impact on the Vogtle Units 1 and 2 B*/H* analysis , which does not take credit for the presence of a divider plate to stub runner weld or the region of the divider plate that has been observed to degrade. The analysis presented in WCAP-16794 utilizes a divider plate (DP) factor of 0.64 which assumes that the divider plate to stub runner weld is completely degraded, but that the divider plate to channel heads welds are intact. This is a valid assumption because these welds are thermally stress relieved, and no degradation has been reported in these welds.

Wolf Creek NRC RAI No. 18

18. Discuss how the ability of the divider plates at Wolf Creek to resist tubesheet deflection (without failure) under operating and accident loads is assured in the short term, pending completion of the EPRI evaluation. Include in this discussion the actions that are planned in the near term to ensure that the divider plates are capable of resisting tubesheet deflection.

Vogtle Units 1 and 2 Response to RAI No. 18:

The current analysis is based on the use of a divider plate factor of 0.64. This factor reflects the structural effect of a divider plate which is welded to the channelhead but assumes that the weld to the stub runner is entirely missing. Justification for the use of this divider plate factor (DP=0.64) was provided previously.

Therefore, divider plate inspections are not necessary to support the H*/B* criteria for the Vogtle Units 1 and 2 steam generators because:

- the H*/B* values do not depend on a direct connection between the divider plate and the tubesheet, and the weld between the divider plate, and
- the channelhead to divider plate welds were stress relieved, have shown no evidence of degradation and are not anticipated to crack.

A.3 REFERENCES

A.1 LTR-SGDA-07-4, Rev. 3, Letter Summary of Changes to B* and H* Analysis Due to New Crevice Pressure and Divider Plate," 9/24/07.

A.2 LTR-CDME-06-58-P, Steam Generator Tube Alternate Repair Criteria for the Portion of the Tube Within the Tubesheet at Vogtle Unit 1 and 2 Electric generating Plant for One Cycle Application," April 2006.

A.3 NCE-88-271, "Assessment of Tube-to-Tubesheet Joint Manufacturing Processes for Sizewell B Steam Generators Using Alloy 690 Tubing," November 1988.

A.4 EPRI Report 1012987, "Steam Generator Tube Integrity Guidelines," Rev. 2.

A.5 Draft Regulatory Guide DG-1074, "Steam Generator Tube Integrity," March 1998.

A.6 NEI-97-06, Rev. 2, "Steam Generator Program Guidelines."

A.7 LTR-CDME-07-72, "Response to NRC Request for Additional Information Relating to LTR-CDME-05-209-P of the Wolf Creek Generating Station (WCGS) Permanent B* License Amendment Request," April 2007.

A.8 WNEP-9725, "The Westinghouse Tube-to-Tubesheet Joint Hydraulic Expansion Process," July 1997.

A.9 WCAP-12522, "Inconel Alloy 600 Tubing-Material Burst and Strength Properties," January 1990.

A.10 Drawing No. 6526D15, Steam Generator Model F Tube Schedule," 11/7/78.

A.11 PR27988-52336, ANTER Laboratories, Inc, April 27, 2007.

A.12 EPRI Report 1014982, "Divider Plate Cracking in Steam Generators; Phase 1 Report," Rev. 0.

A.13 EPRI Report 1003138, "Pressurized Water Reactor Steam Generator Examination Guidelines: Revision 7, Requirements."

A.14 LTR-SGDA-07-213, "Vogtle Units 1 and 2 Model F Steam Generator Faulted Transient Delta-P Evaluation," 9/21/07).

APPENDIX B
LTR-SGDA-07-4, REV. 3
LETTER SUMMARY OF THE CHANGES TO B* AND H* ANALYSIS DUE TO NEW CREVICE PRESSURE AND DIVIDER PLATE DATA

To:	H. O. Lagally		Date: September 24, 2007
cc:	P. R. Nelson	G. W. Whiteman	J. G. Thakkar
	E. P. Morgan	B. A. Bell	W. K. Cullen

From:	C. D. Cassino	Your ref:	
Ext:	724 722-6018	Our ref:	LTR-SGDA-07-4-P, Rev. 3
Fax:	724 722-5889		

Subject: **Letter Summary of Changes to B* and H* Analysis due to New Crevice Pressure and Divider Plate Data**

The technical basis for H* and B* as documented in the Alternate Repair Criteria (ARC) WCAPs and Calc Notes (see Reference 1 for an example) is based, in part, on of the fundamental assumption that leakage through a postulated crack below H* flashes to steam in the crevice. This establishes the pressure in the crevice as the saturation pressure. Test data show that leakage through a crack below H* does not flash to steam and remains a single-phase fluid; therefore, the original assumption is not justified and changes must be made to the B* and H* analysis inputs to reflect the new test results.

The purpose of the test was to determine the pressure in the crevice between the tube and the tubesheet. The tests show that there is a distribution of pressure in the tubesheet crevice that is [ ]^{a,c,e} The results showed that the fluid in the crevice remained [ ]^{a,c,e} Therefore, the crevice pressure is [ ]^{a,c,e} An increased pressure in the crevice will result in:

1. The driving potential on the leaked fluid from the primary side to the crevice has been reduced.

2. The driving potential on the leaked fluid from the crevice to the secondary side is increased at the bottom of the tubesheet and decreased at the top of the tubesheet.

3. The resistance to flow from viscous effects has increased.

4. The tube expansion component of the contact pressure analysis has been reduced.

5. The tube expansion component of the leakage resistance analysis has been reduced.

A discussion of the impact of the test results documented in Reference 1 on H*/B* analyses from a generic perspective is provided. The effects of varying the divider plate factor on a generic H*/B* analysis are also discussed. Note that the flaw in the test specimens discussed in this document was specifically [ ]^{a,c,e} It is possible to maintain a large pressure drop across the tube wall in smaller crack geometries. [ ]^{a,c,e} Therefore, the results described in this letter are bounding for the worst case scenario [ ]^{a,c,e} exists in the tube portion within the tubesheet.

If there are any questions regarding the contents of this letter please contact either Chris Cassino or Herm Lagally.

Author:
C.D. Cassino
Chemistry, Diagnostics and Materials Engineering

Reviewer:
H. O. Lagally
Chemistry, Diagnostics and Materials Engineering

References

1. STD-MC-06-11, Rev. 1.

2. LTR-CDME-05-32-P, Rev. 2.

3. http://www.cee.vt.edu/ewr/environmental/teach/smprimer/outlier/outlier.html, 07/01/2007, 11:34:07 AM EST.

4. M. R. Chernick, "A Note on the Robustness of Dixon's Ratio Test in Small Samples", *American Statistician*, Vol. 36, No. 2 (May, 1982), p. 140.

5. W. B. Middlebrooks, D. L. Harrod, R. E. Gold, "Residual Stresses Associated with the Hydraulic Expansion of Steam Generator Tubing into Tubesheets," Nuclear Engineering and Design 143 (1993) 159-169 North-Holland.

6. LTR-SGDA-06-156.

7. LTR-SGDA-06-157.

8. CN-SGDA-07-6.

9. Terakawa, T., Imai, A., Yagi, Kazushige, Fukada, Y., Okada, K., "Stiffening Effects of Tubes in Heat Exchanger Tube Sheet", Journal of Pressure Vessel Technology Transactions, ASME Vol. 106, No. 3, August 1984.

10. LTR-SGDA-06-160.

11. LTR-SGDA-07-3.

12. TP-SGDA-03-2, Rev. 1.

13. *Divider Plate Cracking in Steam Generators: Results of Phase 1: Analysis of Primary Water Stress Corrosion Cracking and Mechanical Fatigue in the Alloy 600 Stub Runner to Divider Plate Weld Material.* EPRI, Palo Alto, CA: 2007. 1014982.

14. Stress Report: 51 Series Steam Generator Calculated and Measured Strains and Deflections for Steam Generator Tubesheet Channel Head Model Under Limit Conditions, Volume 1, MPR Associates, November 1969.

15. WCAP-16820-P.

16. WCAP-16053-P.

17. LTR-SGDA-07-201.

1.0 Discussion of Crevice Pressure Test Results

The tests documented in Reference 1 were performed to determine the pressure distribution in the crevice of a hydraulically expanded tubesheet region with a postulated through wall flaw near the bottom of the expansion. [

]^{a,c,e} The data from the NOP and SLB tests from both specimens [1], taken after the pressure in the crevice reached steady state conditions, are shown in Table 1 and Table 2 below.

Table 1 Crevice Pressure Specimen Data from Steady State NOP Conditions a,c,e

[

]

Table 2 Crevice Pressure Specimen Data from Steady State SLB Conditions a,c,e

[

]

a,c,e

Figure 1 Picture of Typical Test Specimens Used in Crevice Pressure Experiments.

[

]a,c,e

a,c,e

Figure 2 Plot of Crevice Pressure Ratio as a Function of Depth Ratio into the Test Specimen for Simulated NOP conditions.

a,c,e

Figure 3 Plot of Crevice Pressure Ratio as a Function of Depth Ratio into the Test Specimen for Simulated SLB conditions.

[

]a,c,e

2.0 Discussion of Increased Crevice Pressures relative to an H*/B* Analysis

[

]a,c,e

1. [ ]a,c,e
2. [ ]a,c,e
3. [ ]a,c,e
4. [ ]a,c,e
5. [ ]a,c,e

[

]a,c,e

The contact pressure between the tube wall and the tubesheet hole is calculated in the H* and B* analysis for two reasons:

1. [ ]a,c,e
2. [ ]a,c,e

The components that contribute to the contact pressure between the tube material and the tubesheet crevice are:

- [ ]a,c,e
- [ ]a,c,e

- [
  ]^{a,c,e}
- [
  ]^{a,c,e}

Of these, only the contribution of the [
]^{a,c,e} The contribution of the thermal growth in each material will not be affected by an [ ]^{a,c,e} Similarly, [
]^{a,c,e}

The unrestrained radial expansion of a tube OD due to a pressure differential across the tube wall is a,c,e

[

[

]^{a,c,e}

An interesting observation from Figures 2 and 3 is [

]^{a,c,e}

[

]^{a,c,e}

[

]a,c,e

3.0 Calculation of the Limiting Crevice Pressure Ratio

[

]a,c,e

a,c,e

[

]

Figure 4 Plot of Crevice Pressure Model Comparisons Using Average Test Data Results for the Normal Operating Condition

a,c,e

[ ]

Figure 5 Plot of Crevice Pressure Model Comparisons Using Average Test Data Results for the SLB Accident Condition

[

]a,c,e

There are many sources available for detailed discussions of the application of the mean and the median in statistics. The discussion in the paragraph below is paraphrased from a discussion board hosted by Purdue University (http://www.cyto.purdue.edu/hmarchiv/1998/0824.htm) and several text books. Similar comments can be found in reliability engineering text books (e.g. Statistics, Probability and Reliability for Civil and Environmental Engineers, McGraw-Hill, © 1997).

The median, or 50th centile, is the value that corresponds to the middle item in a ranked list (e.g., sorted by magnitude) of all recorded measurements in a data set. The median is a robust statistical measure in that it doesn't necessarily change in response to small numbers of outliers, or to skewing of the tails of a distribution, whereas the mean is tugged by both. This is why the median is typically described as a "resistant" measure. One situation where the median is perhaps the only valid measure is when data congregate at one or both extremes. However, as long as more than 50% of the data are clear of the extremes a valid median is obtained, but any type of mean (geometric or arithmetic) will be less accurate.

A commonly used statistical tool to determine outliers in a limited population of data is the Dixon Ratio test. The Dixon Ratio test is used to assess the character (i.e., mostly average values, a small number of outliers, entirely composed of outlier values, etc.) of the data set and limit the influence of potential outliers that could affect the limiting crevice pressure ratio result. The following text is adapted from the

tutorial on the detection and accommodation of outliers from the web library of Virginia Polytechnic Institute and State University department of Civil and Environmental Engineering [3]. Dixon's test is generally used for detecting a small number of outliers. This test can be used when the sample size is between 3 and 25 observations [4], but is typically employed whenever a sample set is less than an ideal population to apply standard statistical tools. In a smaller data set, it is less likely to obtain a significant portion of outliers, but the presence of outliers can make a drastic change to statistical interpretations of a small data set. The data is ranked in ascending order and then sorted on the sample size. The τ statistic for the highest value or lowest value is computed. [

]^{a,c,e} The chart below gives a list of how to calculate the appropriate Dixon Ratio values.

Observations	Highest value suspect	Lowest value suspect
3 to 7	$\tau = \frac{x_n - x_{n-1}}{x_n - x_1}$	$\tau = \frac{x_2 - x_1}{x_n - x_1}$
8 to 10	$\tau = \frac{x_n - x_{n-1}}{x_n - x_2}$	$\tau = \frac{x_2 - x_1}{x_{n-1} - x_1}$
11 to 13	$\tau = \frac{x_n - x_{n-2}}{x_n - x_2}$	$\tau = \frac{x_3 - x_1}{x_{n-1} - x_1}$
14 to 20-30	$\tau = \frac{x_n - x_{n-2}}{x_n - x_3}$	$\tau = \frac{x_3 - x_1}{x_{n-2} - x_1}$

The τ statistic is compared to a critical value at a chosen value of α. If the τ statistic is less than the critical value, the null hypothesis is not rejected, and the conclusion is that no outliers are present. If the τ statistic is greater than the critical value, the null hypothesis is rejected, and the conclusion is that the most extreme value is an outlier. To check for other outliers, the Dixon test can be repeated, however, the power of this test decreases as the number of repetitions increases. [

]^{a,c,e}

Table 3 Data Set for Calculating the Dixon Ratio Test NOP Results using Model 1

a,c,e

[

]

Table 4 Data Set for Calculating the Dixon Ratio Test NOP Results Using Model 2

a,c,e

[ ]

Table 5 Data Set for Calculating the Dixon Ratio Test NOP Results Using Model 3

a,c,e

[ ]

Table 6 Data Set for Calculating the Dixon Ratio Test SLB Results Using Model 1 a,c,e

[ ]

Table 7 Data Set for Calculating the Dixon Ratio Test SLB Results Using Model 2 a,c,e

[

]

Table 8 Data Set for Calculating the Dixon Ratio Test SLB Results Using Model 3 a,c,e

[

]

[

]a,c,e

Table 9 Rank Ordered Data Set for NOP Condition

a,c,e

[

]

Table 10 Rank Ordered Data Set for SLB Condition a,c,e

[

]

The equation used to calculate the Dixon Ratio test value for a data set changes based on the size of the data population and whether the higher or lower values are suspect. [

]^{a,c,e} The equation for determining the Dixon ratio test value for the NOP case is:

a,c,e

[

]

Where τ is the Dixon ratio test value, x_n refers to the largest value in the data set, x_2 refers to the second lowest value in the data set and x_1 refers to the lowest value in the data set. The equation for determining the Dixon ratio test value for the SLB case is:

a,c,e

[

]

Where x_3 refers to the third lowest ranked value in the data set and x_{n-1} refers to the second largest value in the data set. Calculating the Dixon ratio test values yield the results shown in Table 11 and Table 12 below.

Table 11 Comparison of Dixon Ratio Test Values for NOP a,c,e

[

]

Table 12 Comparison of Dixon Ratio Test Values for SLB a,c,e

[

]

[

]^{a,c,e} The summary of the calculations is provided in Table 13. The effect of the limiting crevice pressure ratio on the H* and B* inspection distances are evaluated in Section 6.

4.0 The Crevice Pressure Effects on the Loss Coefficient Data

The effective contact pressure between the tube and the tubesheet is a function of four phenomena:

1. thermal growth/mismatch between the tube and the tubesheet,
2. tubesheet displacement resulting in hole dilation,
3. tube expansion due to the pressure differential, and
4. residual mechanical joint strength due to the tube expansion process during installation.

[

]^{a,c,e}

See Appendix C, response to RAI No. 11, in Reference 15 for a discussion of the results of incorporating different crevice pressure assumptions into the loss coefficient versus contact pressure regression analysis. See Reference 16 for the development of the theory of elasticity model used to calculate the contact pressure associated with a primary to secondary pressure differential during a leak rate experiment. See Reference 1 for the data used to calculate the crevice pressure ratios used in the contact pressure analysis.

[

]^{a,c,e} The crevice pressure ratios used with each applied ΔP are summarized in Table 13. The results of the varied crevice pressure with applied ΔP are summarized in Table 14. The spreadsheets and calculation tools used in the analysis are captured in the attachments to Reference 17.

Table 13 Crevice Pressure Ratio Summary for Leak Rate Analysis a,c,e

[

]

Table 14 Summary of Contact Pressure Results for Loss Coefficient Analysis

SG Type	Primary Side Test Pressure (PSI)	Test Temperature (°F)	Contact Pressure (PSI)	Crevice Pressure Differential (PSI)

a,c,e

5.0 The Effect of the Divider Plate Factor on B* and H* Analysis

Indications of cracks in the divider plates have been reported in several steam generators located in France. These indications have been observed in steam generators located at the Chinon, Saint-Laurent, Blayais, Dampierre and Gravelines nuclear power stations. The cracks were observed on the hot leg side of the divider plate in the stub runner divider plate weld, stub runner base metal and also at or in the divider plate itself. See Figure 6 for a sketch of the region where cracking has been observed to occur.

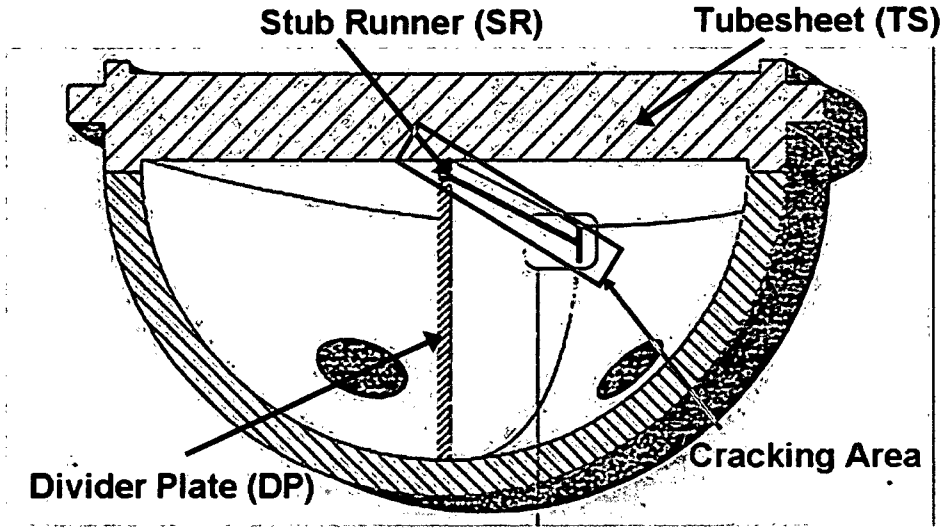

Figure 6 Sketch of Divider Plate, Channel Head and Tubesheet with Potential Cracking Areas Highlighted

The network of cracks has been reported to extend along most of the divider plate (~6 feet) and have also been reported to be relatively shallow with depth, typically less than 2 mm (~75 mils deep).

The French utilities inspected this location to determine if any indications of cracking could be found during a visual inspection because these steam generators used an Alloy 600 material in the divider plate to stub runner weld. During the initial visual inspection it was reported that indications of cracks were observed but that they appeared to be shallow in depth. Various other methods were used in subsequent refueling outages to determine the extent of cracking and to determine the crack growth rate. Available information indicates that these inspections have been performed since 1993 using a combination of liquid penetrant examination (PT) and visual examination (VT) methods with indications of cracking observed in some of these plants. Through the winter of 2005, a total of thirty five inspections using VT and PT were performed in the French 900 megawatt (MW) and 1300 MW units with indications of cracking being found in at least four of the plants as noted above.

Primary water stress corrosion cracking (PWSCC) is a know mechanism of cracking in Alloy 600 and it is likely this is the primary contributor to cracking at this location. However, other potential contributors to cracking have been reported to be defects in the weld or base material, along with deformations associated with loose part impingement and these may be contributing factors. See Reference 13.

The maximum depth of the majority of the cracks observed in the French units has been reported to be about 2 mm (~75 mils). The maximum crack depth indication that has been observed is 7 mm (~0.28 inch) however this indication is the likely result of loose part damage on the hot leg side of the divider plate in the affected generator. Various inspection methods (VT, PT, and then UT) have been used in plants with indications of divider plate cracking. It has been reported that consecutive inspections using identical methods have not been performed to date; therefore, it is not possible to develop an accurate growth rate from the French inspection data. From the available information it can be inferred that the cycle-to-cycle growth rate of the cracks is small based on the following: The difficulty in obtaining an accurate measure of the depth of the crack due to the shallowness of the crack (smaller cracks are harder to detect than larger cracks), the continued reports of finding only shallow depth cracks, and the relatively long period of time that these cracks have been known to exist.

The majority of the cracks included by the French experience are small with a relatively small cycle-to-cycle growth rate; therefore, the effect on the divider plate function is also expected to be small. It would be expected that cracks of the size reported would not affect the general displacement response of the tubesheet since only a very small change in divider plate stiffness would be expected. In addition, it would not be expected that cracks of the size reported would rapidly grow due to mechanically induced loadings resulting from normal/upset events or during a faulted event. However, there may be a potential for long term growth of these cracks which could eventually affect tubesheet displacements and result in an increased rate of crack propagation. See Reference 13 for a conservative analysis estimate of crack growth in the divider plate.

Tubesheet displacements can directly affect multiple regions in the SG that include such areas as:

a. Stress in the tubesheet/shell and tubesheet/channelhead connections
b. Tube stresses and field repairs
c. Plug retention/acceptability issues.

The divider plate is accounted for in B* and H* analyses via a divider plate factor, which is the ratio of the maximum vertical tubesheet displacements with an intact divider plate compared to the maximum vertical displacements of a tubesheet with no divider plate present. The factor is based on the ASME stress report provided for the SGs, which considered both to conservatively calculate stresses in the tubesheet and in the components attached to the tubesheet. The ratio of the maximum tubesheet displacement with and without the benefit of the divider plate is [ ]^{a,c,e}, which means that the maximum vertical displacement of the tubesheet with an intact divider plate is [ ]^{a,c,e} less than the maximum vertical displacement of a tubesheet without a divider plate based on the ASME Code Stress Report for the SGs. This value [ ]^{a,c,e} is used for the divider plate factor in the B* and H* analyses prior to 2007. A value of [ ]^{a,c,e} for the divider plate factor is used in the H* and B* analyses to evaluate the condition where the divider plate does not restrain the vertical tubesheet displacements of the tubesheet.

[

]^{a,c,e}

[

]a,c,e

The effect of a reduced divider plate factor with a non-degraded divider plate will [

]a,c,e

To evaluate the effect of a degraded divider plate, a bounding analysis was performed which assumed that the divider plate provides [

]a,c,e

[

]^{a,c,e}

Evaluation of divider plate degradation is continuing under EPRI sponsorship. The effects of long term operation with postulated larger cracks in the divider plate must be evaluated to determine if the cracks could grow to a point where either rapid crack growth could occur during operation of the SG or if increased tubesheet displacements could affect other aspects of the steam generator, such as tubesheet stress, secondary side shell stress, channel head stress, tube stress, plug retention/acceptability issues and the ARCs [6, 13].

The following conclusions are reached based on the current evaluation of divider plate degradation:

1. The original divider plate factor from the ASME Code stress report, the ratio of the maximum tubesheet displacement assuming a fully effective divider plate to that assuming no contribution from the divider plate, is [ ]^{a,c,e}

2. Based on a more detailed finite element model of the tubesheet/divider plate assembly, the revised divider plate factor is [ ]^{a,c,e}

3. The divider plate factor obtained by comparing the displacements of the tubesheet with and without the contribution of the potentially cracked region of the divider plate is [ ]^{a,c,e}

4. The preliminary conservative estimate of H* and B* assuming no structural contribution from the cracked region of the divider plate is bounded by [ ]^{a,c,e}

5. The presence or absence of the cracked region of the divider plate does not impact a 17 inch inspection depth, since sufficient margin exists between [ ]^{a,c,e} The structural model used for this assessment is the refined finite element model of the tubesheet/divider plate assembly.

6.0 Results from Implementing Changes in H* and B* Analysis

Table 15 below summarizes the limiting crevice pressure ratios [

]a,c,e

Table 15 . Limiting Crevice Pressure Ratios from 3 Models

[a,c,e]

From Section 1, the pressure ratio [

]a,c,e

Therefore, the smallest pressure drop [

]a,c,e

Table 16 H* and B* Prediction for Different Models of Crevice Pressure

(Data based on improved tubesheet/divider plate structural model) a,c,e

[

]

(H* and B* are referenced to the bottom of the expansion transition)

The results [

]a,c,e

The following figures show [

]a,c,e

Figure 7 shows [

]a,c,e

[a,c,e]

Figure 7 Unaltered Data and Methods for B* and H*. Crevice Pressure = $P_{Pri} - P_{Sec}$, DP = 0.76

[ ]a,c,e

[a,c,e]

Figure 8 Updated Input Data and Methods for B* and H*. Crevice Pressure = CP*P_{Pri}, DP = 0.399

The results for the updated analysis input with a divider plate factor of [ ]^{a,c,e} (i.e., no structural restraint provided by the potentially cracked region of the divider plate) are shown in Figure 9.

[a,c,e]

Figure 9 Updated Input Data and Methods for B* and H*. Crevice Pressure = CP*P_{Pri}, DP = 0.64

Comparing the results shown in Figure 7 and Figure 9 proves that the changes in the B* and H* inputs due to the increased crevice pressure and divider plate effects are reasonable and follow similar trends compared to the prior results. The results shown in Figure 9 prove that the generic bounding analysis conditions (using mean ASME material properties and design inputs) in the event that the divider plate to stub runner is fully degraded are still below the previously reported bounding value of 12.50 inches. [

]^{a,c,e}

The choice of crevice pressure model maximizes the B* and H* depths by minimizing the structural and leakage resistance of the tube to tubesheet crevice joint. An alternative method to using a limiting constant crevice pressure ratio is to use a depth based approach. That is, to vary the crevice pressure ratio at each depth based on the available test data so that the pressure difference across the tube varies as a function of tubesheet elevation. The depth based crevice pressure approach [

]^{a,c,e}

1. [

]^{a,c,e}

2. [

]a,c,e

3. [

]a,c,e

The constant crevice pressure approach does yield different results from the depth based approach during accident conditions. [

]a,c,e

In conclusion, [

]a,c,e

7.0 Summary and Conclusions

The following summarizes this "White Paper" regarding the effects of new test data and updated analysis methods on the H*/B* technical justifications:

1. Recently obtained test data indicate that postulated leakage through a tube crack in the tubesheet expansion region [

]a,c,e

2. Updated finite element analysis of the tubesheet/divider plate assembly shows that the ratio of the maximum deflection of the tubesheet with an un-degraded divider plate to the maximum deflection with no structural restraint from the divider plate [

]a,c,e

3. Analysis using the updated divider plate factor shows that the bounding value for H*/B* is about [ ]^{a,c,e} (using mean ASME code material properties and design inputs). Only the "true" B* value will be affected if the divider plate is assumed to be non-functional. Significant margin exists for [ ]^{a,c,e} inch inspection depth.

4. Several models were developed to represent the new crevice pressure test data. The most conservative model, that minimizes the pressure drop from the primary side to the crevice, was identified.

5. Integrated analysis accounting for both the divider plate degradation and revised crevice pressure show that the justification for H* and B* is still valid when the most conservative crevice pressure model and the refined structural model for the tubesheet/divider plate assembly are used.